

---

Electronic Thesis and Dissertation Repository

---

9-21-2016 12:00 AM

## Role of Anterior Cingulate Cortex in Saccade Control

Sahand Babapoor-Farrokhran  
*The University of Western Ontario*

Supervisor  
Dr. Stefan Everling  
*The University of Western Ontario*

Graduate Program in Neuroscience  
A thesis submitted in partial fulfillment of the requirements for the degree in Doctor of  
Philosophy  
© Sahand Babapoor-Farrokhran 2016

Follow this and additional works at: <https://ir.lib.uwo.ca/etd>



Part of the [Cognitive Neuroscience Commons](#), [Other Neuroscience and Neurobiology Commons](#),  
[Systems and Integrative Physiology Commons](#), and the [Systems Neuroscience Commons](#)

---

### Recommended Citation

Babapoor-Farrokhran, Sahand, "Role of Anterior Cingulate Cortex in Saccade Control" (2016). *Electronic Thesis and Dissertation Repository*. 4150.  
<https://ir.lib.uwo.ca/etd/4150>

This Dissertation/Thesis is brought to you for free and open access by Scholarship@Western. It has been accepted for inclusion in Electronic Thesis and Dissertation Repository by an authorized administrator of Scholarship@Western. For more information, please contact [wlsadmin@uwo.ca](mailto:wlsadmin@uwo.ca).

**ABSTRACT:**

Cognitive control is referred to the guidance of behavior based on internal goals rather than external stimuli. The brain areas involved in implementing cognitive control are more developed and have larger proportional spatial extent in humans and non-human primates compared to other species. Studying the mechanisms by which cognitive control is implemented has recently gained more attention. It has been postulated that prefrontal cortex is mainly involved in higher order cognitive functions. Specifically, anterior cingulate cortex (ACC), which is part of the prefrontal cortex, is suggested to be involved in performance monitoring and conflict monitoring that are considered to be cognitive control functions.

Saccades are the fast eye movements that align the fovea on the objects of interest in the environment. Saccade system is one of the most studied motor systems in the brain. This is mainly due to the simplicity of the saccade system and amenability of saccade-related brain areas to electrophysiological recordings. This makes the saccadic system an ideal candidate to study the cognitive control functions.

In this thesis, I have explored the role of ACC in control of saccadic eye movements. First, I performed a resting-state fMRI study to identify areas within the ACC that are functionally connected to the frontal eye fields (FEF). It has been shown that FEF is involved in saccade generation. Therefore, the ACC areas that are functionally connected to FEF could be hypothesized to have a role in saccade control. Then, I performed simultaneous electrophysiological recordings in the ACC and FEF to investigate the mechanisms by which information is transmitted between these areas. Furthermore, I explored whether ACC exerts control over FEF.

In the first chapter, I have shown that ACC has functional connectivity with the FEF. Furthermore, I observed differential functional connectivity of medial and lateral FEF with other brain areas. In the second chapter, I have shown that theta and beta bands are involved in information transmission between FEF and ACC. Finally, using Granger causality analysis, I have shown that ACC exerts control over FEF when monkeys perform saccade-related tasks.

These findings show that ACC is involved in cognitive control of saccades. Furthermore, the ACC and FEF neurons communicate through synchronized theta and beta band activity in these areas. The results of this thesis shine light on the mechanisms by which these brain areas communicate. Moreover, my findings support the notion that ACC and FEF have a unique oscillatory property, and more specifically ACC has a prominent theta band, and to a lesser extent beta band activity.

### Keywords:

Cognitive control, anterior cingulate cortex (ACC), frontal eye field (FEF), resting-state fMRI, functional connectivity, working memory, memory-guided saccade task, pro-/anti-saccade task, local field potentials (LFP), multi-unit recording, brain oscillations, theta band, beta band, spectral power, field-field coherence, spike-field coherence.

## TABLE OF CONTENTS:

<b>ABSTRACT:</b> .....	<b>ii</b>
<b>TABLE OF CONTENTS:</b> .....	<b>iv</b>
<b>CO-AUTHORSHIP STATEMENT:</b> .....	<b>vii</b>
<b>EPIGRAPH:</b> .....	<b>viii</b>
<b>DEDICATION:</b> .....	<b>ix</b>
<b>ACKNOWLEDGEMENTS:</b> .....	<b>x</b>
<b>LIST OF TABLES:</b> .....	<b>xi</b>
<b>LIST OF FIGURES:</b> .....	<b>xii</b>
<b>LIST OF ABBREVIATIONS:</b> .....	<b>xxi</b>
<b>CHAPTER 1:</b> .....	<b>1</b>
<b>1. GENERAL INTRODUCTION:</b> .....	<b>1</b>
<b>1.1. ANTERIOR CINGULATE CORTEX (ACC):</b> .....	<b>1</b>
1.1.1. History: .....	1
1.1.2. ACC subdivisions: .....	2
1.1.3. ACC connectivity: .....	3
1.1.4. ACC functions: .....	4
1.1.4.1. ACC and motor functions: .....	7
1.1.4.2. ACC and the limbic system: .....	8
1.1.4.3. ACC and conflict monitoring: .....	9
1.1.4.4. ACC and performance monitoring: .....	11
<b>1.2. SACCADDES AND THE OCULOMOTOR SYSTEM:</b> .....	<b>14</b>
1.2.1. Frontal eye fields: .....	15
1.2.2. Frontal eye fields and visual functions: .....	18
1.2.3. Memory-guided saccade task: .....	20
1.2.4. Pro-/Anti-saccade task: .....	21
1.2.5. Cingulo-Frontal (ACC-FEF) interaction in saccade tasks: .....	24
1.2.5.1 Resting-state connectivity of the ACC: .....	25
1.2.5.2. Resting-state fMRI: .....	27
1.2.5.3. Analytic approaches for resting-state fMRI: .....	30
1.2.5.4. Resting-state fMRI and clinical applications: .....	31
<b>1.3. BRAIN RHYTHMS:</b> .....	<b>34</b>
1.3.1. Communication through coherence (CTC): .....	35
1.3.2. Theta band: .....	37
1.3.3. Beta band: .....	40
<b>1.4. OBJECTIVES:</b> .....	<b>42</b>
1.4.1. Obtain the functional connectivity map of the FEF: .....	42
1.4.2. Evaluate whether the functionally connected ACC and FEF areas display synchronized neuronal activity: .....	43
1.4.3. Examine the direction of information flow between ACC and FEF: .....	43



1.5. REFERENCES:	44
CHAPTER 2:	56
2. Functional connectivity patterns of medial and lateral macaque frontal eye fields reveal distinct visuomotor networks	56
2.1. ABSTRACT:	56
2.2. INTRODUCTION:	57
2.3. MATERIALS AND METHODS:	59
2.3.1. Data acquisition:	59
2.3.2. Image preprocessing:	61
2.3.3. Statistical analysis:	61
2.3.4. Region-of-interest identification:	63
2.4. RESULTS:	66
2.5. DISCUSSION:	77
2.6. REFERENCES:	84
CHAPTER 3:	92
3. Theta and Beta synchrony coordinate frontal eye fields and anterior cingulate cortex during sensori-motor mapping	92
3.1. ABSTRACT:	92
3.2. INTRODUCTION:	93
3.3. MATERIALS AND METHODS:	94
3.4. RESULTS:	95
3.4.1. Modulation of theta and beta power during the delay period:	97
3.4.2. Task-dependent LFP-LFP coherence between ACC and FEF:	99
3.4.3. Task-dependent Granger-causality between ACC and FEF LFPs:	104
3.4.4. Decreased theta and beta-synchrony between ACC and FEF LFPs on error trials:	105
3.4.5. Modulation of spike-field synchrony during the delay period:	108
3.5. DISCUSSION:	114
3.6. REFERENCES:	123
3.7. SUPPLEMENTARY METHODS:	127
3.7.1. Subjects:	127
3.7.2. Behavioral Task:	127
3.7.3. Electrophysiological Recordings:	129
3.7.4. Data Analysis:	130
3.7.5. Supplementary references:	136
CHAPTER 4:	145
4. GENERAL DISCUSSION:	145
4.1. SUMMARY OF THE MAIN FINDINGS:	145
4.1.1. FEF is functionally connected to the ACC and there is a difference between the functional connectivity of the medial and lateral FEF:	145
4.1.2. Theta and beta band synchronization is involved in the communication between FEF and ACC:	148
4.1.3. ACC affects FEF in memory-guided saccade task:	151
4.2. CAVEATS AND LIMITATIONS:	153

4.2.1. Limited ability to record from multiple sites: .....	153
4.2.2. Lack of specificity with regards to the recorded layer of the cortex: .....	154
<b>4.3. FUTURE DIRECTIONS: .....</b>	<b>155</b>
4.3.1. Investigating the theta- and beta band synchronization of medial and lateral FEF with ACC: .....	155
4.3.2. Investigating the beta and theta band synchronization in pro-/anti-saccade task: .....	155
4.3.3. Identifying specific sub-classes of single units in the ACC and FEF that are coupled with different frequency bands: .....	156
<b>4.4. REFERENCES: .....</b>	<b>156</b>
<b>APPENDIX A: Documentation of Ethics Approval .....</b>	<b>159</b>
<b>CURRICULUM VITAE.....</b>	<b>160</b>

## **CO-AUTHORSHIP STATEMENT:**

**Sahand Babapoor-Farrokhran, Martin Vinck, Joseph S. Gati, Ravi S. Menon, Thilo Womelsdorf, and Stefan Everling.**

As the primary author of the chapters, I (Sahand Babapoor-Farrokhran) have designed the experiments, collected the data, performed the data analysis, and wrote the completed manuscripts. Dr. Stefan Everling supervised all projects and assisted in experiment design, data analysis, and manuscript revisions for all the experimental chapters. Mr. Joseph S. Gati and Dr. Ravi S. Menon kindly assisted in data collection of chapter 2. Dr. Martin Vinck was instrumental in data analysis of chapter 3. Dr. Thilo Womelsdorf provided valuable assistance in the data analysis and writing of chapter 3.

## **EPIGRAPH:**

“It has been said that the beauty is in the eyes of the beholder. As a hypothesis . . . it points clearly enough to the central problem of cognition: . . . The world of experience is produced by the person who experiences it”

- Ulric Neisser (1967)

## **DEDICATION:**

To my parents, they were always available when I needed their support, and provided with the best they could, and encouraged me to pursue my career in science.

## **ACKNOWLEDGEMENTS:**

First, I would like to thank Dr. Everling very much for taking me on as a PhD student, offering me his trust, and teaching me the skills needed to be a dedicated scientist. He has always encouraged me to develop my own ideas, and provided me the opportunity to experiment them. Also, he has always been a supportive supervisor and this has made me more determined to pursue my career in the realm of science.

Secondly, I would like to thank my family: Mom, Dad, Shaghayegh, Savalan, and Ali. They are the people I rely on, and they have always helped me in the long road I have chosen.

I would also like to thank my friends in the Everling lab over the years: Darren, Kevin (Skoblenick), Kevin (Johnston), Jessica, Michelle, Iman, Michael, Sabeeha, Susheel, Jason, Alex, Ramina, Brandon, Liya, Nicole. Thilo Womelsdorf, for helping me analyze the data. Ravi Menon and Joseph Gati for helping me collect the resting-state fMRI data.

Special thanks to Martin, who has helped me perform the sophisticated analysis, sometime till after midnight.

Lastly, I'd like to thank my friends in BMI, back home and all around the world; I have always enjoyed your accompany. Thanks Caroline for the very quick and timely edition of my thesis.

## LIST OF TABLES:

<b>Table 1.1.</b> Statistical analysis and percentage connectivity of FEF seed regions with parietal and premotor areas.....	73
--	----

## LIST OF FIGURES:

### **Figure 1.1. Retrogradely labeling of cells in coronal sections (Top panel), and depiction of labeled cells on the medial hemispheric wall (Bottom panel).**

Cortical maps inset in the middle: Surface view of the right hemisphere showing the location of cortical injection sites (asterisks), and rostrocaudal levels of coronal sections (a-e) indicated by lines labeled with a to e. The letters f-j in the schematic section (to the right of the cortical map) correspond to f-j in the unfolded map at the bottom. In coronal sections and in an unfolded map, each dot represents 2-5 labeled cells. Regions surrounded by elliptical lines indicate approximate territories projecting to the forelimb area of MI and FEF. Arrowhead in the unfolded map indicates the caudal end of arcuate sulcus. Red dots, FB-labeled cells; green dots, DY-labeled cells. SA, superior limb of arcuate sulcus; IA, inferior limb of arcuate sulcus; Spur, spur of arcuate sulcus; PCS, precentral sulcus; CS, central sulcus; ARC, arcuate sulcus; PS, principle sulcus; Cing S, cingulate sulcus; CC, corpus callosum; CMAr, rostral cingulate motor area; CMAAd, dorsal cingulate motor area; CMAv, ventral cingulate motor area; CEFr, rostral cingulate eye field; CEFc, caudal cingulate eye field.....5

### **Figure 1.2. Summary of major connections of FEF with visual cortical areas.**

The location of specific cortical areas is indicated on a dorsolateral view of the macaque brain. The relative amplitude of saccades represented by ventral FEF (area 45) and dorsal FEF (urea 8Ac) is indicated. The solid blue lines indicate major projections to area 8Ac, and the dashed red lines represent major projections to area 45.....17

**Figure 1.3. Cortical patterns of coherent spontaneous BOLD fluctuations are similar to those of task-evoked responses and anatomical connectivity.** a, Conjunction map of BOLD correlations within the oculomotor system on dorsal views of the monkey atlas left and right hemisphere surfaces. Voxels significantly correlated with three (dark blue) or four (light blue) oculomotor ROIs are shown. b, Activation pattern evoked by performance of a saccadic eye movement task. c, Density of cells labelled by retrograde tracer injections into right LIP. The left hemisphere injection data are duplicated by



reflection of the right hemisphere to facilitate visual comparison. Only regions that showed reproducible projections to LIP are shown. AS, arcuate sulcus; CeS, central sulcus; IPS, intraparietal sulcus; SF, sylvian fissure; STS, superior temporal sulcus.....29

#### **Figure 1.4. Communication through Coherence**

(A) Two presynaptic neuronal groups in a lower visual area provide input to a postsynaptic neuronal group in a higher visual area. The lower groups represent two visual stimuli, an apple and a pear. In each neuronal group, network excitation (red) triggers network inhibition (blue), which inhibits the local network. When inhibition decays, excitation restarts the gamma cycle. The gamma rhythm of the apple-representing presynaptic group has entrained the gamma rhythm in the postsynaptic group. Thereby, the apple-representing pre- synaptic group can optimally transmit its representation, whereas the pear-representing presynaptic group cannot transmit its representation.

(B) A simplified illustration in which network excitation and inhibition are combined into network excitability. Red vertical lines indicate excitatory neuron spiking and blue vertical lines inhibitory neuron spiking.....36

**Figure. 2.1. Location of lateral and medial frontal eye field (FEF) spherical seeds in *monkey 1*.** The spherical seed regions have a radius of 2 mm.....65

**Figure 2.2. Right medial (*left*) and right lateral (*right*) FEF seed connectivity maps projected on the F99 template** (Van Essen 2004) (z-score 5 set at cluster significance of  $P$  0.05, corrected for multiple comparisons). The connectivity maps are shown on lateral, medial, dorsal, and ventral views. Asterisks show the location of the seed region. pos, Parieto-occipital sulcus; cas, calcarine sulcus; cs, central sulcus; hs, hippocampal sulcus; cis, cingulate sulcus; sts, superior temporal sulcus; ios, inferior occipital sulcus; lus, lunate sulcus; ots, occipitotemporal sulcus; ps, principal sulcus; L, left; R, right.....68

**Figure 2.3. Left medial (*left*) and right lateral (*right*) FEF seed connectivity maps projected on the F99 template** (Van Essen 2004) (z-score 5 set at cluster significance of

$P$  0.05, corrected for multiple comparisons). The connectivity maps are shown on lateral, medial, dorsal, and ventral views. Asterisks show the location of the seed region.....69

**Figure 2.4. Cortical views of both hemispheres flattened to display spatial overlap connectivity patterns of right medial and lateral FEF (A) and left medial and lateral FEF (B).** Images show the connectivity pattern of the positively functionally connected areas ( $z$ -score 5 set at cluster significance of  $P$  0.05, corrected for multiple comparisons). Areas in red are functionally connected to the medial FEF, areas in green are functionally connected to the lateral FEF, and areas in yellow are functionally connected to both. White lines indicate the boundaries of parietal areas V6 and V6A according to Galletti et al. (1999) and also premotor areas F2, F4, and F5 according to Markov et al. (2011). Asterisks show the location of the seed regions.....71

**Figure 2.5. Cortical views of both hemispheres flattened to display spatial overlap connectivity patterns of right medial and lateral FEF (A) and left medial and lateral FEF (B).** Images show the connectivity pattern of the negatively functionally connected areas ( $z$ -score 5 set at cluster significance of  $P$  0.05, corrected for multiple comparisons). Areas in red are negatively connected to the medial FEF, areas in green are negatively connected to the lateral FEF, and areas in yellow are negatively connected to both. White lines indicate the boundaries of parietal areas V6 and V6A according to Galletti et al. (1999) and also premotor areas F2, F4, and F5 according to Markov et al. (2011). Asterisks show the location of the seed regions.....72

**Figure 2.6. Coronal slices of the functional connectivity patterns of medial and lateral FEF on F99 atlas (Van Essen 2004) as indicated at top.** Red-yellow areas are positively correlated areas, and blue-light blue areas are negatively correlated areas ( $z$ -score 4 set at cluster significance of  $P$  0.05, corrected for multiple comparisons).....75

**Figure 3.1. Experimental paradigm and sample traces of simultaneously recorded activity in ACC and FEF.** (A) Schematic of the memory-guided saccade task and pro/anti-saccade task. (B) The traces show the multi-unit activity, raw LFP signal (0.5-

125 Hz), theta band pass filtered signal (3-9Hz) and beta band pass filtered signal (12-30 Hz) in a trial of memory-guided saccade task. (C) Same as A in another memory-guided saccade task trial. The vertical green dashed lines indicate the 500ms time intervals aligned on stimulus onset.....96

**Figure 3.2. LFP power in FEF and ACC during the memory-guided saccade task.**

(A) Average time frequency spectra of the FEF LFP power across 8 target locations in the memory-guided saccade task. (B) Average time frequency spectra of ACC LFP power across 8 target locations in the memory-guided saccade task. The dashed lines demarcate the time of the onset and offset of the target stimulus. The black boxes on top of each graph demarcate the delay period.....98

**Figure 3.3. Increased theta and beta coherence between ACC and FEF.**

(A) Time-Frequency spectrum of the wpli-debiased coherence between the FEF and ACC in memory-guided saccade task for the population of ACC-FEF channel pairs (n=674). The white contour shows the area in which the subsequent analyses were performed (see Methods). The dashed lines demarcate the time of the onset and offset of the target stimulus. (B) WPLI-debiased FEF-ACC coherence spectrum of the individual monkeys in the delay period across all recording pairs (n=674). (C) Theta band (3-9 Hz) time course of the ACC-FEF WPLI-debiased phase synchronization. (D) Beta band (12-30 Hz) time course of the ACC-FEF WPLI-debiased phase synchronization. (E) Comparison of WPLI-debiased coherence between baseline and delay period of the contra-verse and ipsi-verse memory-guided saccades (\*\*\*:  $p < 0.001$ , t-test). Error bars indicate SEM. (F) Comparison of the overall Granger causality effect of ACC over FEF ( $G_{ACC \rightarrow FEF} - G_{FEF \rightarrow ACC}$ ) between baseline and delay period of the contra-verse and ipsi-verse memory-guided saccades (\*\*\*:  $p < 0.001$ , \*\*:  $p < 0.01$ , t-test, n=275). Error bars indicate SEM. (G) Comparison of beta band WPLI-debiased coherence between baseline and delay period of the contra-verse and ipsi-verse memory-guided saccades (\*\*:  $p < 0.01$ , \*:  $p < 0.05$ ; t-test). Error bars indicate SEM. (H) Comparison of the beta band overall Granger effect of ACC over FEF ( $G_{ACC \rightarrow FEF} - G_{FEF \rightarrow ACC}$ ) between baseline and

delay period of the contra-verse and ipsi-verse memory-guided saccades (\*\*\*:  $p < 0.001$ ; t-test). Error bars indicate SEM.....102

**Figure 3.4. Correct task performance is dependent on field-field coherence but not on LFP power.** (A) Shown the comparison of theta (columns 1 and 2) and beta-band (columns 3 and 4) WPLI-debiased coherence between correct and error memory-guided saccades in the delay period of the memory guided saccade task (400-1100ms following target stimulus onset) and the preparatory period (400-1100ms following fixation onset) of the anti-saccade task. (B) Same as A, but shown normalized ACC theta and beta-band power. (C) Same as A but for normalized FEF power. \*:  $p < 0.05$ ; \*\*:  $p < 0.01$ ; \*\*\*:  $p < 0.001$ , t-test. Error bars indicate SEM.....107

**Figure 3.5. Percentage of units with significant spike-field coupling in theta and beta band.** (A) Percentage of the ACC-units-to-FEF-LFP pairs showing significant changes in phase-locking across the theta and beta frequency range. Comparison between baseline and delay of contra-verse saccades (left), comparison between baseline and delay of ipsi-verse saccades (middle) and comparison between the contra- and ipsi-verse saccades in the delay period (right). (B) Same as (A), but now depicted the percentage of the FEF-units-to-ACC-LFP pairs showing significant changes in phase-locking across the theta and beta frequency range. Statistical testing was performed using two-sided permutation tests, such that chance level is 2.5%.....111

**Figure 3.6. Pairwise phase consistencies (PPCs) across delta and theta band.** (A) PPC spike-field coherence spectrum of the population of the ACC-units-to-FEF-LFP pairs across the delta and theta frequency range. Comparison between baseline and delay of contra-verse saccades (left), comparison between baseline and delay of ipsi-verse saccades (middle) and comparison between the contra- and ipsi-verse saccades in the delay period (right). (B) PPC spike-field coherence spectrum of the population of the FEF-units-to-ACC-LFP pairs across the delta and theta frequency range. Comparison between baseline and delay of contra-verse saccades (left), comparison between

baseline and delay of ipsi-verse saccades (middle) and comparison between the contra- and ipsi-verse saccades in the delay period (right). It should be noted that the same significant differences between ipsi-verse and contra-verse trials were seen even after we compared the contra- versus ipsi-verse conditions using a permutation test as described in the methods section. Error bars denote SEM in all panels. \*:  $p < 0.05$ , paired t-test). The rose plots on the side of each graph show the histogram of the coupling angles of the population of the ACC/FEF units.....112

**Figure 3.7. Pairwise phase consistencies (PPCs) across beta band.** (A) PPC spike-field coherence spectrum of the population of the ACC-units-to-FEF-LFP pairs across the beta frequency range. Comparison between baseline and delay of contra-verse saccades (left), comparison between baseline and delay of ipsi-verse saccades (middle) and comparison between the contra- and ipsi-verse saccades in the delay period (right). (B) PPC spike-field coherence spectrum of the population of the FEF-units-to-ACC-LFP pairs across the beta frequency range. Comparison between baseline and delay of contra-verse saccades (left), comparison between baseline and delay of ipsi-verse saccades (middle) and comparison between the contra- and ipsi-verse saccades in the delay period (right). Error bars denote SEM in all panels. \*:  $p < 0.05$ , paired t-test).....113

**Figure 3.8. Illustration of recorded brain area locations and summary of main inter-areal ACC-FEF modulations observed in this study.** (A) ACC and FEF recording locations (in red shading) shown on a rendering of a semi-inflated macaque brain. (B, C) Illustration of main inter-areal effects in the theta (B) and beta (C) band with the thickness of connections indicating the strength or prevalence of the effects. LFP-LFP coherence (top row) was modulated during the delay in  $> 75\%$  of LFP-LFP pairs in both frequencies (with increased coherence in the largest majority). Granger causality (middle row) increased during the delay for both ACC-FEF and FEF-ACC directions, but the ACC to FEF granger causal flow was stronger than FEF to ACC granger causal flow at both, theta and beta frequencies. Spike-LFP coherence (bottom row) increased for both

directions during the delay in the theta band, but was different between delay and baseline merely in one beta frequency bin (at 22Hz) for ACC spike to FEF LFP sites for contra-verse saccades. Reduced inter-area modulation prior to error commission was evident in both frequencies across different measures and is described in the text.....122

**Supplementary Figure 3.1. Schematic reconstruction of the recording sites.** The recording sites are overlaid on the F99 surface (using Caret software, Van Essen lab) according to the composite atlas of Van Essen et al. (2012)<sup>2</sup>. The left column is the reconstruction of the ACC recording sites shown on a fiducial (up), inflated (middle) and flat surface map. The arrows on the top and middle panels denote the location of the angle of the Arcuate sulcus. Similarly, the left column shows the reconstruction of the FEF recording sites.....138

**Supplementary Figure 3.2. WPLI-debiased spectrum.** (A) The phase synchronization spectrum between ACC and FEF in memory-guided saccades is depicted across all recording pairs (n=674). The panel shows larger ACC-FEF phase synchronization across theta and beta bands in the delay period (400-1100ms following the stimulus onset, blue) compared to the baseline (700ms prior to the fixation onset, black). (B) The phase synchronization spectrum between ACC and FEF in pro-/anti-saccades is depicted across all recording pairs (n=674). The panel shows larger ACC-FEF phase synchronization across theta and beta bands in the preparatory period (400-1100 ms following the fixation onset, blue) compared to the baseline (700 ms prior to the fixation onset, black). The shading shows +/- SEM.....139

**Supplementary Figure 3.3. Increased theta-coherence between ACC and FEF after event-related signal subtraction.** (A) Time-Frequency spectra of the WPLI-debiased coherence between the FEF and ACC in memory-guided saccade task after subtraction of the averaged event-related potentials from the raw signal. The white contour shows the area in which the subsequent analyses were performed (see Methods). The dashed lines demarcate the time of the onset and offset of the target stimulus. (B) WPLI-debiased FEF-ACC coherence spectrum of the individual monkeys in the delay period across all recording pairs (n=674). (C) Theta band (3-9 Hz) time course of the ACC-FEF WPLI-

debiased phase synchronization. (D) Beta band (12-30 Hz) time course of the ACC-FEF WPLI-debiased phase synchronization.....140

**Supplementary Figure 3.4. Granger causality spectrum between ACC and FEF.** (A) Causality effect of ACC over FEF ( $G_{ACC \rightarrow FEF}$ ) in the delay period (400-1100ms following the stimulus onset, blue) and the baseline (700 ms prior to fixation onset, black). The causality effect of ACC over FEF is larger in the delay period across theta and beta frequency range. (B) Causality effect of FEF over ACC ( $G_{FEF \rightarrow ACC}$ ) in the delay period (red) and the baseline (black). The causality effect of FEF over ACC is larger in the delay period across theta and beta frequency range. (C) Causality effect of ACC over FEF ( $G_{ACC \rightarrow FEF}$ , blue) is higher than the causality effect of FEF over ACC ( $G_{FEF \rightarrow ACC}$ , red) in the delay period across theta and beta frequency range. The shading depicts  $\pm$  SEM. The ACC-FEF channel pairs (n=275) that displayed reversed Granger causality following the reversal of time series are included in this figure.....141

**Supplementary Figure 3.5. Pairwise phase consistencies (PPCs) across alpha band.** (A) PPC spike-field coherence spectrum of the population of the ACC units with the LFP's recorded in the FEF across the alpha frequency range. Comparison between baseline and delay of contra-verse saccades (left), comparison between baseline and delay of ipsi-verse saccades (middle) and comparison between the contra- and ipsi-verse saccades in the delay period (right). (B) PPC spike-field coherence spectrum of the population of the FEF units with the LFP's recorded in the ACC across the alpha frequency range. Comparison between baseline and delay of contra-verse saccades (left), comparison between baseline and delay of ipsi-verse saccades (middle) and comparison between the contra- and ipsi-verse saccades in the delay period (right). Error bars denote SEM in all panels. \*:  $p < 0.05$ , paired t-test).....142

**Supplementary Figure 3.6. Pairwise phase consistencies (PPCs) across gamma band.** (A) PPC spike-field coherence spectrum of the population of the ACC units with the LFP's recorded in the FEF across the gamma frequency range. Comparison between baseline and delay of contra-verse saccades (left), comparison between baseline and delay of ipsi-verse saccades (middle) and comparison between the contra- and ipsi-verse saccades in the delay period (right). (B) PPC spike-field coherence spectrum of

the population of the FEF units with the LFP's recorded in the ACC across the gamma frequency range. Comparison between baseline and delay of contra-verse saccades (left), comparison between baseline and delay of ipsi-verse saccades (middle) and comparison between the contra- and ipsi-verse saccades in the delay period (right). Error bars denote SEM in all panels. \*:  $p < 0.05$ , paired t-test).....143

**Supplementary Figure 3.7. Pairwise phase consistencies (PPCs) spectrum.** (A) PPC spike-field coherence spectrum of the population of the ACC units with the LFP's recorded in the FEF across the frequency range of 1.5-100 Hz in the delay period of memory-guided saccade task. (B) PPC spike-field coherence spectrum of the population of the FEF units with the LFP's recorded in the ACC across the frequency range of 1.5-100 Hz in the delay period of memory-guided saccade task. In both panels, the peak spike-field coupling is observed in theta frequency range. Shades denote +/- SEM.....144



## LIST OF ABBREVIATIONS:

ACC	– Anterior Cingulate Cortex
AIP	– Anterior IntraParietal area
AS	– Arcuate Sulcus;
BOLD	– Blood Oxygenation Level Dependent
CEFc	– caudal Cingulate Eye Field
CEFr	– rostral Cingulate Eye Field
CeS	– Central Sulcus
CMA <sub>d</sub>	– dorsal Cingulate Motor Area
CMA <sub>r</sub>	– rostral Cingulate Motor Area
CMA <sub>v</sub>	– ventral Cingulate Motor Area
CS	– Central Sulcus
CTC	– Communication Through Coherence
dl-PFC	– DorsoLateral Prefrontal Cortex
DMN	– Default Mode Network
EEG	– ElectroEncephaloGram
ERN	– Error Related negativity
ERP	– Event Related Potential
FC	– Functional Connectivity
FEF	– Frontal Eye Field
fMRI	– functional Magnetic Resonance Imaging
FM $\theta$	– Frontal Midline Theta
G	– Granger causality
Hz	– Hertz
ICA	– Independent Component Analysis
IPS	– IntraParietal Sulcus
LFP	– Local Field Potential
LIP	– Lateral IntraParietal area
LOP	– Lateral Occipital Parietal area
LUS	– Lunate Sulcus;

MDP	– Medial Dorsal Parietal area
min	– minute
MIP	– Medial IntraParietal area
mmHg	– millimeters of mercury
MRI	– Magnetic Resonance Imaging
ms	– Millisecond
MST	– Medial Superior Temporal area
MT	– Middle Temporal area
OTS	– OccipitoTemporal Sulcus
PCS	– PreCentral Sulcus
PFC	– PreFrontal Cortex
PIP	– Posterior IntraParietal area
PO	– Parietal-Occipital area
PPC	– Pairwise Phase Consistency
PS	– Principle Sulcus
ROI	– Region Of Interest
RS-fMRI	– Resting-State fMRI
RSN	– Resting State Network
SC	– Superior Colliculus
sec	– second
SF	– Sylvian Fissure
SMA	– Supplementary Motor Area
STS	– Superior Temporal Sulcus
VIP	– Ventral IntraParietal area
vl-PFC	– VentroLateral Prefrontal Cortex
VOT	– Ventral OccipitoTemporal area
VP	– Ventral Posterior area
WPLI	– Weighted phase Lag Index

## **CHAPTER 1:**

### **1. GENERAL INTRODUCTION:**

Cognitive control refers to the adjustments made in the processing of sensory inputs and motor outputs to serve internal goals (Miller and Cohen 2001). A few examples of cognitive control functions are attention, working memory, and decision making (Miller and Cohen 2001). A network of brain areas is involved in cognitive control including the prefrontal cortex (Fuster 2008). The prefrontal cortex performs cognitive control functions through exerting top-down control on other cortical areas. Top-down control is needed when the behavior is not driven by merely the sensory stimuli, but also by internal intentions and goals (Miller and Cohen 2001). The medial prefrontal cortex and in particular, the anterior cingulate cortex (ACC) has been suggested to exert top-down control on other cortical areas. The ACC has been suggested to be involved in a multitude of cognitively demanding tasks, and therefore, a brief review of literature surrounding ACC function is provided in below.

#### ***1.1. ANTERIOR CINGULATE CORTEX (ACC):***

##### ***1.1.1. History:***

The cingulate cortex was initially thought of as a cortical area associated with the limbic system (MacLean 1990). However, substantial evidence that gathered through neuroimaging and electrophysiological experiments in 1990s and thereafter, casted doubt on this theory. In fact, it was shown that large parts of the cingulate cortex are involved in visual, motor, and higher cognitive functions (Vogt 2009). Additionally, the rostral and

subgenual ACC possess autonomic properties that could be considered as limbic functions (Dum and Strick 2002). Further studies found that the ACC is comprised of cytoarchitectonically distinct subdivisions that are involved in a variety of functions. Below, I will describe the subdivisions and the most commonly studied functions of the ACC.

### ***1.1.2. ACC subdivisions:***

ACC is part of the medial prefrontal cortex. The cingulate cortex was viewed as a single functional unit for the most part of the last century. In separate reports, Papez (1937) and MacLean (1954) have defined the cingulate cortex as part of the limbic system and they emphasized that the cingulate cortex is involved in emotional responses (Maclean 1954; Papez 1995). This view of cingulate function did not consider the motor and visuo-spatial properties of the cingulate cortex. In a different model of the cingulate cortex structure based on the cytoarchitectonic characteristics, the dual subdivision for the cingulate cortex, the anterior and the posterior cingulate cortices, was proposed (Brodmann and Garey 1994). The dual model of the cingulate cortex provides a more precise description of the functional and cytological properties of the cingulate cortex. For example, the anterior cingulate cortex is mainly involved in executive functioning whereas the posterior cingulate cortex is involved in evaluative processes (Vogt 2009). The dual model of the cingulate cortex subdivision is a dominant model and is used in many current reports to refer to the cingulate cortex. However, recent functional neuroimaging and immunohistochemical studies have shown that even the dual model needs to be revised. For example, a recent study demonstrated that the rostral and caudal ACC display distinct patterns of receptor density (Palomero-Gallagher et al. 2008; Palomero-

Gallagher et al. 2009). The authors argued that the difference between rostral and caudal ACC is so pronounced that these two areas should be considered two distinct neuroanatomical divisions. Consequently, the concept of mid-cingulate cortex (MCC) has emerged (Vogt 2009). It has been suggested that the MCC includes the cingulate motor areas and is involved in evaluation of feedback and reward (Procyk et al. 2016).

In humans, the ACC includes the areas 24c, 24, 25, 32 and 33 (Vogt 2009) and the MCC includes the cytoarchitectonic areas 24a' , 24b' , 24c' , 24d, 33' , and 32' (Palomero-Gallagher et al. 2008; Vogt et al. 1995). Monkeys and humans have similar ACC subdivisions. However, area 32 in humans is larger and more elaborated (Vogt 2009). Furthermore, area 24 in humans is larger and expanded more than in monkeys. With regards to the MCC, the major difference between humans and monkeys is the absence of area 32' and ectocollosal divisions of area 33' in monkeys. The absence of a paracingulate sulcus in monkeys is the gross neuroanatomical difference between monkeys and humans.

### ***1.1.3. ACC connectivity:***

The ACC displays extensive connectivity with cortical and subcortical areas. It has been shown that ACC has strong functional connectivity with anterior insula (Neubert et al. 2015). The other cortical area with dense reciprocal connectivity with the ACC is the lateral prefrontal cortex. Bates and Goldman-Rakic have shown that cingulate motor areas are reciprocally connected with areas 8a, 11, and 46 in the prefrontal cortex (Bates and Goldman-Rakic 1993). In another anatomical tracing study, Wang and colleagues found areas within the ACC with direct projection to the frontal eye fields (Figure 1.1). These findings support the notion that ACC is involved in the integration of cognitive

functions with sensori-motor commands (Naito et al. 2000). The findings from anatomical tracing studies are also in line with results from resting-state functional connectivity, which will be discussed in section 1.2.5.1 below; e.g. see (Hutchison et al. 2012).

#### ***1.1.4. ACC functions:***

The ACC has been described as one of the prefrontal areas exerting top-down control over other brain regions (Silvetti et al. 2014). Some of the functions that the ACC has been suggested to be involved in include conflict monitoring, reward monitoring, performance monitoring, and working memory (Brignani et al. 2010). Furthermore, the ACC has been shown to have motor as well as emotional and motivational functions (Silvetti et al. 2014). Thus, there are a multitude of sensori-motor and cognitive functions that have been attributed to the ACC. Some of these functions, and also the models that have been developed in recent years to describe the ACC role in cognitive control, will be briefly discussed next.

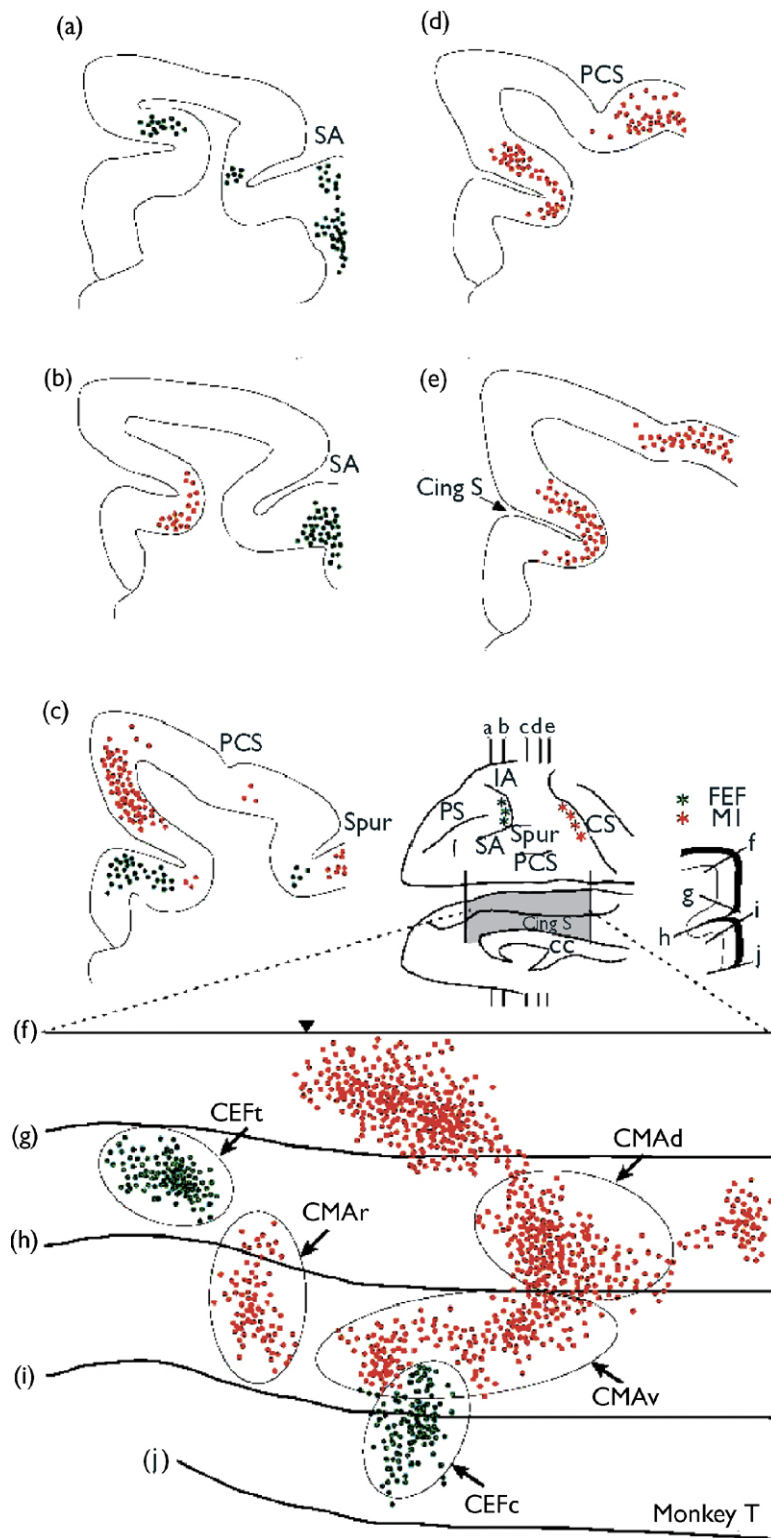


**Figure 1.1. Retrogradely labeling of cells in coronal sections (Top panel), and depiction of labeled cells on the medial hemispheric wall (Bottom panel).**

Cortical maps inset in the middle: Surface view of the right hemisphere showing the location of cortical injection sites (asterisks), and rostrocaudal levels of coronal sections (a-e) indicated by lines labeled with a to e. The letters f-j in the schematic section (to the right of the cortical map) correspond to f-j in the unfolded map at the bottom. In coronal sections and in an unfolded map, each dot represents 2-5 labeled cells. Regions surrounded by elliptical lines indicate approximate territories projecting to the forelimb area of MI and FEF. Arrowhead in the unfolded map indicates the caudal end of arcuate sulcus. Red dots, FB-labeled cells; green dots, DY-labeled cells. SA, superior limb of arcuate sulcus; IA, inferior limb of arcuate sulcus; Spur, spur of arcuate sulcus; PCS, precentral sulcus; CS, central sulcus; ARC, arcuate sulcus; PS, principle sulcus; Cing S, cingulate sulcus; CC, corpus callosum; CMAR, rostral cingulate motor area; CMAd, dorsal cingulate motor area; CMAv, ventral cingulate motor area; CEFr, rostral cingulate eye field; CEFc, caudal cingulate eye field.

With permission from (Wang et al. 2004).



#### ***1.1.4.1. ACC and motor functions:***

The ACC displays a variety of motor properties. Electrical micro-stimulation of the ACC results in complex movements of the mouth and forelimbs in macaque monkeys (Luppino et al. 1991). It has been shown that the eye and face movement-related activity in cingulate cortex is more prevalent in rostral cingulate cortex, whereas forelimb movement-related activity is most commonly observed in caudal cingulate cortex (Procyk et al. 2016). Furthermore, micro-stimulation of the monkey ACC can elicit vocalizations together with autonomic emotional motor responses (Muller-Preuss et al. 1980; Paus 2001). The involvement of ACC in vocalizations has also been observed in other mammals, e.g., the elicited vocalizations in bats exhibited a tonotopic organization within the ACC with a distinct frequency map, similar to somatotopic pattern of the motor functions (Gooler and O'Neill 1987). Yet, micro-stimulation of the human ACC does not result in vocalizations (Devinsky et al. 1995). Indeed, the ACC motor map in humans is organized in a caudal-to-rostral gradient, with the highest density of neurons with motor and premotor activities located in the caudal ACC (Dum and Strick 2002). The caudal ACC in this map corresponds with areas ventral to the supplementary motor area.

It has also been suggested that the ACC is involved in the control of saccadic eye movements (Kennerley and Wallis 2009; Wang et al. 2004). Indeed, Wang and colleagues have shown that there are areas within the ACC with direct projections to the frontal eye fields (FEF) as shown in Figure 1.1 (Wang et al. 2004). They named these areas the cingulate eye fields. However, the activity of ACC neurons in these “cingulate eye fields” has yet to be characterized.

According to the above mentioned studies, it can be concluded that motor and cognitive signals are represented simultaneously in the ACC. Paus has argued that the presence of motor activity in combination with the cognitive control function within the ACC serves as an advantage to transform goals and intentions into actions (Paus 2001).

#### ***1.1.4.2. ACC and the limbic system:***

The ACC has been classically considered to be part of the limbic system (Papez 1995). It has been shown that it has strong anatomical connections with the hippocampus through the parahippocampal gyrus (Nieuwenhuys et al. 1981; Silvetti et al. 2014). Electrical micro-stimulation of the ACC could evoke motivational and emotional responses (Parvizi et al. 2013). In the study conducted by Parvizi et al., it was shown that stimulation of the ACC triggered expectations of impending challenge coupled with a “will to persevere” (Parvizi et al. 2013). Correspondingly, there have been studies showing that ACC micro-stimulation leads to autonomic responses such as changes in blood pressure, heart rate, and penile erection (Devinsky et al. 1995; Parvizi et al. 2013). The visceral and autonomic functions of the ACC follow a rostro-caudal gradient with rostral ACC possessing higher levels of autonomic functions (Dum and Strick 2002). Finally, the ACC receives nociceptive projections from thalamus (Vogt et al. 1979).

Similar to motor functions of the ACC, the autonomic and motivational responses in the ACC are prominently linked to the cognitive demands of the tasks (Critchley and Mathias 2003; Gabriel et al. 1991) and therefore, ACC could be considered as an area that integrates these various functions.

#### ***1.1.4.3. ACC and conflict monitoring:***

One of the key capabilities of humans and non-human primates is their ability to effectively adjust their behavior in response to a wide variety of behavioral challenges they encounter. This becomes more important when the challenges include choosing between competing stimuli or suppression of a prepotent response. The first steps in processing and responding to these challenging situations are the timely detection of conflict and subsequent allocation of adequate cognitive resources to overcome the challenges imposed by these conflicting situations. It is widely believed that the ACC provides the main neural substrates for conflict detection (Carter and van Veen 2007). Some of the earlier evidence for its involvement in conflict monitoring came from experiments using the Stroop task (Stroop 1935); for a review see (MacLeod and MacDonald 2000). In the classic Stroop task, the subjects name the color in which the words are presented. It has been observed that subjects respond faster when the name of the color matches the word itself (congruent trials), whereas the response time is significantly longer in trials when words refer to different colors (incongruent trials) (Botvinick et al. 2004). It has been demonstrated that ACC is activated when subjects perform incongruent trials of the Stroop task (Botvinick et al. 2004; MacLeod and MacDonald 2000). Moreover, the ACC is involved in a variety of other cognitive tasks where a prepotent response has to be suppressed in favor of a task-relevant behavior (Braver et al. 2001; Paus et al. 1993). It has been suggested that ACC activation in high conflict trials recruits more cognitive resources to perform the desired task. This suggestion has been supported in an experiment where there was a smaller interference effect (shorter reaction time) in incongruent trials following a high ACC activation in the

preceding trials (Kerns et al. 2004). In the same study, it has been observed that dorso-lateral prefrontal cortex (dl-PFC) is activated following strong activation of the ACC. This finding supports a conflict-monitoring role for the ACC according to which the ACC detects conflict and recruits the dl-PFC to exert additional top-down control to successfully perform the tasks.

The proposal for a conflict monitoring role of the ACC originates mainly from human neuroimaging and electrophysiological studies (Herrmann et al. 2004; Kerns et al. 2004); for review articles see (Beldzik et al. 2015; Botvinick et al. 2004; Cole et al. 2009). However, early single neuron recording experiments in monkeys failed to demonstrate such a role for ACC in non-human primates (Ito et al. 2003; Johnston et al. 2007). Similarly, single unit recordings in humans did not provide convincing support in favor of the presence of conflict-related signal in the ACC (Davis et al. 2005; Sheth et al. 2012). Indeed, these studies proposed a performance monitoring role or a more general top-down role for the ACC rather than conflict monitoring (Hayden et al. 2011; Ito et al. 2003; Johnston et al. 2007). A great deal of effort has been made to describe the discrepancy between results from human studies showing a conflict-monitoring role for ACC with studies that failed to replicate these results. Some researchers suggested that the ACC in the non-human primates might not be the homologous area for human ACC and there are fundamental neuroanatomical differences between the human and monkey ACC (Cole et al. 2009). Other studies pointed towards methodological differences between the experiments conducted in humans and monkeys. For instance, most of the monkey single unit studies that failed to find conflict-monitoring signal in the ACC used eye movement tasks (Ito et al. 2003; Johnston et al. 2007) and therefore, it is difficult to

generalize the findings from the oculomotor tasks to other motor systems. Furthermore, these studies used go/no-go or task-switching paradigms that might not be truly equivalent to the Stroop task. In a recent study, the investigators employed a Stroop-like task, which induced conflict both at the stimulus level and response level (Michelet et al. 2016). The authors were able to demonstrate conflict-related signal in the ACC and provided evidence that the ACC in humans and non-human primates could be homologous areas.

So far I have discussed the ACC's role in conflict monitoring. There are also several studies suggesting a performance monitoring role for the ACC. Below, I will briefly review some of these studies.

#### ***1.1.4.4. ACC and performance monitoring:***

Numerous models have been proposed with regards to the dynamics of optimized control of behavior to obtain favorable outcomes. According to the Actor-Critic models, the critic predicts the reward and expected outcome based on the actions performed and information obtained from the environment. This estimated reward is subsequently compared with the actual reward obtained. Any unexpected discrepancy between the expected and actual outcomes triggers a signal used by the Actor to adjust the subsequent behavior and maximize the favorable outcome (Montague et al. 2004; Procyk et al. 2008). The involvement of the ACC in monitoring the behavioral outcomes and valuating the actions is ubiquitous in the cognitive control literature, and performance monitoring signals have been documented in the ACC (Carter and van Veen 2007; Ito et al. 2003; Quilodran et al. 2008). In this context, ACC could be perceived as the "Critic" component of the Actor-Critic model. It has been suggested that the ACC together with

orbito-frontal cortex sends performance monitoring-related signals to the locus coeruleus (Aston-Jones and Cohen 2005). The locus coeruleus subsequently modulates the activity of lateral prefrontal cortex neurons via adrenergic projections to influence the animal's behavior (Aston-Jones and Cohen 2005). Furthermore, the ACC has dopaminergic connections to mesencephalic areas such as the ventral tegmental area (Divac et al. 1978). These connections might mediate the sensation of reward and reinforce the behavior following the correct behavioral performance (Watanabe 1990).

ACC and dl-PFC work in concert to provide efficient control of behavior. In a study previously conducted in our lab, it has been shown that the activity of ACC neurons increase in the first trials of a block in a task-switching paradigm (Johnston et al. 2007). In each block, the task rule switched without any previous cue to the monkey and the only way the monkey notices the rule-change is by making repeated performance errors. It was suggested that ACC detects the performance errors and participates in cognitive control in the first trials following the task switch. Thereafter, dl-PFC neurons increase their activity to provide the necessary control signals and maintain the new task rule to maximize the reward (Johnston et al. 2007). The dense reciprocal connectivity between ACC and PFC supports the notion that these areas act in concert to control behavior (Bates and Goldman-Rakic 1993; Paus et al. 2001).

The role of ACC in performance monitoring can be explained not only by detection of errors but also by the detection of unexpected reward and positive feedback (Amiez et al. 2006; Toda et al. 2012). It has been shown that the firing rate of ACC neurons is modulated based on the amount of reward obtained by the monkeys (Amiez et al. 2006). In another similar study, Procyk and colleagues have shown that ACC activity

reflects the representations of expected reward values in sequential behaviors as well as the negative and positive feedbacks used in adapting such behaviors (Procyk et al. 2000). The ultimate goal of detecting reward or any other sort of feedback could be realized in the context of influencing the actions to produce the maximized favorable outcomes. ACC could play an ideal role in this respect because it could integrate the reward-related activity into the motor commands due to the simultaneous presence of reward and motor-related signals in the ACC. In fact, it has been shown that the spatial selectivity of ACC neurons can be modulated by reward value (Kennerley and Wallis 2009).

Shenhav and colleagues have recently proposed a model of the “expected value of control (EVC)” (Shenhav et al. 2013). According to this model, three factors should act in concert to produce the most favorable outcome. First, the current state of the organism should be determined and the expected outcomes of the behavioral alternatives be estimated. The conflict and/or performance monitoring functions of the ACC fit this component of the EVC model. Second, the amount of control signal required to perform each alternative should be evaluated. Further, the system should integrate the expected value of the behavioral alternatives in the selection process. Indeed, it has been shown that the value signals and task-selective signals are simultaneously represented in ACC neuronal activity (Hayden and Platt 2010; Kaping et al. 2011). Third, the final decision should be made not only based on the expected value of the action but also the cost of the control required to perform a certain action. It has been shown that the ACC is also involved in computing the cost of control, i.e. in computing the estimated amount of cognitive effort an organism requires to correctly perform a task (Magno et al. 2006; McGuire and Botvinick 2010). The EVC model can explain the apparently diverse

neuronal activities observed in the ACC and these processes could be conducted in parallel (Rushworth et al. 2012).

### ***1.2. SACCADDES AND THE OCULOMOTOR SYSTEM:***

Saccades are the fast eye movements that align the fovea on the objects of interest in the environment (Gilchrist 2011). The oculomotor system consists of a number of cortical and subcortical areas that control the performance of saccades in response to behavioral demands. This system is the best-studied motor system in primates due to the simplicity of tracking eye movements and advancements in the neuronal recording techniques (Johnston and Everling 2008). Furthermore, there are only 12 extra-ocular muscles in both eyes (Gray and Russo 2008) that generate saccades, which simplifies the study of saccade system. Moreover, the saccade generators are located in the brainstem (Hepp and Henn 1983) and electrophysiological recordings are easier to perform in brainstem than in spinal cord. The saccade network is comprised of a number of cortical and subcortical areas that display functional and structural connectivity. Some of the cortical areas involved in saccade generation and saccade control are the frontal eye fields (FEF), lateral intraparietal area (LIP), and dorsolateral prefrontal cortex (Bruce and Goldberg 1985; Funahashi et al. 1991; Shibutani et al. 1984). FEF is more directly involved in saccade generation whereas more anterior prefrontal structures are mainly involved in saccade control (Bruce et al. 1985; Funahashi et al. 1991). These areas send neuronal projections to the midbrain structure superior colliculus (SC) in which the neurons have prominent saccade-related activity (Selemon and Goldman-Rakic 1988; 1985). The SC neurons in turn send direct projections to the brainstem saccade generators to initiate saccades (Munoz et al. 2000; Scudder et al. 2002; Sparks 2002).



As mentioned above, the oculomotor network consists of cortical and subcortical areas that are primarily involved in saccade generation. Other cortical areas, in particular the prefrontal cortex, are involved in the top-down modulation of the saccadic eye movements. Depending on the goals of a research project, different components of the oculomotor network can be explored including the higher cognitive functions. For instance, saccades and oculomotor system have been used to investigate attention, reward, and decision making (Kennerley et al. 2006; Moore and Armstrong 2003; Sato and Schall 2003; Sugrue et al. 2004). Also, saccadic eye movements have been used to identify the cognitive impairments in patients with psychiatric and neurologic impairments (Broerse et al. 2001; Leigh and Zee 2006). Patients with schizophrenia exhibit impairments in the anti-saccade task performance that requires the subjects to perform a saccade to the opposite location of a peripheral visual stimulus (Broerse et al. 2001; Fukushima et al. 1990). The memory-guided saccade task and anti-saccade task will be discussed in further detail in below.

### ***1.2.1. Frontal eye fields:***

FEF is located in the rostral bank of the arcuate sulcus in nonhuman primates. There is also an analogous FEF in human frontal cortex located in the junction of the superior frontal sulcus and superior precentral sulcus (Paus 1996; Schall 2015). Early studies have shown that micro-stimulation of the FEF with very low threshold currents ( $<50 \mu\text{Amp}$ ) can trigger saccades (Bruce et al. 1985). The amplitude of the electrically evoked saccades follows a certain anatomical pattern. Stimulation of the more medial FEF sites elicits saccades with larger amplitude and lateral FEF sites give rise to smaller amplitude saccades (Bruce et al. 1985). Furthermore, the medial and lateral FEF have distinct

anatomical connectivity with parietal and temporal areas. Schall and colleagues demonstrated that the medial FEF has structural connectivity with areas in the parietal cortex and dorsal visual stream whereas the lateral FEF has connectivity with temporal areas and ventral stream of visual processing as shown in Figure 1.2 (Schall et al. 1995). Furthermore, the same study demonstrated that lateral FEF receives inputs from retinotopic areas with foveal representations whereas medial FEF receives projections from peripheral representations of the retinotopically organized cortical areas (Schall et al. 1995; Ungerleider et al. 2008).

The dorsal stream of visual processing is responsible for spatial vision and visually-guided motor responses, and the major role of the ventral stream of visual processing is object perception and identification (Goodale and Milner 1992). The response field of visual neurons in the FEF follows a similar pattern as for saccades, i.e. the peripheral visual field is represented in the medial FEF and central visual field in the more lateral FEF (Suzuki and Azuma 1983). In this regard, it can be postulated that the connectivity between medial FEF and the dorsal visual stream is mainly involved in the motor planning of the eye movements; because medial FEF generates a larger range of eye movements. The lateral FEF, which generates smaller saccades, is mainly connected with the ventral visual stream to aid in a more detailed and meticulous examination of the objects of interest in the environment. A more detailed description of the functional connectivity of the FEF is discussed in the second chapter. Apart from its prominent role in saccade generation, FEF is also involved in a multitude of actions such as visual search, target selection, and transformation of visual signals to saccade commands, which will be briefly discussed in below.

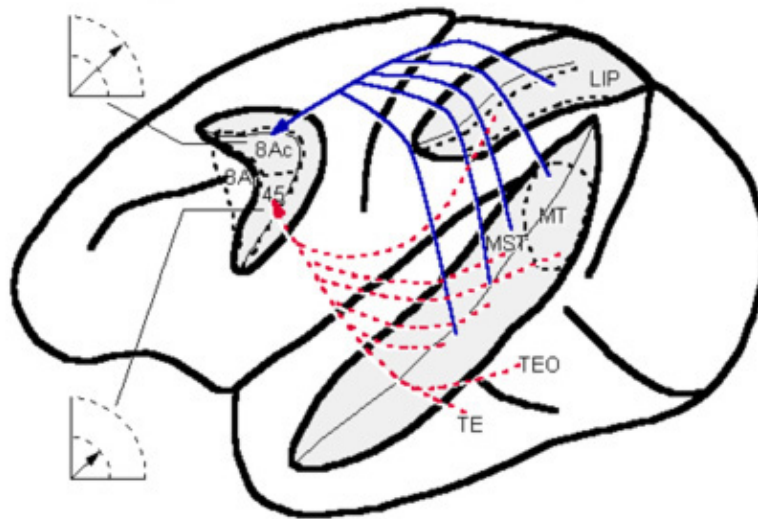


**Figure 1.2. Summary of major connections of FEF with visual cortical areas.**

The location of specific cortical areas is indicated on a dorsolateral view of the macaque brain. The relative amplitude of saccades represented by ventral FEF (area 45) and dorsal FEF (area 8Ac) is indicated. The solid blue lines indicate major projections to area 8Ac, and the dashed red lines represent major projections to area 45.

Modified with permission from (Schall et al. 1995)

### ***1.2.2. Frontal eye fields and visual functions:***

As mentioned above, FEF has significant connectivity with cortical visual areas and there is a plenty of evidence suggesting the presence of visual signals in the FEF (Bruce and Goldberg 1985). Some neurons in the FEF respond exclusively to the visual stimuli appearing in their response field (visual neurons) and some FEF neurons increase their activity both in response to visual stimuli and saccades (visuo-movement neurons) (Bruce and Goldberg 1985). Therefore, the FEF is considered to be a visual and motor area.

The visual neurons in the FEF do not exhibit feature selectivity unless under restricted training conditions (Peng et al. 2008). However, the presence of both visual and saccade-related signals in the FEF makes it an ideal candidate for transformation of the visual signals into saccade (and/or gaze) commands. In fact, it has been shown that the FEF performs a preliminary visual-motor transformation and further transformation into motor frames occurs in downstream subcortical areas (Sajad et al. 2015). Moreover, it was shown that FEF is also involved in memory to motor transformation, although this transformation is imperfect (Sajad et al. 2016). Additionally, the FEF has been implicated in guiding saccades to moving objects through modulation of the pre-saccadic activity in relation to target velocity (Cassanello et al. 2008). All this evidence indicates that FEF receives information related to visual stimuli, processes this information, and relays it to other areas for further processing.

FEF is also involved in top-down control of visual processing. Several studies have shown that FEF is involved in visual search paradigms in which the subjects have to

discriminate a visual target among distractors (Gregoriou et al. 2012; Schall 2015; Zhou and Desimone 2011). In visual search paradigms, the visual neurons in the FEF primarily respond to the array of visual stimuli in a non-selective manner. However, prior to the initiation of the saccade towards the target stimulus, these neurons display increased activity when the target falls into their response field compared to the distractors (Thompson et al. 1996; Thompson and Schall 2000). The target selection process in the FEF involves spike-field coupling mechanisms as well as spike timing competition and cooperation (Cohen et al. 2010; Gregoriou et al. 2012). A causal effect of FEF in visual search has been proved in studies where the target selection was impaired following the inactivation of the FEF (Wardak et al. 2006).

Further evidence with regards to the top-down control role of the FEF comes from the studies of covert spatial attention. Covert spatial attention occurs when humans or non-human primates attend to an object or a stimulus in the peripheral visual field without shifting their gaze towards that stimulus (Posner 1980). According to the premotor theory of attention, covert spatial attention originates from latent eye movement activity despite absence of an apparent saccade or eye movements (Moore and Armstrong 2003; Rizzolatti et al. 1987). However, Thompson and colleagues used a spatial attention task that did not require monkeys to preform a subsequent saccade towards the location of the covertly attended target (Thompson et al. 2005). The authors concluded that the activity of the visual neurons that signal spatial attention was independent of the saccade command signals (Thompson et al. 2005). In a separate study, it was shown that electrical micro-stimulation of the FEF by currents below the threshold needed to elicit saccades can enhance the activity of the visual neurons in area V4 (Moore and Armstrong 2003).

Interestingly, this enhancement was observed when the response fields of the FEF and V4 sites matched. In the experiments in which the response fields of the FEF and V4 sites were different, the FEF stimulation led to suppression of the activity of the V4 neurons (Moore and Armstrong 2003). This evidence suggests that although FEF can be considered a motor area with a prominent saccade generation role, it also exerts influence on other cortical and subcortical areas.

As noted above, there are multiple cortical and subcortical areas that are involved in saccade control. FEF is a saccade generating area with connectivity to other cortical and subcortical areas. In this project, I was interested in the mechanisms by which higher cortical areas exert control on generation of saccades. I utilized a memory-guided saccade task and pro-/anti-saccade task to study cognitive saccade control that will be discussed in below.

### ***1.2.3. Memory-guided saccade task:***

This task is used to examine the short-term memory and/or working memory (Johnston and Everling 2008). In this task, the subject fixates at a central fixation point for a period of time, then a target stimulus is presented briefly in a peripheral location. However, the subject is instructed to maintain fixation during the target stimulus presentation and during the subsequent delay period. The delay period can vary between a few hundred milliseconds to a few seconds depending on the study design (Hutton 2008). The offset of the central fixation point signals the subject to perform a saccade towards the remembered target location. Different brain areas have been shown to be involved in performance of the memory-guided saccade task. In this respect, single neurons in the dl-PFC increase their activity in the delay period of the memory-guided saccade task

(Funahashi et al. 1991; 1990). The activity of dl-PFC neurons exhibit spatial tuning, i.e., the neurons' firing rate is highest when they perform a saccade towards a certain target location which is generally biased towards the contralateral space (Funahashi et al. 1991). Also, the direction towards which the neurons exhibit maximal visual response appears to correspond with that of the delay and saccadic epochs (Funahashi et al. 1989; 1991; 1990). Similar neuronal responses across different epochs of the memory-guided saccade task have been observed in other brain areas such as FEF, lateral intraparietal area (LIP) and superior colliculus (SC) (Colby et al. 1996; Pare and Wurtz 1997; Schall 2015). However, there are slight differences in the activation pattern of different brain areas. For instance, the percentage of neurons with visual response is higher in LIP than dl-PFC and the opposite is true for the saccadic activity (Johnston and Everling 2008). The neuronal signals related to different epochs of memory-guided saccade task is shown to be sent from FEF (Sommer and Wurtz 2000; 2001), LIP (Pare and Wurtz 1997), and dl-PFC (Johnston and Everling 2006) to SC. Therefore, it can be concluded that coordinated neuronal activity in these areas is necessary for correct performance of the memory-guided saccade task. Furthermore, other areas might also be involved in performance on this task. For example a network of fronto-parietal areas was activated during memory-guided saccade performance (Brown et al. 2004). Further studies could reveal more information in this regard.

#### ***1.2.4. Pro-/Anti-saccade task:***

The pro-saccade task is interchangeably called the visually-guided saccade task. In this task, a central fixation point appears for a certain period and subsequently the target stimulus is displayed in a peripheral location. The subjects are required to perform a

saccade towards the target stimulus (Hutton 2008). There are different variations of the pro-saccade task. In the step task, the onset of the target stimulus and offset of the central fixation point occur simultaneously, whereas in the overlap task, the central fixation point remains illuminated. In the gap task, the central fixation point disappears before the target stimulus is presented (Hutton 2008). Saccadic reaction time is significantly lower in gap tasks and higher in overlap tasks compared to step trials (Reuter-Lorenz et al. 1991). This finding is generally referred to as the “gap effect” (Saslow 1967). One explanation for the gap effect is that in gap trials, the attention is disengaged from the fixation point before the appearance of the target stimulus and therefore, there is less time needed to re-allocate the attention towards the stimulus, although this notion has been challenged in some studies (Dorris et al. 1997). The pro-saccade task elicits a relatively automatic and prepotent response and pro-saccade performance does not appear to employ a great deal of cognitive resources. The anti-saccade task can address this shortcoming of the pro-saccade task.

The anti-saccade task was first introduced by Peter Hallett (Hallett 1978). This task can probe the top-down control. Similar to pro-saccades, the participants fixate at a central fixation point and then a peripheral target stimulus appears. In the anti-saccade task, the participants are instructed to look towards the mirror location of the target stimulus on the screen (Munoz and Everling 2004). In order to correctly perform this task, the participants have to suppress an automatic saccade towards the stimulus, transform the prepotent saccade vector (pro-saccade) to the opposite movement vector (anti-saccade), and generate a voluntary saccade command (Munoz and Everling 2004). A variety of brain areas are suggested to be involved in anti-saccade performance



including the dl-PFC, FEF, SEF, and SC (Munoz and Everling 2004). For instance, single neurons with saccade related activity in FEF and SC decreased their firing rate before the initiation of anti-saccades whereas fixation neurons in these areas increased their activity before anti-saccades (Everling et al. 1999). The source of inhibitory signal that leads to decreased firing of the saccadic neurons in the FEF and SC appears to be in dl-PFC and the extensive projections from the dl-PFC to SC (Leichnetz et al. 1981) and FEF (Selemon and Goldman-Rakic 1988) support this notion. However, a study conducted in our lab showed that dl-PFC does not appear to suppress the saccade-related activity of SC neurons (Everling and Johnston 2013; Johnston et al. 2014). Other possible sources of the inhibitory signal to the FEF and SC could be the supplementary eye fields and substantia nigra pars reticulata (Munoz and Everling 2004).

The signal for saccade vector inversion in the anti-saccade task might originate in the lateral intraparietal area (LIP) (Munoz and Everling 2004; Zhang and Barash 2004). Certain neurons in area LIP were identified that became active when the saccade vector but not the visual stimulus were aligned on their response field (Zhang and Barash 2000). However, the response latency of these neurons was about 50 ms following the target stimulus onset that corresponds with the latency for visual neurons in the LIP. The authors argued that the presence of this response could be indicative of a re-mapped visual response that could contribute to the saccade vector inversion in anti-saccade task (Zhang and Barash 2000; 2004).

Other brain areas might also be involved in the response inhibition and saccade vector inversion. ACC is a candidate in this regard because of its role in cognitive control

as well as motor functions. Further experiments are needed to elucidate the role of ACC in anti-saccade performance.

#### ***1.2.5. Cingulo-Frontal (ACC-FEF) interaction in saccade tasks:***

It has been shown time and time again that prefrontal cortex is involved in top-down control of behavior (Fuster 2008). The coordinated activity between different sub-regions in the prefrontal cortex is a pre-requisite to correctly perform the behavioral tasks. In this context, co-activation of the ACC and FEF has been observed in functional imaging studies when subjects performed oculomotor tasks (Brown et al. 2004; Ford et al. 2009). It has also been shown that ACC and FEF are more activated when monkeys performed blocks of anti-saccades than blocks of pro-saccades (Ford et al. 2009). In another report, the activity in FEF and ACC was increased following a switch in task rule (Lee et al. 2011). It was shown that the change in task rule introduces more errors in task performance and this could trigger the activation of ACC and FEF. These findings are consistent with the reports from our lab showing that ACC neurons increased their activity following the switch trials (Johnston et al. 2007). The increased ACC activity could provide top-down control over FEF in task-switching paradigms (Johnston et al. 2007; Lee et al. 2011). In another study, it was shown that ACC was activated in the delay period of a memory-guided saccade task (Brignani et al. 2010). The ACC remained activated until the trials ended and FEF was co-activated with ACC during the peri-saccadic epoch (Brignani et al. 2010). The authors argued that ACC provided attentive control and conflict monitoring to correctly select the appropriate response.

Alternatively, ACC could inhibit the saccades during the delay period of the memory-guided saccade paradigm (Brignani et al. 2010).

Similar ACC-FEF co-activation has been observed in other paradigms (Beldzik et al. 2015; Burrell et al. 2012; Jamadar et al. 2015; Pierce and McDowell 2016; Richards 2013) and this co-activation could serve a functional role in the correct performance of the tasks. The mechanisms by which the ACC and FEF communicate remain to be clarified.

#### ***1.2.5.1 Resting-state connectivity of the ACC:***

The functional connectivity of the ACC has been the subject of a number of resting-state fMRI studies. In a recent macaque resting-state fMRI study in our lab, it has been shown that ACC connectivity displays a distinct rostro-caudal pattern (Hutchison et al. 2012). Rostral ACC regions were mainly connected to prefrontal areas suggestive of involvement in cognitive processes. On the other hand, caudal ACC areas were connected to premotor and primary sensori-motor areas (Hutchison et al. 2012). Margulies and colleagues have reported transition zones within the ACC between the rostral and caudal regions that displayed functional connectivity with dorsal and ventral brain regions (Margulies et al. 2007). The authors hypothesized that these “transition zones” serve the integration of affective and cognitive signals needed to perform the conflict and performance monitoring functions of the ACC (Margulies et al. 2007).

Hutchison et al. (2012) have observed that distinct ACC subregions have connectivity with certain functional networks. In this respect, a caudal ACC cluster across dorsal, ventral, and fundus of the cingulate sulcus displayed connectivity with pre- and post-central sulcus as well as supramarginal gyrus. Therefore, this ACC cluster was

considered to be connected to the somatomotor network (Hutchison et al. 2012). Another ACC area rostral to the previously mentioned cluster, displayed connectivity mainly with the lateral intraparietal area, FEF and dl-PFC, and thus this area was designated as the attention-orientation cluster. More anteriorly, the ACC areas exhibited connectivity with other prefrontal areas suggesting that these areas were part of the executive control network (Hutchison et al. 2012). Finally, the most rostral ACC areas formed a cluster with strong connectivity to limbic regions such as hippocampal and parahippocampal areas, insular cortex, amygdala, and rostral caudate nucleus (Hutchison et al. 2012). These ACC functional connectivity networks were outstandingly in concert with the anatomical connectivity patterns of the ACC as well as electrophysiological and neuroimaging results (Barbas et al. 1999; Dum and Strick 2002; Vogt and Pandya 1987). For instance, as mentioned above, the limbic and autonomic functions of the ACC follow a rostro-caudal gradient with higher limbic activity in the rostral ACC areas (Dum and Strick 2002).

It should be mentioned that cortical parcellation efforts using resting-state fMRI functional connectivity (as in Hutchison et al. 2012) have some challenges. One challenge could be related to the limited sampling rate of functional images, and the relatively small data points collected for resting-state fMRI parcellation analyses (Cole et al. 2010). Furthermore, occasionally there is an overlap between the boundaries of cortical parcellations and exact boundaries cannot be defined. Therefore, it is important to compare the resting-state functional connectivity results with the existing anatomical connectivity literature (Seeley et al. 2007).

#### ***1.2.5.2. Resting-state fMRI:***

Our brain uses ~20% of the total body's energy, although it constitutes only 2% of the body weight. This energy expenditure occurs even when the subjects do not perform any tasks and essentially are at rest. Furthermore, the brain energy expenditure increases only by 2-5% of the baseline brain activity, when the subjects actively perform tasks. Therefore, a significant aspect of the brain activity is not taken into consideration when only studying the brain activity in response to behavioral paradigms. Previously, the spontaneous fluctuations in the BOLD signal were attributed to the respiratory and cardiac activity and were considered to be the background "noise". However, Biswal et al. (1995) found that the brain areas that were originally activated in response to a hand movement task displayed highly correlated activity even at rest. The authors performed a low pass filter ( $< 0.08$  Hz) on the resting-state BOLD activity and this BOLD activity was correlated across bilateral sensori-motor areas. This was the seminal study that established the concept of functional connectivity through exploring the low frequency BOLD signal fluctuations at rest. Even further, the authors suggested that brain anatomical connectivity could be related to the functional connectivity acquired through resting-state fMRI.

Further studies used resting-state fMRI functional connectivity maps to identify resting-state networks (RSN) in the brain. One of the first reports in this regard was Vincent and colleagues' paper, in which the authors have shown that the correlated low frequency BOLD signal fluctuations in different brain networks persist even during light anesthesia (Vincent et al. 2007). The authors showed three networks (oculomotor, somatosensory, and visual) in the brain that displayed coherent spontaneous activity

despite deep anesthesia levels. Another interesting finding of this study was that the authors demonstrated that the functional connectivity maps derived from resting-state fMRI studies had substantial similarities to the maps acquired when subjects performed behavioral tasks. Interestingly, the anatomical connectivity maps obtained from tracer injections in the brain also exhibited a substantial overlap with functional connectivity maps as shown in Figure 1.3 below (Vincent et al. 2007). The authors concluded that these coherent spontaneous BOLD signal fluctuations could not solely represent the processing of ongoing cognitive tasks. Indeed, the authors suggested that the resting-state fMRI functional connectivity might reflect functional brain organizations that persist regardless of different levels of consciousness.

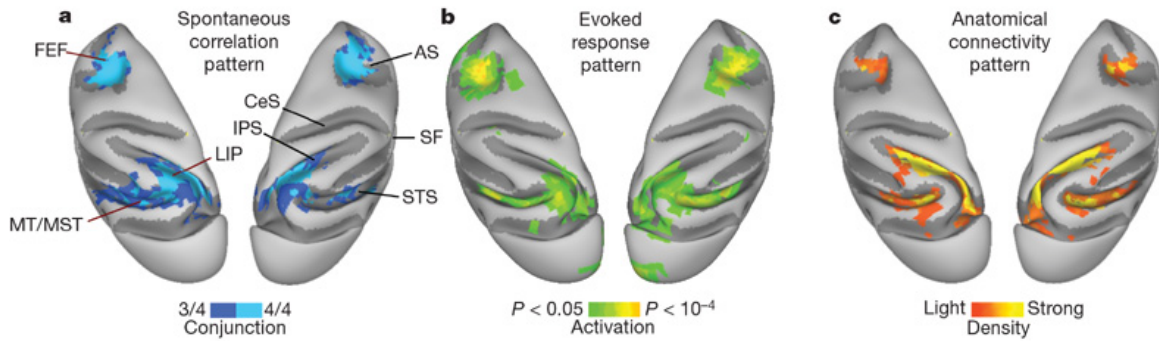


**Figure 1.3. Cortical patterns of coherent spontaneous BOLD fluctuations are similar to those of task-evoked responses and anatomical connectivity.** a, Conjunction map of BOLD correlations within the oculomotor system on dorsal views of the monkey atlas left and right hemisphere surfaces. Voxels significantly correlated with three (dark blue) or four (light blue) oculomotor ROIs are shown. b, Activation pattern evoked by performance of a saccadic eye movement task. c, Density of cells labelled by retrograde tracer injections into right LIP. The left hemisphere injection data are duplicated by reflection of the right hemisphere to facilitate visual comparison. Only regions that showed reproducible projections to LIP are shown. AS, arcuate sulcus; CeS, central sulcus; IPS, intraparietal sulcus; SF, sylvian fissure; STS, superior temporal sulcus.

With permission from (Vincent et al. 2007).

#### ***1.2.5.3. Analytic approaches for resting-state fMRI:***

So far I have described that spontaneous BOLD signal fluctuations at rest or even during anesthesia could provide valuable information about brain structure and function. This signifies the necessity of utilizing appropriate analytical tools to study resting-state brain functions using fMRI. Different analytical approaches have been developed to analyze the so-called resting-state fMRI data. The two most commonly used approaches are seed-based analyses, and principal component analysis.

The seed based analysis is probably the first method used to analyze the resting-state fMRI data (Biswal et al. 1995). In this method, a particular region of interest in the brain is selected, and then the BOLD signal time course of this area is extracted. Subsequently, the extracted time course is correlated with every other voxel in the brain generating the functional connectivity maps of the region of interest. Seed based analysis is not a data-driven method and the investigator should have an a priori knowledge of seed area (Lee et al. 2013). I have used the seed based analysis in my research paper that will be explained in chapter 2.

The next analytical approach that will be discussed here is independent component analysis (ICA). This method utilizes a data-driven approach with no previous assumption about the functional connectivity of the brain. The only condition of this method is that it assumes the data is composed of a number of independent components that are orthogonal to each other. However, it compels the investigator to identify, which components are RSNs and which ones are noise. Also, the investigator determines the optimal number of components in the ICA, although some efforts have been made to automate this process (Tohka et al. 2008). Despite the apparent difference in the seed



based and ICA, it has been shown that these two methods yield similar results in groups of healthy subjects (Rosazza et al. 2012).

So far, I have discussed the basic concepts of the resting-state fMRI and different approaches to data analysis. This technique has been used in a few clinical studies. Below, I will briefly review this literature.

#### ***1.2.5.4. Resting-state fMRI and clinical applications:***

Resting-state fMRI seems to be a good candidate for clinical applications because of a number of advantages. For instance, there is no need for the subjects to perform tasks. Thus, it can be used irrespective of the patients' cognitive capabilities. Moreover, it can be used in patients with altered levels of consciousness and even in anesthetized patients. However, there are some issues with the use of resting-state fMRI in patient populations. The main concerns regarding the use of resting-state fMRI are the test-retest reproducibility and inter-subject variability (Hagmann et al. 2010; Lee et al. 2013; Sporns and Honey 2013). Some studies have suggested that RSNs can be identified across recording sessions and different subjects, however, there could be some differences in certain loci in the brain across subjects (Biswal et al. 2010; Shehzad et al. 2009). Despite these disadvantages, resting-state fMRI is gaining attention as an imaging modality to diagnose psychiatric or neurologic conditions. Further advances in image acquisition techniques and improvements in image quality can ultimately help in the more widespread use of resting-state fMRI as a diagnostic modality. Some examples of the resting-state fMRI use in clinical applications will be discussed in below.

Resting-state fMRI has been previously used to identify patients with Alzheimer's disease. It was shown that Alzheimer's patients had significantly lower clustering

coefficients in the hippocampus (Supekar et al. 2008). Koch et al. also investigated the utility of resting-state fMRI in the diagnosis of Alzheimer's disease. They used a combination of ICA and seed-based analysis with regions of interest within the default mode network. Using a multivariate model, they achieved 97% accuracy in diagnosing Alzheimer's disease (Koch et al. 2012). Interestingly, a separate study found that the default mode network is important in the diagnosis of Alzheimer's disease (Dai et al. 2012). Resting-state fMRI has also been used to diagnose and differentiate other kinds of dementia such as fronto-temporal dementia (Zhou et al. 2010).

The other potential application of resting-state fMRI is the early diagnosis and management of psychiatric conditions such as schizophrenia and depression. In a number of studies, it has been suggested that schizophrenia is associated with abnormal functional connectivity in the default mode network (Karbasforoushan and Woodward 2012). However, the types of abnormalities reported were somewhat inconsistent, with some reporting increased and some decreased connectivity across the default mode network (Karbasforoushan and Woodward 2012). Furthermore, some studies have shown hypo-connectivity across frontal areas in schizophrenic patients (Woodward et al. 2011). Indeed, there is a great deal of inconsistency regarding resting-state functional connectivity fMRI characteristics of schizophrenia. This could be related to the fact that schizophrenia is a multi-factorial disorder with a multitude of cognitive and behavioral dysfunctions. Thus, the observed heterogeneity in the functional connectivity could be related to the degree of cognitive functioning and also, the subtype of the schizophrenia. In this respect a systematic review conducted by Sheffield and Barch (2016) could not identify a specific cognitive domain showing a particular pattern in the resting-state fMRI

function connectivity associated with certain cognitive abilities in schizophrenia (Sheffield and Barch 2016). The authors suggested that the observed functional connectivity abnormalities might contribute to a general cognitive dysfunction in schizophrenia rather than specific cognitive domains.

Similar efforts have been made to identify functional connectivity abnormalities associated with depression; for a review, see (Dutta et al. 2014). The default mode network was one of the networks extensively studied in depressive disorders. It has been shown that the functional connectivity across DMN networks increases in depressive disorders, e.g. see (Guo et al. 2013). Interestingly, (Li et al. 2013) reported that the increased functional connectivity in default mode network was normalized following the treatment with anti-depressant medications. Also, there are several papers investigating the functional connectivity of individual brain areas such as anterior and posterior cingulate cortex, orbito-frontal cortex, limbic structures and so on in depression (Dutta et al. 2014). This evidence suggests that the concept of functional connectivity has a valuable potential in diagnosis and management of many neurologic and psychiatric conditions.

### ***1.3. BRAIN RHYTHMS:***

Buildings, bridges, engines and many other systems in nature vibrate. The same is true for neuronal activity, and the oscillatory brain activity was observed since the very first experiment that recorded the electrical brain activity (Berger 1929). The question that arises here is whether these neuronal oscillations are just a byproduct of neural activity or whether they serve a functional role in information processing. It has been shown that even single neurons oscillate at certain frequencies and their activity pattern is dependent on the undergoing cognitive or sensori-motor processes (Hutcheon and Yarom 2000). Even further, neuronal oscillatory patterns during sleep were shown to be related to the prior experiences during the awake period (Buzsaki 1989). These reports were among the first studies suggesting the involvement of neuronal oscillations in information processing (Buzsaki and Draguhn 2004). A multitude of subsequent studies provided further support for this notion.

Neuronal populations in the brain oscillate across a range of frequency bands. These frequencies can be as low as 0.05 Hz, and up to 500 Hz or even higher (Buzsaki and Draguhn 2004; Gulyas and Freund 2015). The power density of the recorded electroencephalogram (EEG) or local field potentials (LFP) signals follows a  $1/f$  pattern (Buzsaki and Draguhn 2004). This means that the spectral power of low frequency neuronal oscillations is orders of magnitude higher than the power of high frequency oscillations. When the power of recorded EEG or LFP signal is depicted against the frequency, we observe a number of peaks at certain frequencies and this gives rise to the concept of different frequency bands (Buzsaki and Draguhn 2004). There are slight variations in the exact definition of each frequency band but generally delta frequencies

are between 0.5-3Hz, theta is between 3-9 Hz, alpha between 9-12 Hz, beta between 12-30 Hz, and gamma between 30-120 Hz (Buzsaki and Draguhn 2004; Liebe et al. 2012). There are also definitions for higher frequencies that are beyond the scope of this thesis. Each of these frequency bands is considered to be involved in certain aspects of information processing in the brain. Below, I will discuss the communication through coherence (CTC) hypothesis that suggests a functional role for the oscillatory brain activity in facilitation (or inhibition) of information transmission between neurons.

### ***1.3.1. Communication through coherence (CTC):***

The CTC hypothesis was first suggested by Pascal Fries (Fries 2005). The mainstay of the CTC hypothesis is that the neuronal synchronization across certain frequency bands affects neuronal communication (Fries 2005; 2015). A plethora of evidence has accumulated in recent years in support of the CTC hypothesis; for a review see (Fries 2015). According to CTC, the spike output and sensitivity to synaptic input can be synchronized with rhythmic excitation and inhibition cycles. The inputs that consistently arrive at the peak excitability window of the post-synaptic neuronal groups are more likely to trigger post-synaptic action potentials and this results in a higher degree of effective connectivity (Fries 2015). Therefore, in order to maintain a stronger effective connectivity, the pre- and post-synaptic neuronal groups should exhibit rhythmic synchronization or in other words they should exhibit “coherence”. On the other hand, the inputs that arrive at random phases of the post-synaptic excitability are less likely to trigger an action potential and there would be a lesser degree of effective connectivity (Figure 1.4).

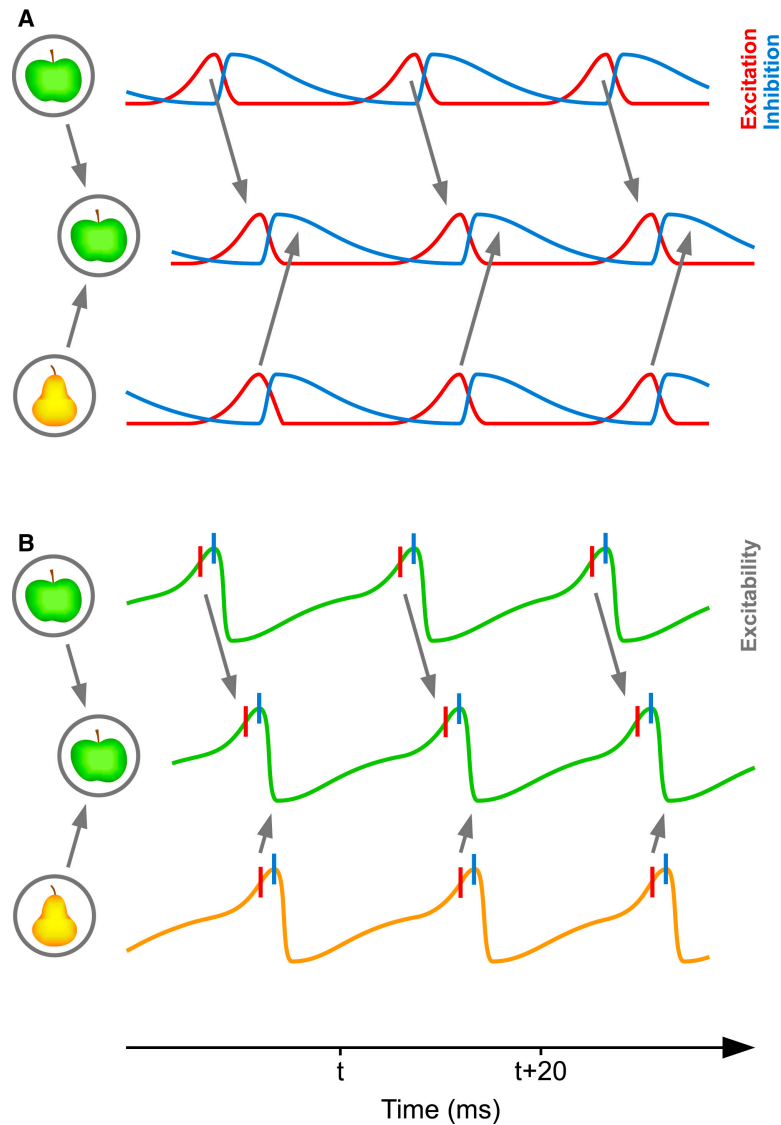


**Figure 1.4. Communication through Coherence**

(A) Two presynaptic neuronal groups in a lower visual area provide input to a postsynaptic neuronal group in a higher visual area. The lower groups represent two visual stimuli, an apple and a pear. In each neuronal group, network excitation (red) triggers network inhibition (blue), which inhibits the local network. When inhibition decays, excitation restarts the gamma cycle. The gamma rhythm of the apple-representing presynaptic group has entrained the gamma rhythm in the postsynaptic group. Thereby, the apple-representing pre-synaptic group can optimally transmit its representation, whereas the pear-representing presynaptic group cannot transmit its representation.

(B) A simplified illustration in which network excitation and inhibition are combined into network excitability. Red vertical lines indicate excitatory neuron spiking and blue vertical lines inhibitory neuron spiking.

With permission from (Fries 2015).

There is a time lapse for the action potential to travel from the soma to the axon ending and this latency depends on the distance between the soma and axon ending, the axon's myelination, and the axon's diameter. Neuronal groups at varying distances synchronize across different frequency bands based on the time latency of the action potentials to reach from one group to the other. Distant neuronal groups synchronize across lower frequencies (e.g., beta band) and adjacent neuronal groups synchronize across higher frequencies (e.g., gamma band) (Fries 2005). Furthermore, it has been suggested that synchronization across each frequency band has a certain functional role in information processing. For instance, visual stimuli induce synchronized gamma band activity in the primary visual cortex and this could influence the bottom-up stimulus salience (Bosman et al. 2012; Cannon et al. 2014). The role of theta and beta band synchronization in cognitive and sensori-motor processing will be discussed in more detail in below.

### ***1.3.2. Theta band:***

The theta frequency range is generally referred to as the frequencies between 3-9 Hz, however there is a slight variation between different references (Buzsaki and Draguhn 2004; Liebe et al. 2012). Involvement of theta frequency oscillations have been extensively studied in the rat hippocampus; for a review see (Buzsaki 2002). However, theta activity has been implicated in a variety of cognitive functions such as working memory, attention, and detecting the need for top-down control (Cavanagh and Frank 2014). Furthermore, theta band oscillations have been observed broadly across cortical areas in humans and monkeys, more specifically during the performance of higher cognitive functions (Cohen 2011; Raghavachari et al. 2006).

Theta band oscillatory activity has been robustly reported in frontal midline electrodes of EEG recordings (Cohen 2011). This frontal-midline theta (FM $\theta$ ) activity has been suggested as the primary constituent of the event-related potential (ERP) modulations related to functions such as response conflict monitoring, aversive feedback, and novelty detection (Cavanagh and Frank 2014). Different source estimation techniques and also invasive recordings in humans and monkeys have established that the ACC and/or MCC are the main generators of the FM $\theta$  activity (Cohen and Ranganath 2007; Womelsdorf et al. 2010a). The theta rhythmic activity across a variety of cognitively demanding tasks could provide a temporal template to organize the neuronal processes in the mid-frontal cortex in response to increased control demands (Cavanagh and Frank 2014). Furthermore, synchronized theta activity of different neuronal populations in distant areas creates a time frame, so that information can be effectively transferred (Womelsdorf et al. 2010a). In this respect, the action potentials that arrive at a brain region in a theta phase with peak excitability are more likely to be effective and therefore, single neurons at distant areas synchronize their activity with the theta rhythm. This theta band spike-field coherence has been previously reported between prefrontal and visual areas (Liebe et al. 2012). Furthermore, it has been shown that there is a correlation between the strength of white matter connectivity and theta band synchronization between various brain areas (Cohen 2011).

From a functional perspective, FM $\theta$  has been implicated to encode various cognitive functions. Some studies have suggested that the increased FM $\theta$  activity could be indicative of a surprise, i.e., occurrence of an unexpected “good” or “bad” outcome (Cavanagh and Frank 2014). The surprise signal can elicit further adjustment in behavior



to produce more favorable outcomes (Danielmeier and Ullsperger 2011). Supporting this claim, it has been shown that theta power is correlated with increased reaction time in the subsequent trials (Cavanagh and Shackman 2015). Alternatively, the surprise signal can trigger a set of processes that increase the learning rate and adjust the future behaviors (O'Reilly 2013).

Another set of experiments has suggested that FM $\theta$  could reflect the uncertainty surrounding the behavioral stimuli or responses (Cavanagh and Frank 2014). This view is consistent with the notion that the ACC (generator of FM $\theta$ ) is involved in conflict monitoring. Furthermore, the involvement of FM $\theta$  in novelty detection can be explained in this respect. In fact, theta band could facilitate the integration of different inputs (reward, memory, etc.) to conduct efficient action selection (Womelsdorf et al. 2010b).

The above-mentioned FM $\theta$  activity is mainly related to the processing of outcome and/or conflict related signals. However, the theta band is also involved in stimulus-response mapping (Womelsdorf et al. 2010b). The involvement of theta band synchrony in performance of working memory-related paradigms could be mentioned in this regard. As previously described, prefrontal cortex has been robustly implicated in coding the working memory activity. Indeed, it has been shown that the spiking activity of the prefrontal single neurons can be strongly coupled to the theta band oscillations in distant areas such as visual cortex or hippocampus (Liebe et al. 2012; Siapas et al. 2005). Furthermore, the hippocampal formation has also been suggested to be involved in working memory especially when multiple stimuli and task relevant associations have to be maintained in working memory (Axmacher et al. 2010). It has been shown that the working memory representations across hippocampal neurons are mediated by theta band

activity (Lisman and Buzsaki 2008). In addition to the spatial working memory, visual working memory is also mediated by the coupling of the neuronal spiking activity to the theta band in the visual cortex. It has been shown that the theta band spike-field coherence of the neurons in visual cortex becomes stronger towards the end of the delay period of working memory, and the theta band spike-field coupling could convey visual information (Lee et al. 2005). The gradually increased theta band coupling of the visual cortical neurons in the delay period is a clear reflection of top-down control, because there is no visual stimuli during the delay period to induce bottom-up influence (Womelsdorf et al. 2010b).

These findings suggest that theta band is involved in a variety of higher order cognitive functions. Furthermore, theta band is involved in top-down control and it could facilitate the transmission of task relevant information between distant brain areas.

### ***1.3.3. Beta band:***

Similar to theta band, beta band activity has been implicated in a broad range of cognitive and sensori-motor functions. Beta band is historically associated with motor functions. It has been shown that beta band activity is more pronounced during iso-metric contractions and decreased while performing planned movements (Chakarov et al. 2009; Sanes and Donoghue 1993). The prominence of beta band rhythms at rest has led to naming this rhythm as the “idling rhythm” with regards to the motor system (Engel and Fries 2010; Pfurtscheller et al. 1996). Alternatively, the beta band has been suggested to reflect an active process in favor of the current movement, and attenuates the processing of the subsequent movement (Gilbertson et al. 2005; Pogosyan et al. 2009). In this respect, Gilbertson and colleagues have shown that increased beta band activity is correlated with

slowed voluntary movements (Gilbertson et al. 2005). An explanation to reconcile these findings could be that the beta band is involved in the feedback monitoring (e.g. proprioceptive inputs) of the movements and re-adjusting and correcting the unwanted motor responses (Engel and Fries 2010). This suggestion is supported by the notion that the somatosensory cortex exerts causal effect across beta band over motor and parietal cortices (Brovelli et al. 2004).

In addition to its involvement in motor control, the beta band is also suggested to be involved in cognitive functions (Bressler and Richter 2015; Engel and Fries 2010). Similar to its involvement in motor control, the beta band seems to be more active while maintaining top-down control in cognitively demanding tasks and it diminishes when the task rule switches or when the task rule is stimulus driven and does not involve endogenous cognitive functions (Engel and Fries 2010). As a support of this notion it has been shown that beta band activity is amplified when the task involves internally driven goals compared to stimulus-guided choices (Pesaran et al. 2008). Another interesting finding in this context is reported by (Buschman and Miller 2007). The authors trained monkeys to search for an object either in a pop out or a serial search paradigm. The pop out paradigm essentially engaged a stimulus driven choice selection whereas the serial search paradigm involved an endogenous top-down control. They found that the pop out paradigm led to enhancement in gamma coherence between parietal and frontal areas while serial search regime increased beta band coherence (Buschman and Miller 2007). This study suggests that top-down control in cognitively demanding tasks involves beta band activity. Furthermore, beta band has been implicated in context dependent modulation of the neuronal activity (Bressler and Richter 2015). For instance, single

neurons in the visual cortex have been found to exhibit different responses to the same stimuli across varying task demands (Li et al. 2004). Beta band is a candidate to exert top-down control over neurons in visual cortex and thereby modify their responses according to task demands (Bressler et al. 2007).

Taken together, these findings show that beta band is involved in performance of motor activities as well as cognitive functions. However, more studies are needed to shine light on the role of beta band in cognitive processes.

#### ***1.4. OBJECTIVES:***

##### ***1.4.1. Obtain the functional connectivity map of the FEF:***

The anatomical connectivity of the medial and lateral FEF with parietal and temporal areas has been previously explored (Schall et al. 1995). However, little is known about the functional connectivity of the FEF with other cortical and subcortical areas. More specifically, the difference in functional connectivity of the medial and lateral FEF with medial prefrontal areas is not well understood. In the first part of the project, I will address these questions by investigating the functional connectivity of the medial and lateral FEF using resting-state fMRI. I will perform the functional connectivity analysis utilizing the seed-base analysis approach. To do this, I will place a seed region of interest in the medial and lateral FEF and obtain the functional connectivity map of these areas. The results of this part of the project could be compared with the existing anatomical connectivity literature to verify whether the functional connectivity maps correspond with the anatomical connectivity maps. Furthermore, the resting-state fMRI functional connectivity maps could aid us to examine whether the areas that are functionally connected share functional and physiological properties.

***1.4.2. Evaluate whether the functionally connected ACC and FEF areas display synchronized neuronal activity:***

It has been suggested that functional brain networks form through synchronization across different frequency bands (Bressler and Richter 2015; Bressler et al. 2007; Buzsaki and Draguhn 2004). Each frequency band has a distinct functional role and this could include top-down or bottom-up processes (Buzsaki and Draguhn 2004). Furthermore, it has been suggested that the neuronal oscillations can facilitate (or inhibit) the communication between neuronal groups (Fries 2005; 2015). In this part of the project, I have performed local field potential (LFP) recordings in ACC and FEF to probe whether these areas display synchronized electrical activity and which frequency band exhibits strongest synchronization. The findings of this project will elucidate the functional role of the LFP synchronization in the transmission of information between FEF and ACC. In this respect, it has been previously suggested that the prominent theta frequency band in the ACC provides a temporal framework for efficient neuronal communication (Womelsdorf et al. 2010a). However, this hypothesis has not been directly tested through simultaneous recordings of ACC with other brain areas and my study will address this question.

***1.4.3. Examine the direction of information flow between ACC and FEF:***

The ACC is generally believed to be an area involved in higher cognitive functions that exerts top-down control over other areas. According to some models of cognitive control, ACC detects the need for control and recruits other areas such as the prefrontal cortex to implement such a control (Shenhav et al. 2013). However, this hypothesis has not been directly tested through simultaneous electrophysiological recordings between frontal

areas and ACC. Here, I will perform simultaneous single neuron and LFP recordings in FEF and ACC to examine whether ACC affects FEF.

### **1.5. REFERENCES:**

**Amiez C, Joseph JP, and Procyk E.** Reward encoding in the monkey anterior cingulate cortex. *Cerebral cortex* 16: 1040-1055, 2006.

**Aston-Jones G, and Cohen JD.** An integrative theory of locus coeruleus-norepinephrine function: adaptive gain and optimal performance. *Annual review of neuroscience* 28: 403-450, 2005.

**Axmacher N, Henseler MM, Jensen O, Weinreich I, Elger CE, and Fell J.** Cross-frequency coupling supports multi-item working memory in the human hippocampus. *Proceedings of the National Academy of Sciences of the United States of America* 107: 3228-3233, 2010.

**Barbas H, Ghashghaei H, Dombrowski SM, and Rempel-Clover NL.** Medial prefrontal cortices are unified by common connections with superior temporal cortices and distinguished by input from memory-related areas in the rhesus monkey. *The Journal of comparative neurology* 410: 343-367, 1999.

**Bates JF, and Goldman-Rakic PS.** Prefrontal connections of medial motor areas in the rhesus monkey. *The Journal of comparative neurology* 336: 211-228, 1993.

**Beldzik E, Domagalik A, Oginska H, Marek T, and Fafrowicz M.** Brain Activations Related to Saccadic Response Conflict are not Sensitive to Time on Task. *Frontiers in human neuroscience* 9: 664, 2015.

**Berger H.** About the human electroencephalogram. *Archiv f Psychiatrie u Nervenkrankheiten* 87: 527-570, 1929.

**Biswal B, Yetkin FZ, Haughton VM, and Hyde JS.** Functional Connectivity in the Motor Cortex of Resting Human Brain Using Echo-Planar Mri. *Magnetic resonance in medicine* 34: 537-541, 1995.

**Biswal BB, Mennes M, Zuo XN, Gohel S, Kelly C, Smith SM, Beckmann CF, Adelstein JS, Buckner RL, Colcombe S, Dogonowski AM, Ernst M, Fair D, Hampson M, Hoptman MJ, Hyde JS, Kiviniemi VJ, Kotter R, Li SJ, Lin CP, Lowe MJ, Mackay C, Madden DJ, Madsen KH, Margulies DS, Mayberg HS, McMahon K, Monk CS, Mostofsky SH, Nagel BJ, Pekar JJ, Peltier SJ, Petersen SE, Riedl V, Rombouts SA, Rypma B, Schlaggar BL, Schmidt S, Seidler RD, Siegle GJ, Sorg C, Teng GJ, Veijola J, Villringer A, Walter M, Wang L, Weng XC, Whitfield-Gabrieli S, Williamson P, Windischberger C, Zang YF, Zhang HY, Castellanos FX, and Milham MP.** Toward discovery science of human brain function. *Proceedings of the National Academy of Sciences of the United States of America* 107: 4734-4739, 2010.

**Bosman CA, Schoffelen JM, Brunet N, Oostenveld R, Bastos AM, Womelsdorf T, Rubehn B, Stieglitz T, De Weerd P, and Fries P.** Attentional stimulus selection through selective synchronization between monkey visual areas. *Neuron* 75: 875-888, 2012.

**Botvinick MM, Cohen JD, and Carter CS.** Conflict monitoring and anterior cingulate cortex: an update. *Trends in cognitive sciences* 8: 539-546, 2004.

**Braver TS, Barch DM, Gray JR, Molfese DL, and Snyder A.** Anterior cingulate cortex and response conflict: effects of frequency, inhibition and errors. *Cerebral cortex* 11: 825-836, 2001.

**Bressler SL, and Richter CG.** Interareal oscillatory synchronization in top-down neocortical processing. *Current opinion in neurobiology* 31: 62-66, 2015.

**Bressler SL, Richter CG, Chen Y, and Ding M.** Cortical functional network organization from autoregressive modeling of local field potential oscillations. *Statistics in medicine* 26: 3875-3885, 2007.

**Brignani D, Bortoletto M, Miniussi C, and Maioli C.** The when and where of spatial storage in memory-guided saccades. *NeuroImage* 52: 1611-1620, 2010.

**Brodmann K, and Garey LJ.** *Brodmann's Localisation in the cerebral cortex*. London: Smith-Gordon, 1994, p. xviii, 300 p.

**Broerse A, Crawford TJ, and den Boer JA.** Parsing cognition in schizophrenia using saccadic eye movements: a selective overview. *Neuropsychologia* 39: 742-756, 2001.

**Brovelli A, Ding M, Ledberg A, Chen Y, Nakamura R, and Bressler SL.** Beta oscillations in a large-scale sensorimotor cortical network: directional influences revealed by Granger causality. *Proceedings of the National Academy of Sciences of the United States of America* 101: 9849-9854, 2004.

**Brown MR, DeSouza JF, Goltz HC, Ford K, Menon RS, Goodale MA, and Everling S.** Comparison of memory- and visually guided saccades using event-related fMRI. *Journal of neurophysiology* 91: 873-889, 2004.

**Bruce CJ, and Goldberg ME.** Primate frontal eye fields. I. Single neurons discharging before saccades. *Journal of neurophysiology* 53: 603-635, 1985.

**Bruce CJ, Goldberg ME, Bushnell MC, and Stanton GB.** Primate frontal eye fields. II. Physiological and anatomical correlates of electrically evoked eye movements. *Journal of neurophysiology* 54: 714-734, 1985.

**Burrell JR, Hornberger M, Carpenter RH, Kiernan MC, and Hodges JR.** Saccadic abnormalities in frontotemporal dementia. *Neurology* 78: 1816-1823, 2012.

**Buschman TJ, and Miller EK.** Top-down versus bottom-up control of attention in the prefrontal and posterior parietal cortices. *Science* 315: 1860-1862, 2007.

**Buzsaki G.** Theta oscillations in the hippocampus. *Neuron* 33: 325-340, 2002.

**Buzsaki G.** Two-stage model of memory trace formation: a role for "noisy" brain states. *Neuroscience* 31: 551-570, 1989.

**Buzsaki G, and Draguhn A.** Neuronal oscillations in cortical networks. *Science* 304: 1926-1929, 2004.

**Cannon J, McCarthy MM, Lee S, Lee J, Borgers C, Whittington MA, and Kopell N.** Neurosystems: brain rhythms and cognitive processing. *The European journal of neuroscience* 39: 705-719, 2014.

**Carter CS, and van Veen V.** Anterior cingulate cortex and conflict detection: an update of theory and data. *Cognitive, affective & behavioral neuroscience* 7: 367-379, 2007.

**Cassanello CR, Nihalani AT, and Ferrera VP.** Neuronal responses to moving targets in monkey frontal eye fields. *Journal of neurophysiology* 100: 1544-1556, 2008.

**Cavanagh JF, and Frank MJ.** Frontal theta as a mechanism for cognitive control. *Trends in cognitive sciences* 18: 414-421, 2014.

**Cavanagh JF, and Shackman AJ.** Frontal midline theta reflects anxiety and cognitive control: meta-analytic evidence. *Journal of physiology, Paris* 109: 3-15, 2015.

**Chakarov V, Naranjo JR, Schulte-Monting J, Omlor W, Huethe F, and Kristeva R.** Beta-range EEG-EMG coherence with isometric compensation for increasing modulated low-level forces. *Journal of neurophysiology* 102: 1115-1120, 2009.

**Cohen JY, Crowder EA, Heitz RP, Subraveti CR, Thompson KG, Woodman GF, and Schall JD.** Cooperation and competition among frontal eye field neurons during visual target selection. *The Journal of neuroscience : the official journal of the Society for Neuroscience* 30: 3227-3238, 2010.

**Cohen MX.** Error-related medial frontal theta activity predicts cingulate-related structural connectivity. *NeuroImage* 55: 1373-1383, 2011.

**Cohen MX, and Ranganath C.** Reinforcement learning signals predict future decisions. *The Journal of neuroscience : the official journal of the Society for Neuroscience* 27: 371-378, 2007.

**Colby CL, Duhamel JR, and Goldberg ME.** Visual, presaccadic, and cognitive activation of single neurons in monkey lateral intraparietal area. *Journal of neurophysiology* 76: 2841-2852, 1996.

**Cole DM, Smith SM, and Beckmann CF.** Advances and pitfalls in the analysis and interpretation of resting-state fMRI data. *Frontiers in systems neuroscience* 4: 8, 2010.

**Cole MW, Yeung N, Freiwald WA, and Botvinick M.** Cingulate cortex: diverging data from humans and monkeys. *Trends in neurosciences* 32: 566-574, 2009.

**Critchley HD, and Mathias CJ.** Blood pressure, attention and cognition: drivers and air traffic controllers. *Clinical autonomic research : official journal of the Clinical Autonomic Research Society* 13: 399-401, 2003.

**Dai Z, Yan C, Wang Z, Wang J, Xia M, Li K, and He Y.** Discriminative analysis of early Alzheimer's disease using multi-modal imaging and multi-level characterization with multi-classifier (M3). *NeuroImage* 59: 2187-2195, 2012.

**Danielmeier C, and Ullsperger M.** Post-error adjustments. *Frontiers in psychology* 2: 233, 2011.

**Davis KD, Taylor KS, Hutchison WD, Dostrovsky JO, McAndrews MP, Richter EO, and Lozano AM.** Human anterior cingulate cortex neurons encode cognitive and emotional demands. *The Journal of neuroscience : the official journal of the Society for Neuroscience* 25: 8402-8406, 2005.

**Devinsky O, Morrell MJ, and Vogt BA.** Contributions of anterior cingulate cortex to behaviour. *Brain : a journal of neurology* 118 ( Pt 1): 279-306, 1995.

**Divac I, Bjorklund A, Lindvall O, and Passingham RE.** Converging projections from the mediodorsal thalamic nucleus and mesencephalic dopaminergic neurons to the neocortex in three species. *The Journal of comparative neurology* 180: 59-71, 1978.

**Dorris MC, Pare M, and Munoz DP.** Neuronal activity in monkey superior colliculus related to the initiation of saccadic eye movements. *The Journal of neuroscience : the official journal of the Society for Neuroscience* 17: 8566-8579, 1997.

**Dum RP, and Strick PL.** Motor areas in the frontal lobe of the primate. *Physiology & behavior* 77: 677-682, 2002.

**Dutta A, McKie S, and Deakin JF.** Resting state networks in major depressive disorder. *Psychiatry research* 224: 139-151, 2014.



**Engel AK, and Fries P.** Beta-band oscillations--signalling the status quo? *Current opinion in neurobiology* 20: 156-165, 2010.

**Everling S, Dorris MC, Klein RM, and Munoz DP.** Role of primate superior colliculus in preparation and execution of anti-saccades and pro-saccades. *The Journal of neuroscience : the official journal of the Society for Neuroscience* 19: 2740-2754, 1999.

**Everling S, and Johnston K.** Control of the superior colliculus by the lateral prefrontal cortex. *Philosophical transactions of the Royal Society of London Series B, Biological sciences* 368: 20130068, 2013.

**Ford KA, Gati JS, Menon RS, and Everling S.** BOLD fMRI activation for anti-saccades in nonhuman primates. *NeuroImage* 45: 470-476, 2009.

**Fries P.** A mechanism for cognitive dynamics: neuronal communication through neuronal coherence. *Trends in cognitive sciences* 9: 474-480, 2005.

**Fries P.** Rhythms for Cognition: Communication through Coherence. *Neuron* 88: 220-235, 2015.

**Fukushima J, Morita N, Fukushima K, Chiba T, Tanaka S, and Yamashita I.** Voluntary control of saccadic eye movements in patients with schizophrenic and affective disorders. *Journal of psychiatric research* 24: 9-24, 1990.

**Funahashi S, Bruce CJ, and Goldman-Rakic PS.** Mnemonic coding of visual space in the monkey's dorsolateral prefrontal cortex. *Journal of neurophysiology* 61: 331-349, 1989.

**Funahashi S, Bruce CJ, and Goldman-Rakic PS.** Neuronal activity related to saccadic eye movements in the monkey's dorsolateral prefrontal cortex. *Journal of neurophysiology* 65: 1464-1483, 1991.

**Funahashi S, Bruce CJ, and Goldman-Rakic PS.** Visuospatial coding in primate prefrontal neurons revealed by oculomotor paradigms. *Journal of neurophysiology* 63: 814-831, 1990.

**Fuster JM.** *The prefrontal cortex*. Amsterdam ; Boston: Academic Press/Elsevier, 2008, p. xiii, 410 p.

**Gabriel M, Vogt BA, Kubota Y, Poremba A, and Kang E.** Training-stage related neuronal plasticity in limbic thalamus and cingulate cortex during learning: a possible key to mnemonic retrieval. *Behavioural brain research* 46: 175-185, 1991.

**Ghilchrist ID.** Saccades. In: *The Oxford handbook of Eye Movements*, edited by Livessedge SP, Gilchrist ID, and Everling S. Oxford: Oxford university press, 2011.

**Gilbertson T, Lalo E, Doyle L, Di Lazzaro V, Cioni B, and Brown P.** Existing motor state is favored at the expense of new movement during 13-35 Hz oscillatory synchrony in the human corticospinal system. *The Journal of neuroscience : the official journal of the Society for Neuroscience* 25: 7771-7779, 2005.

**Goodale MA, and Milner AD.** Separate visual pathways for perception and action. *Trends in neurosciences* 15: 20-25, 1992.

**Gooler DM, and O'Neill WE.** Topographic representation of vocal frequency demonstrated by microstimulation of anterior cingulate cortex in the echolocating bat, *Pteronotus parnelli parnelli*. *Journal of comparative physiology A, Sensory, neural, and behavioral physiology* 161: 283-294, 1987.

**Gray S, and Russo K.** *Gray's anatomy*. Woodstock, Ill.: Dramatic Publishing, 2008, p. 69 p.

**Gregoriou GG, Gotts SJ, and Desimone R.** Cell-type-specific synchronization of neural activity in FEF with V4 during attention. *Neuron* 73: 581-594, 2012.

**Gulyas AI, and Freund TT.** Generation of physiological and pathological high frequency oscillations: the role of perisomatic inhibition in sharp-wave ripple and interictal spike generation. *Current opinion in neurobiology* 31: 26-32, 2015.

**Guo WB, Liu F, Liu JR, Yu LY, Zhang ZK, Zhang J, Chen HF, and Xiao CQ.** Is there a cerebellar compensatory effort in first-episode, treatment-naive major depressive disorder at rest? *Prog Neuro-Psychoph* 46: 13-18, 2013.

**Hagmann P, Cammoun L, Gigandet X, Gerhard S, Grant PE, Wedeen V, Meuli R, Thiran JP, Honey CJ, and Sporns O.** MR connectomics: Principles and challenges. *Journal of neuroscience methods* 194: 34-45, 2010.

**Hallett PE.** Primary and secondary saccades to goals defined by instructions. *Vision research* 18: 1279-1296, 1978.

**Hayden BY, Heilbronner SR, Pearson JM, and Platt ML.** Surprise signals in anterior cingulate cortex: neuronal encoding of unsigned reward prediction errors driving adjustment in behavior. *The Journal of neuroscience : the official journal of the Society for Neuroscience* 31: 4178-4187, 2011.

**Hayden BY, and Platt ML.** Neurons in anterior cingulate cortex multiplex information about reward and action. *The Journal of neuroscience : the official journal of the Society for Neuroscience* 30: 3339-3346, 2010.

**Herrmann MJ, Rommner J, Ehrlis AC, Heidrich A, and Fallgatter AJ.** Source localization (LORETA) of the error-related-negativity (ERN/Ne) and positivity (Pe). *Brain research Cognitive brain research* 20: 294-299, 2004.

**Hepp K, and Henn V.** Spatio-temporal recoding of rapid eye movement signals in the monkey paramedian pontine reticular formation (PPRF). *Experimental brain research* 52: 105-120, 1983.

**Hutcheon B, and Yarom Y.** Resonance, oscillation and the intrinsic frequency preferences of neurons. *Trends in neurosciences* 23: 216-222, 2000.

**Hutchison RM, Womelsdorf T, Gati JS, Leung LS, Menon RS, and Everling S.** Resting-state connectivity identifies distinct functional networks in macaque cingulate cortex. *Cerebral cortex* 22: 1294-1308, 2012.

**Hutton SB.** Cognitive control of saccadic eye movements. *Brain and cognition* 68: 327-340, 2008.

**Ito S, Stuphorn V, Brown JW, and Schall JD.** Performance monitoring by the anterior cingulate cortex during saccade countermanding. *Science* 302: 120-122, 2003.

**Jamadar SD, Johnson BP, Clough M, Egan GF, and Fielding J.** Behavioral and Neural Plasticity of Ocular Motor Control: Changes in Performance and fMRI Activity Following Antisaccade Training. *Frontiers in human neuroscience* 9: 653, 2015.

**Johnston K, and Everling S.** Monkey dorsolateral prefrontal cortex sends task-selective signals directly to the superior colliculus. *The Journal of neuroscience : the official journal of the Society for Neuroscience* 26: 12471-12478, 2006.

**Johnston K, and Everling S.** Neurophysiology and neuroanatomy of reflexive and voluntary saccades in non-human primates. *Brain and cognition* 68: 271-283, 2008.

**Johnston K, Koval MJ, Lomber SG, and Everling S.** Macaque dorsolateral prefrontal cortex does not suppress saccade-related activity in the superior colliculus. *Cerebral cortex* 24: 1373-1388, 2014.

**Johnston K, Levin HM, Koval MJ, and Everling S.** Top-down control-signal dynamics in anterior cingulate and prefrontal cortex neurons following task switching. *Neuron* 53: 453-462, 2007.

**Kaping D, Vinck M, Hutchison RM, Everling S, and Womelsdorf T.** Specific contributions of ventromedial, anterior cingulate, and lateral prefrontal cortex for attentional selection and stimulus valuation. *PLoS biology* 9: e1001224, 2011.

**Karbasforoushan H, and Woodward ND.** Resting-state networks in schizophrenia. *Current topics in medicinal chemistry* 12: 2404-2414, 2012.

**Kennerley SW, and Wallis JD.** Encoding of reward and space during a working memory task in the orbitofrontal cortex and anterior cingulate sulcus. *Journal of neurophysiology* 102: 3352-3364, 2009.

**Kennerley SW, Walton ME, Behrens TE, Buckley MJ, and Rushworth MF.** Optimal decision making and the anterior cingulate cortex. *Nature neuroscience* 9: 940-947, 2006.

**Kerns JG, Cohen JD, MacDonald AW, 3rd, Cho RY, Stenger VA, and Carter CS.** Anterior cingulate conflict monitoring and adjustments in control. *Science* 303: 1023-1026, 2004.

**Koch W, Teipel S, Mueller S, Benninghoff J, Wagner M, Bokde AL, Hampel H, Coates U, Reiser M, and Meindl T.** Diagnostic power of default mode network resting state fMRI in the detection of Alzheimer's disease. *Neurobiology of aging* 33: 466-478, 2012.

**Lee AK, Hamalainen MS, Dyckman KA, Barton JJ, and Manoach DS.** Saccadic preparation in the frontal eye field is modulated by distinct trial history effects as revealed by magnetoencephalography. *Cerebral cortex* 21: 245-253, 2011.

**Lee H, Simpson GV, Logothetis NK, and Rainer G.** Phase locking of single neuron activity to theta oscillations during working memory in monkey extrastriate visual cortex. *Neuron* 45: 147-156, 2005.

**Lee MH, Smyser CD, and Shimony JS.** Resting-state fMRI: a review of methods and clinical applications. *AJNR American journal of neuroradiology* 34: 1866-1872, 2013.

**Leichnetz GR, Spencer RF, Hardy SG, and Astruc J.** The prefrontal corticotectal projection in the monkey; an anterograde and retrograde horseradish peroxidase study. *Neuroscience* 6: 1023-1041, 1981.

**Leigh RJ, and Zee DS.** *The neurology of eye movements*. New York: Oxford University Press, 2006, p. x, 763 p.

**Li B, Liu L, Friston KJ, Shen H, Wang L, Zeng LL, and Hu D.** A treatment-resistant default mode subnetwork in major depression. *Biological psychiatry* 74: 48-54, 2013.

**Li W, Piech V, and Gilbert CD.** Perceptual learning and top-down influences in primary visual cortex. *Nature neuroscience* 7: 651-657, 2004.

**Liebe S, Hoerzer GM, Logothetis NK, and Rainer G.** Theta coupling between V4 and prefrontal cortex predicts visual short-term memory performance. *Nature neuroscience* 15: 456-462, S451-452, 2012.

**Lisman J, and Buzsaki G.** A neural coding scheme formed by the combined function of gamma and theta oscillations. *Schizophrenia bulletin* 34: 974-980, 2008.

**Luppino G, Matelli M, Camarda RM, Gallese V, and Rizzolatti G.** Multiple representations of body movements in mesial area 6 and the adjacent cingulate cortex: an intracortical microstimulation study in the macaque monkey. *The Journal of comparative neurology* 311: 463-482, 1991.

**Maclean PD.** The limbic system and its hippocampal formation; studies in animals and their possible application to man. *Journal of neurosurgery* 11: 29-44, 1954.

**MacLean PD.** *The triune brain in evolution : role in paleocerebral functions*. New York: Plenum Press, 1990, p. xxiv, 672 p.

**MacLeod CM, and MacDonald PA.** Interdimensional interference in the Stroop effect: uncovering the cognitive and neural anatomy of attention. *Trends in cognitive sciences* 4: 383-391, 2000.

**Magno E, Foxe JJ, Molholm S, Robertson IH, and Garavan H.** The anterior cingulate and error avoidance. *The Journal of neuroscience : the official journal of the Society for Neuroscience* 26: 4769-4773, 2006.

**Margulies DS, Kelly AM, Uddin LQ, Biswal BB, Castellanos FX, and Milham MP.** Mapping the functional connectivity of anterior cingulate cortex. *NeuroImage* 37: 579-588, 2007.

**McGuire JT, and Botvinick MM.** Prefrontal cortex, cognitive control, and the registration of decision costs. *Proceedings of the National Academy of Sciences of the United States of America* 107: 7922-7926, 2010.

**Michelet T, Bioulac B, Langbour N, Goillandeau M, Guehl D, and Burbaud P.** Electrophysiological Correlates of a Versatile Executive Control System in the Monkey Anterior Cingulate Cortex. *Cerebral cortex* 26: 1684-1697, 2016.

**Miller EK, and Cohen JD.** An integrative theory of prefrontal cortex function. *Annual review of neuroscience* 24: 167-202, 2001.

**Montague PR, Hyman SE, and Cohen JD.** Computational roles for dopamine in behavioural control. *Nature* 431: 760-767, 2004.

**Moore T, and Armstrong KM.** Selective gating of visual signals by microstimulation of frontal cortex. *Nature* 421: 370-373, 2003.

**Muller-Preuss P, Newman JD, and Jurgens U.** Anatomical and physiological evidence for a relationship between the 'cingular' vocalization area and the auditory cortex in the squirrel monkey. *Brain research* 202: 307-315, 1980.

**Munoz DP, Dorris MC, Pare M, and Everling S.** On your mark, get set: brainstem circuitry underlying saccadic initiation. *Canadian journal of physiology and pharmacology* 78: 934-944, 2000.

**Munoz DP, and Everling S.** Look away: the anti-saccade task and the voluntary control of eye movement. *Nature reviews Neuroscience* 5: 218-228, 2004.

**Naito E, Kinomura S, Geyer S, Kawashima R, Roland PE, and Zilles K.** Fast reaction to different sensory modalities activates common fields in the motor areas, but the anterior cingulate cortex is involved in the speed of reaction. *Journal of neurophysiology* 83: 1701-1709, 2000.

**Neubert FX, Mars RB, Sallet J, and Rushworth MF.** Connectivity reveals relationship of brain areas for reward-guided learning and decision making in human and monkey frontal cortex. *Proceedings of the National Academy of Sciences of the United States of America* 112: E2695-2704, 2015.

**Nieuwenhuys R, Voogd J, and Huijzen Cv.** *The human central nervous system : a synopsis and atlas*. Berlin ; New York: Springer-Verlag, 1981, p. viii, 253 p.

**O'Reilly JX.** Making predictions in a changing world-inference, uncertainty, and learning. *Frontiers in neuroscience* 7: 105, 2013.

- Palomero-Gallagher N, Mohlberg H, Zilles K, and Vogt B.** Cytology and receptor architecture of human anterior cingulate cortex. *The Journal of comparative neurology* 508: 906-926, 2008.
- Palomero-Gallagher N, Vogt BA, Schleicher A, Mayberg HS, and Zilles K.** Receptor architecture of human cingulate cortex: evaluation of the four-region neurobiological model. *Human brain mapping* 30: 2336-2355, 2009.
- Papez JW.** A proposed mechanism of emotion. 1937. *The Journal of neuropsychiatry and clinical neurosciences* 7: 103-112, 1995.
- Pare M, and Wurtz RH.** Monkey posterior parietal cortex neurons antidromically activated from superior colliculus. *Journal of neurophysiology* 78: 3493-3497, 1997.
- Parvizi J, Rangarajan V, Shirer WR, Desai N, and Greicius MD.** The will to persevere induced by electrical stimulation of the human cingulate gyrus. *Neuron* 80: 1359-1367, 2013.
- Paus T.** Location and function of the human frontal eye-field: a selective review. *Neuropsychologia* 34: 475-483, 1996.
- Paus T.** Primate anterior cingulate cortex: where motor control, drive and cognition interface. *Nature reviews Neuroscience* 2: 417-424, 2001.
- Paus T, Castro-Alamancos MA, and Petrides M.** Cortico-cortical connectivity of the human mid-dorsolateral frontal cortex and its modulation by repetitive transcranial magnetic stimulation. *The European journal of neuroscience* 14: 1405-1411, 2001.
- Paus T, Petrides M, Evans AC, and Meyer E.** Role of the human anterior cingulate cortex in the control of oculomotor, manual, and speech responses: a positron emission tomography study. *Journal of neurophysiology* 70: 453-469, 1993.
- Peng X, Sereno ME, Silva AK, Lehky SR, and Sereno AB.** Shape selectivity in primate frontal eye field. *Journal of neurophysiology* 100: 796-814, 2008.
- Pesaran B, Nelson MJ, and Andersen RA.** Free choice activates a decision circuit between frontal and parietal cortex. *Nature* 453: 406-409, 2008.
- Pfurtscheller G, Stancak A, Jr., and Neuper C.** Post-movement beta synchronization. A correlate of an idling motor area? *Electroencephalography and clinical neurophysiology* 98: 281-293, 1996.
- Pierce JE, and McDowell JE.** Modulation of cognitive control levels via manipulation of saccade trial-type probability assessed with event-related BOLD fMRI. *Journal of neurophysiology* 115: 763-772, 2016.
- Pogosyan A, Gaynor LD, Eusebio A, and Brown P.** Boosting cortical activity at Beta-band frequencies slows movement in humans. *Current biology : CB* 19: 1637-1641, 2009.
- Posner MI.** Orienting of attention. *The Quarterly journal of experimental psychology* 32: 3-25, 1980.
- Procyk E, Amiez C, Quilodran R, and Josef JP.** Modulation of prefrontal activity related to cognitive control and performance monitoring. In: *Sensorimotor foundations of higher cognition, Attention and performance*, edited by Haggard P, Rossetti Y, and Kawato M. Oxford: Oxford University Press, 2008, p. 27-46.
- Procyk E, Tanaka YL, and Joseph JP.** Anterior cingulate activity during routine and non-routine sequential behaviors in macaques. *Nature neuroscience* 3: 502-508, 2000.

**Procyk E, Wilson CR, Stoll FM, Faraut MC, Petrides M, and Amiez C.** Midcingulate Motor Map and Feedback Detection: Converging Data from Humans and Monkeys. *Cerebral cortex* 26: 467-476, 2016.

**Quilodran R, Rothe M, and Procyk E.** Behavioral shifts and action valuation in the anterior cingulate cortex. *Neuron* 57: 314-325, 2008.

**Raghavachari S, Lisman JE, Tully M, Madsen JR, Bromfield EB, and Kahana MJ.** Theta oscillations in human cortex during a working-memory task: evidence for local generators. *Journal of neurophysiology* 95: 1630-1638, 2006.

**Reuter-Lorenz PA, Hughes HC, and Fendrich R.** The reduction of saccadic latency by prior offset of the fixation point: an analysis of the gap effect. *Perception & psychophysics* 49: 167-175, 1991.

**Richards JE.** Cortical sources of ERP in prosaccade and antisaccade eye movements using realistic source models. *Frontiers in systems neuroscience* 7: 27, 2013.

**Rizzolatti G, Riggio L, Dascola I, and Umiltà C.** Reorienting attention across the horizontal and vertical meridians: evidence in favor of a premotor theory of attention. *Neuropsychologia* 25: 31-40, 1987.

**Rosazza C, Minati L, Ghielmetti F, Mandelli ML, and Bruzzone MG.** Functional connectivity during resting-state functional MR imaging: study of the correspondence between independent component analysis and region-of-interest-based methods. *AJNR American journal of neuroradiology* 33: 180-187, 2012.

**Rushworth MF, Kolling N, Sallet J, and Mars RB.** Valuation and decision-making in frontal cortex: one or many serial or parallel systems? *Current opinion in neurobiology* 22: 946-955, 2012.

**Sajad A, Sadeh M, Keith GP, Yan X, Wang H, and Crawford JD.** Visual-Motor Transformations Within Frontal Eye Fields During Head-Unrestrained Gaze Shifts in the Monkey. *Cerebral cortex* 25: 3932-3952, 2015.

**Sajad A, Sadeh M, Yan X, Wang H, and Crawford JD.** Transition from Target to Gaze Coding in Primate Frontal Eye Field during Memory Delay and Memory-Motor Transformation. *eNeuro* 3: 2016.

**Sanes JN, and Donoghue JP.** Oscillations in local field potentials of the primate motor cortex during voluntary movement. *Proceedings of the National Academy of Sciences of the United States of America* 90: 4470-4474, 1993.

**Saslow MG.** Effects of components of displacement-step stimuli upon latency for saccadic eye movement. *Journal of the Optical Society of America* 57: 1024-1029, 1967.

**Sato TR, and Schall JD.** Effects of stimulus-response compatibility on neural selection in frontal eye field. *Neuron* 38: 637-648, 2003.

**Schall JD.** Visuomotor Functions in the Frontal Lobe. *Annual Review of Vision Science* 1: 469-498, 2015.

**Schall JD, Morel A, King DJ, and Bullier J.** Topography of visual cortex connections with frontal eye field in macaque: convergence and segregation of processing streams. *The Journal of neuroscience : the official journal of the Society for Neuroscience* 15: 4464-4487, 1995.

**Scudder CA, Kaneko CS, and Fuchs AF.** The brainstem burst generator for saccadic eye movements: a modern synthesis. *Experimental brain research* 142: 439-462, 2002.

**Seeley WW, Menon V, Schatzberg AF, Keller J, Glover GH, Kenna H, Reiss AL, and Greicius MD.** Dissociable intrinsic connectivity networks for salience processing

and executive control. *The Journal of neuroscience : the official journal of the Society for Neuroscience* 27: 2349-2356, 2007.

**Selemon LD, and Goldman-Rakic PS.** Common cortical and subcortical targets of the dorsolateral prefrontal and posterior parietal cortices in the rhesus monkey: evidence for a distributed neural network subserving spatially guided behavior. *The Journal of neuroscience : the official journal of the Society for Neuroscience* 8: 4049-4068, 1988.

**Selemon LD, and Goldman-Rakic PS.** Longitudinal topography and interdigitation of corticostriatal projections in the rhesus monkey. *The Journal of neuroscience : the official journal of the Society for Neuroscience* 5: 776-794, 1985.

**Sheffield JM, and Barch DM.** Cognition and resting-state functional connectivity in schizophrenia. *Neuroscience and biobehavioral reviews* 61: 108-120, 2016.

**Shehzad Z, Kelly AM, Reiss PT, Gee DG, Gotimer K, Uddin LQ, Lee SH, Margulies DS, Roy AK, Biswal BB, Petkova E, Castellanos FX, and Milham MP.** The resting brain: unconstrained yet reliable. *Cerebral cortex* 19: 2209-2229, 2009.

**Shenhav A, Botvinick MM, and Cohen JD.** The expected value of control: an integrative theory of anterior cingulate cortex function. *Neuron* 79: 217-240, 2013.

**Sheth SA, Mian MK, Patel SR, Asaad WF, Williams ZM, Dougherty DD, Bush G, and Eskandar EN.** Human dorsal anterior cingulate cortex neurons mediate ongoing behavioural adaptation. *Nature* 488: 218-221, 2012.

**Shibutani H, Sakata H, and Hyvarinen J.** Saccade and blinking evoked by microstimulation of the posterior parietal association cortex of the monkey. *Experimental brain research* 55: 1-8, 1984.

**Siapas AG, Lubenov EV, and Wilson MA.** Prefrontal phase locking to hippocampal theta oscillations. *Neuron* 46: 141-151, 2005.

**Silvetti M, Alexander W, Verguts T, and Brown JW.** From conflict management to reward-based decision making: actors and critics in primate medial frontal cortex. *Neuroscience and biobehavioral reviews* 46 Pt 1: 44-57, 2014.

**Sommer MA, and Wurtz RH.** Composition and topographic organization of signals sent from the frontal eye field to the superior colliculus. *Journal of neurophysiology* 83: 1979-2001, 2000.

**Sommer MA, and Wurtz RH.** Frontal eye field sends delay activity related to movement, memory, and vision to the superior colliculus. *Journal of neurophysiology* 85: 1673-1685, 2001.

**Sparks DL.** The brainstem control of saccadic eye movements. *Nature reviews Neuroscience* 3: 952-964, 2002.

**Sporns O, and Honey CJ.** Topographic dynamics in the resting brain. *Neuron* 78: 955-956, 2013.

**Stroop JR.** Studies of interference in serial verbal reactions. Nashville, Tenn.: George Peabody College for Teachers, George Peabody College for Teachers, 1935, p. 19 p.

**Sugrue LP, Corrado GS, and Newsome WT.** Matching behavior and the representation of value in the parietal cortex. *Science* 304: 1782-1787, 2004.

**Supekar K, Menon V, Rubin D, Musen M, and Greicius MD.** Network analysis of intrinsic functional brain connectivity in Alzheimer's disease. *PLoS computational biology* 4: e1000100, 2008.

**Suzuki H, and Azuma M.** Topographic studies on visual neurons in the dorsolateral prefrontal cortex of the monkey. *Experimental brain research* 53: 47-58, 1983.

**Thompson KG, Biscoe KL, and Sato TR.** Neuronal basis of covert spatial attention in the frontal eye field. *The Journal of neuroscience : the official journal of the Society for Neuroscience* 25: 9479-9487, 2005.

**Thompson KG, Hanes DP, Bichot NP, and Schall JD.** Perceptual and motor processing stages identified in the activity of macaque frontal eye field neurons during visual search. *Journal of neurophysiology* 76: 4040-4055, 1996.

**Thompson KG, and Schall JD.** Antecedents and correlates of visual detection and awareness in macaque prefrontal cortex. *Vision research* 40: 1523-1538, 2000.

**Toda K, Sugase-Miyamoto Y, Mizuhiki T, Inaba K, Richmond BJ, and Shidara M.** Differential encoding of factors influencing predicted reward value in monkey rostral anterior cingulate cortex. *PloS one* 7: e30190, 2012.

**Tohka J, Foerde K, Aron AR, Tom SM, Toga AW, and Poldrack RA.** Automatic independent component labeling for artifact removal in fMRI. *NeuroImage* 39: 1227-1245, 2008.

**Ungerleider LG, Galkin TW, Desimone R, and Gattass R.** Cortical connections of area V4 in the macaque. *Cerebral cortex* 18: 477-499, 2008.

**Vincent JL, Patel GH, Fox MD, Snyder AZ, Baker JT, Van Essen DC, Zempel JM, Snyder LH, Corbetta M, and Raichle ME.** Intrinsic functional architecture in the anaesthetized monkey brain. *Nature* 447: 83-86, 2007.

**Vogt BA.** *Cingulate neurobiology and disease*. Oxford ; New York: Oxford University Press, 2009, p. xxxiv, 829 p.

**Vogt BA, Nimchinsky EA, Vogt LJ, and Hof PR.** Human cingulate cortex: surface features, flat maps, and cytoarchitecture. *The Journal of comparative neurology* 359: 490-506, 1995.

**Vogt BA, and Pandya DN.** Cingulate cortex of the rhesus monkey: II. Cortical afferents. *The Journal of comparative neurology* 262: 271-289, 1987.

**Vogt BA, Rosene DL, and Pandya DN.** Thalamic and cortical afferents differentiate anterior from posterior cingulate cortex in the monkey. *Science* 204: 205-207, 1979.

**Wang Y, Matsuzaka Y, Shima K, and Tanji J.** Cingulate cortical cells projecting to monkey frontal eye field and primary motor cortex. *Neuroreport* 15: 1559-1563, 2004.

**Wardak C, Ibos G, Duhamel JR, and Olivier E.** Contribution of the monkey frontal eye field to covert visual attention. *The Journal of neuroscience : the official journal of the Society for Neuroscience* 26: 4228-4235, 2006.

**Watanabe M.** Prefrontal unit activity during associative learning in the monkey. *Experimental brain research* 80: 296-309, 1990.

**Womelsdorf T, Johnston K, Vinck M, and Everling S.** Theta-activity in anterior cingulate cortex predicts task rules and their adjustments following errors. *Proceedings of the National Academy of Sciences of the United States of America* 107: 5248-5253, 2010a.

**Womelsdorf T, Vinck M, Leung LS, and Everling S.** Selective theta-synchronization of choice-relevant information subserves goal-directed behavior. *Frontiers in human neuroscience* 4: 210, 2010b.

**Woodward ND, Rogers B, and Heckers S.** Functional resting-state networks are differentially affected in schizophrenia. *Schizophrenia research* 130: 86-93, 2011.



**Zhang M, and Barash S.** Neuronal switching of sensorimotor transformations for antisaccades. *Nature* 408: 971-975, 2000.

**Zhang M, and Barash S.** Persistent LIP activity in memory antisaccades: working memory for a sensorimotor transformation. *Journal of neurophysiology* 91: 1424-1441, 2004.

**Zhou H, and Desimone R.** Feature-based attention in the frontal eye field and area V4 during visual search. *Neuron* 70: 1205-1217, 2011.

**Zhou J, Greicius MD, Gennatas ED, Growdon ME, Jang JY, Rabinovici GD, Kramer JH, Weiner M, Miller BL, and Seeley WW.** Divergent network connectivity changes in behavioural variant frontotemporal dementia and Alzheimer's disease. *Brain : a journal of neurology* 133: 1352-1367, 2010.

## CHAPTER 2:

### **2. Functional connectivity patterns of medial and lateral macaque frontal eye fields reveal distinct visuomotor networks<sup>1</sup>**

#### **2.1. ABSTRACT:**

It has been previously shown that small- and large-amplitude saccades have different functions during vision in natural environments. Large saccades are associated with reaching movements toward objects, whereas small saccades facilitate the identification of more detailed object features necessary for successful grasping and manual manipulation. To determine whether these represent dichotomous processing streams, I used resting-state functional MRI to examine the functional connectivity patterns of the medial and lateral frontal eye field (FEF) regions that encode large- and small-amplitude saccades, respectively. I found that the spontaneous blood oxygen level-dependent signals of the medial FEF were functionally correlated with areas known to be involved in reaching movements and executive control processes, whereas lateral FEF was functionally correlated with cortical areas involved in object processing and in grasping, fixation, and manipulation of objects. The results provide strong evidence for two distinct visuomotor network systems in the primate brain that likely reflect the alternating phases of vision for action in natural environments.

---

<sup>1</sup> A version of Chapter 2 is published as S Babapoor-Farrokhran, R.M. Hutchison, J.S. Gati, R.S. Menon, and S Everling, (2013): Functional connectivity patterns of medial and lateral macaque frontal eye fields reveal distinct visuomotor networks. *Journal of Neurophysiology*.

## ***2.2. INTRODUCTION:***

Saccades are rapid movements of the eyes that shift the line of sight to a new location in the visual field. Although saccades are remarkably stereotypical across a wide range of amplitudes (Bahill et al. 1975), studies of human gaze behavior in natural and dynamic environments have demonstrated that small- and large-amplitude saccades serve very different behavioral functions (Foerster et al. 2012; Hayhoe et al. 2003; Johansson et al. 2001; Land et al. 1999; Land 2009; Land and Hayhoe 2001). Large saccades, often accompanied by a head movement, are made to task-relevant objects in the environment and are followed by a reaching movement toward the object. In many cases, these large gaze movements are themselves preceded by an orienting movement of the trunk that is likely guided by memory (Land 2009). The initial large saccade toward the object is typically followed by a series of considerably smaller saccades on the object, which are thought to provide the necessary visual information about the object's shape and texture for grasping and manipulation. In most cases, the eyes will then leave the object before manual manipulation has ended.

It is presently unknown how the brain achieves the tight temporal relationship between large saccades and reaching movements, and between small saccades, grasping, and object processing. In the present study I tested the hypothesis that separate functional networks underlie these behavioral couplings. Prime candidates for testing this hypothesis are the frontal eye fields (FEF) that are located bilaterally in the anterior banks of the arcuate sulci in macaque monkeys (Bruce and Goldberg 1985; Bruce et al. 1985) and in the ventral branch of the superior precentral sulcus in humans (Amiez et al. 2006b; Luna et al. 1998; Paus 1996). Although it is presently unknown how large and small

saccades are encoded in human FEF, it is well known that the macaque FEF contains a topographical map for contralateral saccadic eye movements, with lateral FEF encoding small saccades and medial FEF encoding large saccades and head movements (Bruce et al. 1985; Elsley et al. 2007; Robinson and Fuchs 1969). Tracer studies support separate divisions of macaque FEF, showing that medial and lateral FEF differ in both their anatomic connectivity and cytoarchitecture (Schall et al. 1995; Stanton et al. 1993, 1995). Therefore, the known organization of macaque FEF and their widespread usage as a primate model for the neural control of saccades (Johnston and Everling 2008), reaching, and grasping movements (Davare et al. 2011) makes these monkeys ideal subjects for investigating the neural networks associated with small and large saccades.

Resting-state functional magnetic resonance imaging (RS-fMRI) is quickly becoming the method of choice for investigating the organization of functional brain networks (Fox and Raichle 2007) across multiple species (Hutchison and Everling 2012) and their alterations across various psychiatric, neurological, and developmental disorders in the absence of experimental tasks (Greicius 2008; Menon 2011). Resting-state functional connectivity (FC) is largely constrained by the underlying anatomic architecture (Greicius et al. 2009; Honey et al. 2009; Shen et al. 2012; Vincent et al. 2007) and is presumed to be a hemodynamic manifestation of FC between slow fluctuations in neuronal activity (Scholvinck et al. 2010; Shmuel and Leopold 2008; for reviews see Fox and Raichle 2007; Leopold and Maier 2011).

In this study, I used the RS-fMRI technique to directly determine the FC of medial and lateral FEF in macaque monkeys. I found that medial and lateral FEF form largely separate functional neural networks that may underlie the distinct behavioral roles

of large and small saccades in the visual control of action.

### **2.3. MATERIALS AND METHODS:**

*Subjects.* Five naive male macaque monkeys (3 *Macaca mulatta* and 2 *Macaca fascicularis*), weighing between 5 and 8.5 kg, were the subjects in this study. These data have not been published in our previous reports (Hutchison et al. 2011a, 2011b, 2012, in press; Shen et al. 2012) and functional data have been acquired at a higher spatial resolution (see below). All experimental methods were carried out in accordance with the Canadian Council of Animal Care policy on the use of laboratory animals and approved by the Animal Use Subcommittee of the University of Western Ontario Council on Animal Care.

#### **2.3.1. Data acquisition:**

Data acquisition procedures followed in this study have been used to derive functional connectivity maps in previous studies (Hutchison et al. 2011a, 2011b, 2012). On the day of scanning, the monkeys were anesthetized by intramuscular injections of atropine (0.4 mg/kg), ipratropium (0.025 mg/kg), and ketamine hydrochloride (7.5 mg/kg). Afterwards, 3 ml of propofol (10 mg/ml) were administered intravenously and oral intubation was carried out. Maintenance of anesthesia was conducted by using 1.5% isoflurane mixed with oxygen. Animals had spontaneous respiration throughout the duration of the experiment. The animals were placed in a custom-built chair and head-fixed while they were in the magnet bore. Isoflurane level was reduced to 1% during functional image acquisition. The animals' vital signs were monitored throughout the duration of the image acquisition [rectal temperature via a fiber-optic temperature probe (FISO, Quebec City, QC, Canada), respiration via bellows (Siemens, Union, NJ), and

end-tidal CO<sub>2</sub> via capnometer (Covidien-Nellcor, Boulder, CO)]. Physiological parameters were in the normal range throughout the image acquisition procedure (temperature: 36.8°C; respiration: 24–32 breaths/min; end-tidal CO<sub>2</sub>: 31–40 mmHg). A heating disk (SnuggleSafe; Littlehampton, West Sussex, UK) and thermal insulation were used to maintain body temperature. Anesthesia was used in this study because there are fewer motion artifacts, less physiological stress, and no training requirements. Regardless of the vasodilator properties of isoflurane and its effects on cerebrovascular activity (Farber et al. 1997), network connectivity and synchronous blood oxygen level-dependent (BOLD) fluctuations under isoflurane anesthesia have been robustly reported elsewhere (Hutchison et al. 2012; Vincent et al. 2007). The data were acquired on an actively shielded 7-Tesla 68-cm horizontal bore scanner with a DirectDrive console (Agilent, Santa Clara, CA) and a Siemens AC84 gradient subsystem (Erlangen, Germany) operating at a slew rate of 350 mT·m<sup>-1</sup>·s<sup>-1</sup>. An in-house-designed and -manufactured conformal five-channel transceive primate head radiofrequency coil was used for acquiring magnetic resonance (MR) images. The coil consisted of an array of elements wrapped 270° circumferentially around the head. Magnetic field optimization (B<sub>0</sub> shimming) was performed using an automated three-dimensional mapping procedure over the specific imaging volume of interest. For each monkey, 10 runs of 150 continuous echo-planar imaging (EPI) functional volumes [TR 2,000 ms, TE 16 ms, flip angle 70°, matrix 96×96, field of view (FOV) 96×96 mm, acquisition voxel size 1×1×1mm] were acquired, with each scan totaling 5 min. EPI images were acquired with phase encoding in the left-right direction using GRAPPA at an acceleration factor of 2. Every image was corrected for physiological fluctuations using navigator echo

correction. A high-resolution gradient echo (GRE) anatomic MR image was acquired along the same orientation as the functional images (TR 1,100 ms, TE 8 ms, matrix 256×256, FOV 96×96 mm, acquisition voxel size 375  $\mu\text{m}$  × 375  $\mu\text{m}$  × 1 mm). Also, for every monkey, a T1-weighted anatomic image (TE 2.5 ms, TR 2,300 ms, TI 800 ms, FOV 96×96 mm, 750-  $\mu\text{m}$  isotropic resolution) was acquired.

### ***2.3.2. Image preprocessing:***

Functional MRI preprocessing was carried out using the FSL software package (<http://www.fmrib.ox.ac.uk>). The preprocessing procedure included motion correction (6-parameter affine transformation), brain extraction, spatial smoothing (full-width at half-maximum 2 mm), high-pass temporal filtering (Gaussian- weighted least-squares straight line fitting with 100 s), low-pass temporal filtering (half-width at half-maximum 2.8 s, Gaussian filter), and nonlinear registration (fMRIB nonlinear image registration tool: FNIRT; <http://www.fmrib.ox.ac.uk/fsl/fslwiki/FNIRT>) to the individual monkey's T2-weighted image. Global mean signal was not regressed out from the data because of its propensity for finding more anticorrelations (Murphy et al. 2009) and because it might remove physiologically important signals (Scholvinck et al. 2010).

### ***2.3.3. Statistical analysis:***

For each monkey, spherical seed regions (radius: 2 mm) were selected individually in the medial and lateral FEF of the right and left hemisphere in the T2-weighted anatomic images (Figure 2.1). There was no overlap between medial and lateral FEF seed regions, and the distance between the two seeds was at least 4 mm. The mean time course of the signal for each seed region was extracted for each subject and each scanning session and was used as the regressor in a generalized linear regression analysis. The regression

model included the four seed time series as predictors and also nuisance covariates [6 motion parameters, white matter, and cerebrospinal fluid (CSF)]. Cardiac and respiratory activity was monitored but not recorded during MR image acquisition, and thus white matter and CSF nuisance covariates were included in the model to further regress out the physiological noise from the data. This approach has been previously used to remove physiological noise in human and monkey RS-fMRI studies (Hutchison et al. 2011a, 2011b, 2012; Lund and Hanson 2001; Margulies et al. 2007; Shim et al. 2010). The cardiac rate is in the range of 1–2 Hz, and thus the cardiac signal can be aliased in the RS-fMRI BOLD signal that has a lower frequency (0.01–0.1 Hz). There is no consensus in the literature about the best method of eliminating physiological noise from fMRI data (Churchill et al. 2012). Including the CSF and white matter nuisance covariates in my analysis is one of the preferable methods for physiological noise reduction because it does not interfere with detection of functional activation (Shmueli et al. 2007). However, physiological noise can still affect my results (e.g., due to the different effects of cardiac and respiratory signal on CSF, white matter, and gray matter), although I speculate that the impact of physiological noise on the results is not substantial.

The first level of the analysis was carried out on the individual subjects at each scanning session. In the second level, the analysis results from the first level were normalized to the F99 atlas template (Van Essen 2004) and functional connectivity maps across 10 scans for each monkey were generated by implementing a second-level fixed-effects analysis using the FSL software package ([http://www. fmrib.ox.ac.uk](http://www.fmrib.ox.ac.uk)). The group-level analysis was conducted by implementing a third-level fixed-effects analysis. Corrections for multiple comparisons were performed at the cluster level using Gaussian



random field theory ( $z > 5$ ; cluster significance:  $P < 0.05$ , corrected). It should be noted that the results obtained using the fixed-effects model cannot be extended to the population, and thus the results should be interpreted cautiously (Woolrich et al. 2004). A mixed effects analysis was not carried out due to the low subject number in my study. I also implemented another third-level analysis in which I contrasted medial and lateral FEF to determine whether the connectivity strength of an area is greater with medial or lateral FEF. All group-level  $z$ -score maps were projected from volume data to the F99 cortical surface using the CARET (<http://www.nitrc.org/projects/caret>) enclosed voxel method (Van Essen et al. 2001). The F99 template is from a *Macaca mulatta* but has also been successfully used as a template for *Macaca fascicularis* (Hutchison et al. 2011a, 2011b). A  $z$ -score threshold of 5 was used for the group maps to allow better visualization of the segregation between functionally connected areas. I overlaid a map of cortical subdivision by Van Essen (2004) that has been previously mapped to both hemispheres of the F99 template (<http://sumsdb.wustl.edu/sums/index.jsp>).

#### ***2.3.4. Region-of-interest identification:***

In Table 1, I show the calculated percent connectivity of parietal areas MIP, V6A, and VIP and premotor areas F2, F4, and F5 with medial and lateral FEF, and I provide corresponding statistics. The region of interest (ROI) of areas MIP and VIP are based on anatomic landmarks mentioned in the atlas of Van Essen et al. (2012). The composite atlas of Van Essen et al. (2012) does not include area V6A; the ROIs corresponding to area V6A were defined on the basis of landmarks described by Galletti et al. (1999). Also, because premotor areas in most of the reaching/grasping literature are designated differently than the nomenclature used by Van Essen et al. (2012), ROIs of premotor

areas F2, F4, and F5 were selected on the basis of boundaries defined in the atlas of Markov et al. (2011).

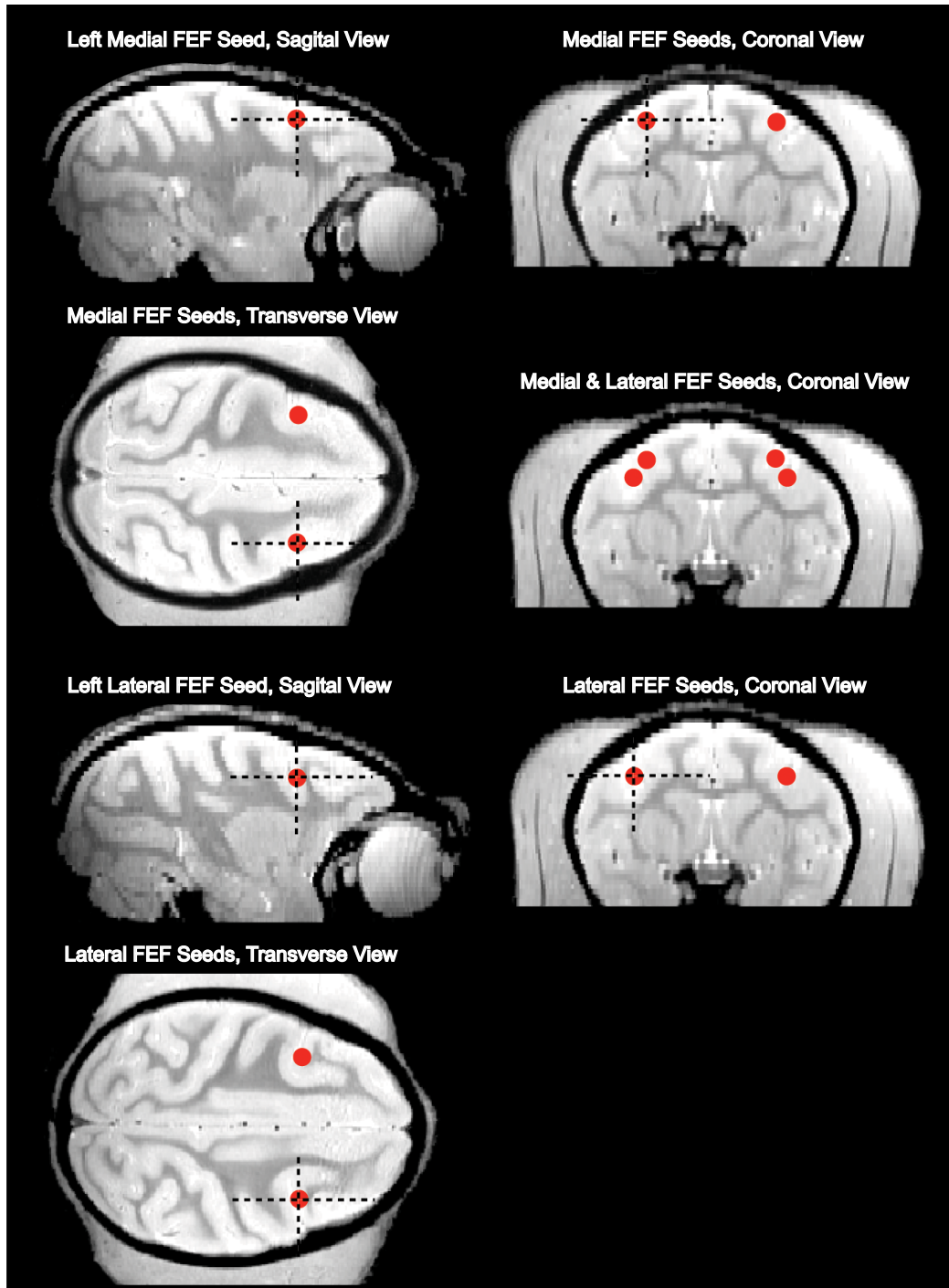


**Figure. 2.1. Location of lateral and medial frontal eye field (FEF) spherical seeds in *monkey 1*. The spherical seed regions have a radius of 2 mm.**

## **2.4. RESULTS:**

I placed spherical seeds in medial FEF regions corresponding to area 8Ac and portions of areas 8Am and 8As, and in lateral FEF regions corresponding to area 6Vam and portions of area 45 (Van Essen et al. 2012) (Figure 2.1). Figure 2.2 shows the FC of the right medial and lateral FEF superimposed on inflated ipsilateral and contralateral cortical surfaces (see Figure. 2.3 for seeds in medial and lateral FEF in the left hemisphere). For a more detailed comparison of the FC and previously identified cytoarchitectonic areas in the macaque, I superimposed the architectonical map by Van Essen et al. (2012) on the flattened cortical surfaces of the left and right hemisphere. Red and green areas indicate regions that displayed FC with medial and lateral FEF, respectively. Areas in yellow indicate overlapping FC between lateral and medial FEF. These connectivity maps for the ipsilateral hemisphere indicate that areas in the intraparietal sulcus (IPS), lateral intraparietal area (LIP), parietal-occipital area (area PO), posterior intraparietal area (PIP), medial dorsal parietal area (MDP), medial intraparietal area (MIP), area 7a, area 5D and dorsomedial areas in V1, V2, V3 are functionally connected to the medial FEF. Area PO has been subdivided into dorsal area V6A and ventral area V6 (Galletti et al. 1996), and I will use the V6A and V6 nomenclature in the rest of this article because of its widespread use in reaching/grasping literature. In the right hemisphere, I found almost no FC of medial FEF with inferotemporal areas, whereas some areas such as TE in the left hemisphere showed FC. Also, I found large areas in the anterior bank of the superior temporal sulcus (STS), dorsal parts of middle temporal area (MT), and medial superior temporal area (MST) that showed positive FC with the medial FEF. Furthermore, the connectivity maps show that medial FEF is functionally connected to the dorsal

somatosensory cortex (areas 1, 2, 3a, and 3b), dorsal primary motor cortex (area 4), dorsal premotor areas (6DR, 6Ds, and 6DC, or area F2 according to the atlas of Markov et al. 2011), and supplementary motor area (SMA). Premotor areas involved in reaching/grasping are most commonly referred to as F2, F4, and F5 in the literature (e.g., see Luppino et al. 1999). Area F2 includes areas 6DC, 6Ds, and 6DR; area F4 encompasses ventral area 4C and caudal portions of areas 6Val and 6Vb; and area F5 includes ventrorostral area 6Val and rostral area 6Vb (Markov et al. 2011) as shown in Figures. 2.4 and 2.5. I will use both terminologies to make it easier to compare my results with existing literature. In the prefrontal cortex, several areas, including ventral area 46 along the principal sulcus, areas 9, 10, and 14, showed FC to the medial FEF. Interestingly, my results show that the medial FEF has strong FC with medial wall of the ipsilateral hemisphere; i.e., medial FEF is connected to parts of the anterior cingulate cortex (ACC) and posterior cingulate cortex (areas 24 and 23, respectively). I also observed negative FC of the right medial FEF with ventral premotor areas, ventral areas in central sulcus, and portions of area V4. In the contralateral hemisphere (Figure 2.2 A), I found contralateral medial FEF functionally connected to the medial FEF seed. The connectivity pattern of the medial FEF seed region in the contralateral hemisphere is very similar to that of the same seed region in the ipsilateral hemisphere. However, the positively correlated areas in the contralateral hemisphere are smaller in their spatial extent than in the ipsilateral hemisphere.

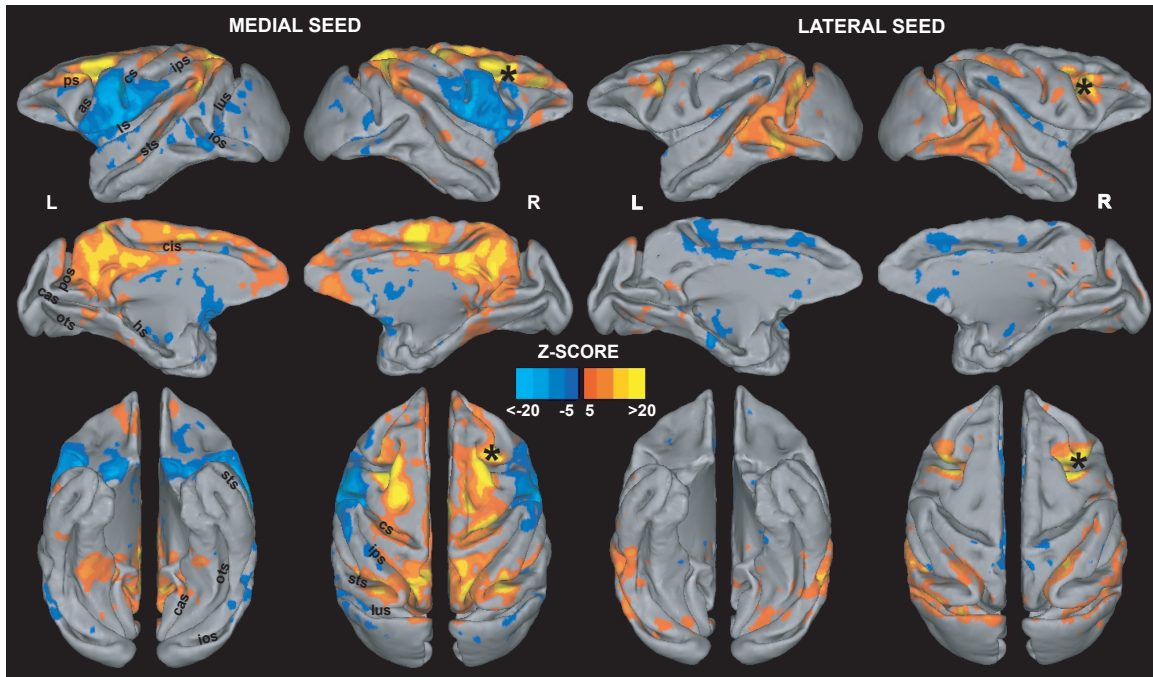


**Figure 2.2. Right medial (*left*) and right lateral (*right*) FEF seed connectivity maps projected on the F99 template (Van Essen 2004) (z-score 5 set at cluster significance of  $P$  0.05, corrected for multiple comparisons). The connectivity maps are shown on lateral, medial, dorsal, and ventral views. Asterisks show the location of the seed region. pos, Parieto-occipital sulcus; cas, calcarine sulcus; cs, central sulcus; hs, hippocampal sulcus; cis, cingulate sulcus; sts, superior temporal sulcus; ios, inferior occipital sulcus; lus, lunate sulcus; ots, occipitotemporal sulcus; ps, principal sulcus; L, left; R, right.**

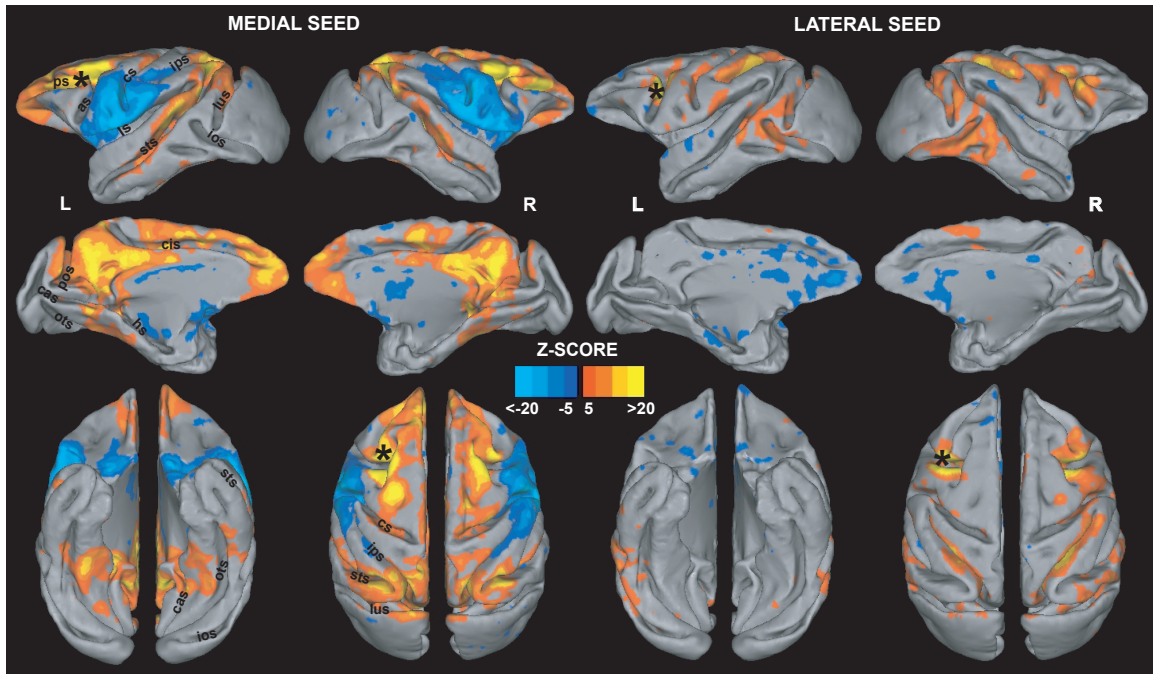


**Figure 2.3.** Left medial (*left*) and right lateral (*right*) FEF seed connectivity maps projected on the F99 template (Van Essen 2004) ( $z$ -score 5 set at cluster significance of  $P$  0.05, corrected for multiple comparisons). The connectivity maps are shown on lateral, medial, dorsal, and ventral views. Asterisks show the location of the seed region.

Lateral FEF in the ipsilateral hemisphere is positively correlated with ventrolateral areas in the central sulcus, area 7t, anterior intraparietal area (AIP), area LIP, and ventral intraparietal area (VIP). It should be noted that rostral LIP displayed higher FC with lateral FEF than with medial FEF. In the visual cortex, ventrolateral areas in V1, V2, V3, and a large portion of V4 and the ventral posterior area (VP) showed FC with the lateral FEF. In the left hemisphere, I also found strong FC with inferotemporal areas, such as TE and ventral occipitotemporal area (VOT). In addition, ventral premotor areas exhibited FC with the lateral FEF. In the contralateral hemisphere, I observed almost the same areas as in the ipsilateral hemisphere that are functionally connected to the lateral FEF seed. Negatively correlated areas with the lateral FEF seed were found within the cingulate cortex, lateral sulcus, and small areas in the parahippocampal cortex.

Although the FC of medial and lateral FEF differed substantially, I also found overlapping FC between lateral and medial FEF (yellow areas in Figure 2.4). Overlapping FC was present in portions of areas 4C and 6Ds, corresponding to premotor area F4, caudal area LIP, lateral occipital parietal area (LOP), dorsal areas in the IPS such as VIP, area V3A, and small areas in the MST. I have quantified the overlap in FC for several key parietal and premotor areas in Table 1. Little overlap was found for negatively correlated areas (Figure 2.5).



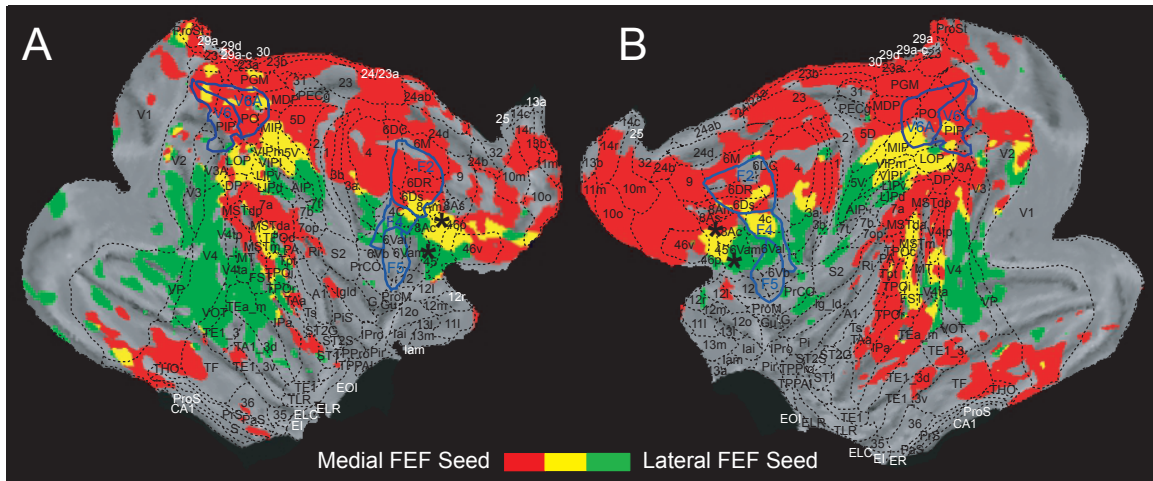


**Figure 2.4. Cortical views of both hemispheres flattened to display spatial overlap connectivity patterns of right medial and lateral FEF (A) and left medial and lateral FEF (B).** Images show the connectivity pattern of the positively functionally connected areas ( $z$ -score 5 set at cluster significance of  $P$  0.05, corrected for multiple comparisons). Areas in red are functionally connected to the medial FEF, areas in green are functionally connected to the lateral FEF, and areas in yellow are functionally connected to both. White lines indicate the boundaries of parietal areas V6 and V6A according to Galletti et al. (1999) and also premotor areas F2, F4, and F5 according to Markov et al. (2011). Asterisks show the location of the seed regions.

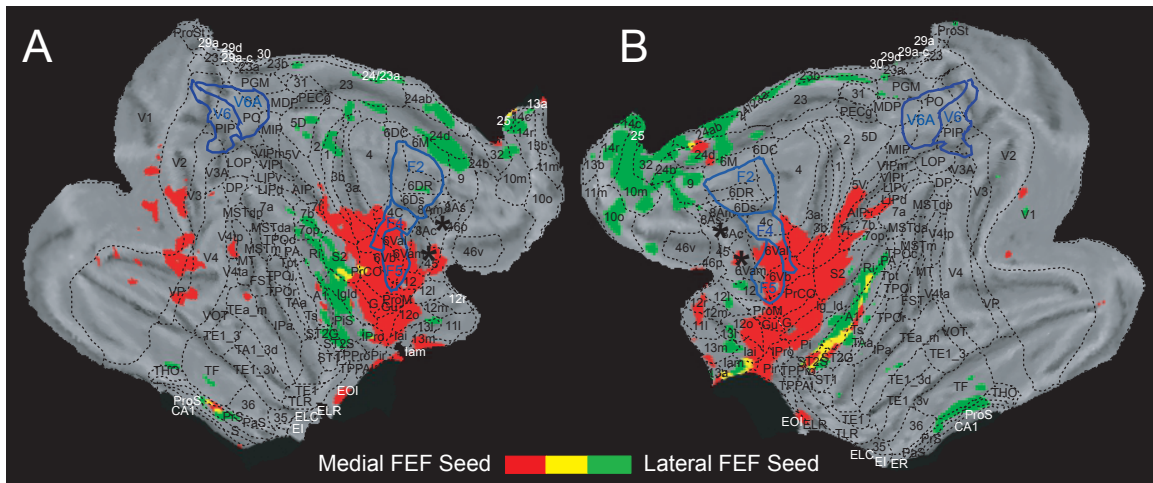


**Figure 2.5. Cortical views of both hemispheres flattened to display spatial overlap connectivity patterns of right medial and lateral FEF (A) and left medial and lateral FEF (B).** Images show the connectivity pattern of the negatively functionally connected areas ( $z$ -score 5 set at cluster significance of  $P$  0.05, corrected for multiple comparisons). Areas in red are negatively connected to the medial FEF, areas in green are negatively connected to the lateral FEF, and areas in yellow are negatively connected to both. White lines indicate the boundaries of parietal areas V6 and V6A according to Galletti et al. (1999) and also premotor areas F2, F4, and F5 according to Markov et al. (2011). Asterisks show the location of the seed regions.

Table 1.1.

Statistical analysis and percentage connectivity of FEF seed regions with parietal and premotor areas

	Posterior Parietal Cortex				Premotor Cortex		
	MIP	V6A	VIP	AIP	F2	F4	F5
Medial FEF > Lateral FEF (z-score)	3.5*	1.96	0.09	0	4.06*	0.59	0
Lateral FEF > Medial FEF (z-score)	0.02	0.22	4.88*	11.98*	0.38	7.95*	7.96*
% Connectivity to medial FEF seed	74.66	71	42.8	3	94.75	35	0
% Connectivity to lateral FEF seed	25.34	29	57.2	97	5.25	65	100

Note: \*: statistically significant. % Connectivity to medial FEF seed =  $(Z_m / (Z_m + Z_l)) * 100$ . % Connectivity to lateral FEF seed =  $(Z_l / (Z_m + Z_l)) * 100$ .  $Z_m$ : Mean connectivity z-score to medial FEF seed.  $Z_l$ : Mean connectivity z-score to lateral FEF seed

Both the medial and lateral seeds were negatively correlated with the caudate nucleus and the rostral putamen (Figure 2.6 at 0–10 mm anterior to the anterior commissure). Positive correlations were found in the caudal putamen and globus pallidus (Figure 2.6 at 5 and 10 mm posterior to the anterior commissure). There also were bilateral positive correlations of the medial FEF seed with regions 20 mm posterior to the anterior commissure, which might correspond to the superior colliculi, although the regions are located slightly too far dorsally for accurate identification.

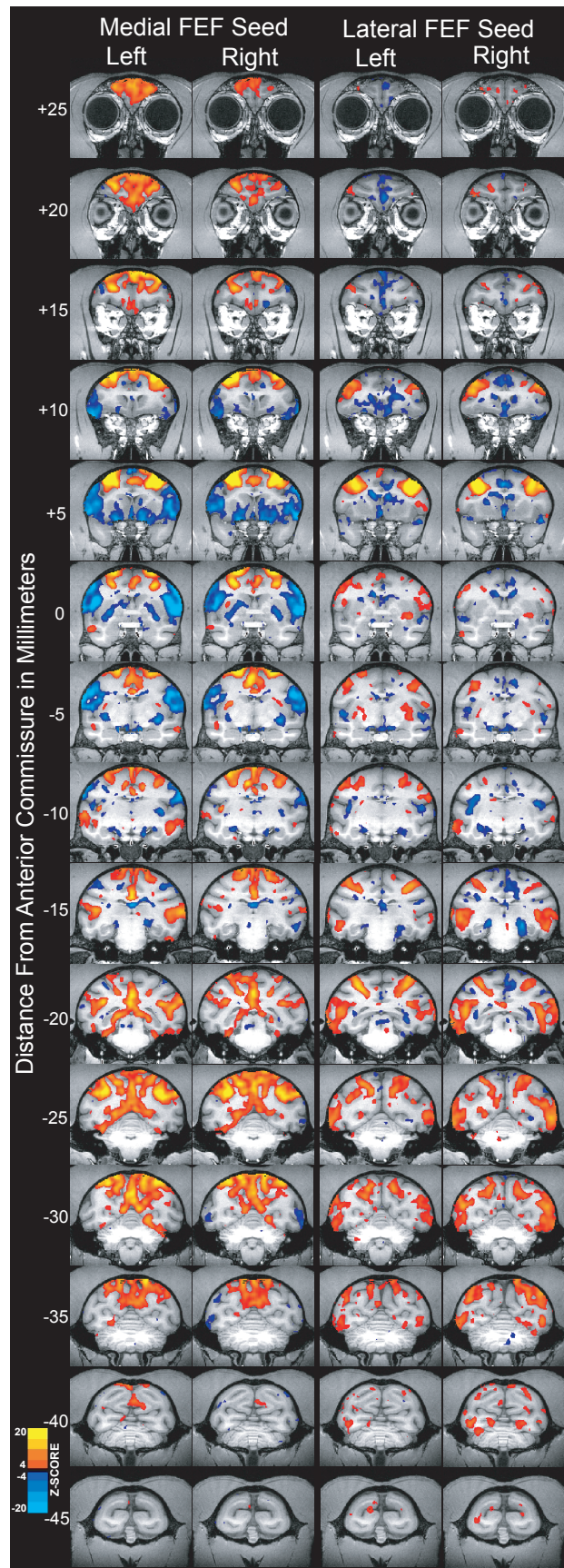


**Figure 2.6. Coronal slices of the functional connectivity patterns of medial and lateral FEF on F99 atlas** (Van Essen 2004) as indicated at *top*. Red-yellow areas are positively correlated areas, and blue-light blue areas are negatively correlated areas ( $z$ -score 4 set at cluster significance of  $P$  0.05, corrected for multiple comparisons).

## **2.5. DISCUSSION:**

Behavioral studies have demonstrated that small and large saccades have different functions during vision in natural environments (Foerster et al. 2012; Hayhoe et al. 2003; Johansson et al. 2001; Land et al. 1999; Land 2009). Large saccades are associated with reaching and trunk movements toward objects, whereas small saccades likely promote the identification of more detailed object features for successful grasping and manual manipulation. In the present study I used RS-fMRI in the macaque to test the hypothesis that this tight temporal coupling is reflected in the FC of medial and lateral FEF regions, which encode large- and small-amplitude saccades, respectively (Bruce et al. 1985; Robinson and Fuchs 1969). I found that the spontaneous BOLD signal of areas known to be involved in reaching movements and executive control processes were more functionally connected with medial FEF than with lateral FEF, whereas cortical areas involved in object processing and in grasping, fixation, and manipulation of objects showed stronger FC to lateral FEF than to medial FEF. The results critically extend a previous RS-fMRI study that only placed a single seed region in the FEF (Hutchison et al. 2012; Vincent et al. 2007) and previous traditional tracer studies (Schall et al. 1995; Stanton et al. 1993, 1995) and suggest that the FC of lateral and medial FEF reflect the different behavioral roles of small and large saccades in natural vision.

The limited visual acuity of the peripheral retina in primates necessitates gaze shifts that bring the high-resolution fovea onto ROIs (Gilchrist 2012). Gaze shifts toward targets of more than 20° in amplitude also require a contribution of the head (Freedman and Sparks 1997). In many cases, gaze shifts do not just serve a visual search function but provide the necessary location information for a subsequent reaching movement. In the

present study I found that medial FEF is functionally correlated with parietal areas (e.g., PIP, MDP, MIP, 7a, V6A, and 5D) and dorsal premotor areas (6DR, 6Ds, and 6DC, or area F2) that are known to be involved in reaching movements in macaques (Fattori et al. 2001; Grefkes and Fink 2005; Wise et al. 1997). I also found FC of medial FEF with cingulate areas (areas 23 and 24) and dorsal primary motor cortex, dorsal somatosensory cortex, and supplementary motor cortex that contain proximal and distal representations of the arm (Dum and Strick 2002; Strick et al. 1998). For visual areas, FC was found with V1, V2, V3, MT, and MST. This FC of medial FEF is consistent with the tight temporal coupling of large saccades and arm movements in eye-hand coordination (Angel et al. 1970; Biguer et al. 1982; Gribble et al. 2002; Prablanc et al. 1979). In addition, I observed strong FC of medial FEF with areas in prefrontal cortex (46, 9, 10, and 14) that are involved in executive control (Fuster 2008). Whereas “free viewing” experiments have shown that salient visual features such as color, intensity, contrast, and sudden onsets influence the selection of saccade targets (Itti and Koch 2000), studies that have investigated gaze behavior under natural conditions have demonstrated that behavioral goals play a more dominant role in determining the distribution of gaze (Ballard and Hayhoe 2009; Tatler et al. 2011). Land (2009) has proposed that the dorsolateral prefrontal cortex is associated with setting and reprogramming these behavioral goals that determine the location of gaze and reaching movements. In addition, I found FC of the medial FEF seed with areas in the posterior, medial, and anterior cingulate cortex that are known to have reward, performance, and outcome-monitoring activity (Amiez et al. 2006a; Emeric et al. 2008; Hayden et al. 2008; Ito et al. 2003; McCoy et al. 2003; Shima and Tanji 1998). Strong FC of medial FEF with these areas is consistent with the



framework proposed by Tatler et al. (2011) in which gaze is allocated on the basis of reward maximization.

The FC of lateral FEF was consistent with the functional role of small saccades in vision and action in natural environments. In addition to early visual areas such as V1, V2, and V3, lateral FEF was functionally correlated to V4 and areas such as TEa and VOT in the caudal inferior temporal cortex that show color and orientation selectivity (Desimone and Schein 1987; Nakamura et al. 1994). I also found that lateral FEF had FC with parietal area AIP and ventral premotor area F5, and interestingly, areas AIP and F5 are reciprocally connected (Rizzolatti and Luppino 2001). Area AIP is considered a part of the lateral-dorsal stream (Galletti et al. 2003). This area contains neurons that code for specific kinds of grasping or manipulation movements and that have visual responses that may be encoding three-dimensional object characteristics (Murata et al. 2000; Sakata et al. 1995). A direct role of area AIP in grasping has been demonstrated by transient inactivation of the area in monkeys, which impairs the appropriate hand posture toward grasped objects (Gallese et al. 1994). Interestingly, fMRI studies have suggested that there might be an area homologous to macaque AIP in humans (Cavina-Pratesi et al. 2007; Culham et al. 2003).

As mentioned before, lateral FEF displayed FC with ventral premotor cortex (such as F5) that contains different classes of grasp-related neurons (Raos et al. 2006). Inactivation of area F5 in the posterior bank of the arcuate sulcus impairs the appropriate shaping of the hands during the grasping of objects (Fogassi et al. 2001). A direct role for ventral premotor cortex in saccade control has been demonstrated by Fuji et al. (1998), who found a subregion on the gyral surface of the premotor cortex where saccades could

be evoked by electrical micro- stimulation and where neurons were active during saccade tasks without arm movements.

The concept of two parallel processing streams within the dorsal visual stream (Jeannerod et al. 1995) has been challenged and discussed recently (Fattori et al. 2010; Galletti et al. 2003; Mon-Williams and McIntosh 2000; Rizzolatti and Matelli 2003; Smeets and Brenner 1999). Although my results provide support for the existence of two substreams within the dorsal visual stream, there is a substantial overlap in FC between these two substreams (see Table 1). For instance, lateral FEF still exhibits weak FC with the medial parietal and dorsal premotor areas (Table 1). This finding has been supported by recent electrophysiological studies in monkeys. Fattori et al. (2010) found grasping neurons in V6A, and also area F2 has been shown to contain neurons with distal as well as proximal forelimb movement fields (Raos et al. 2003). Based on the present results, it can be posited that FC of the lateral and medial FEF with reaching/grasping areas falls into a continuum; medial parietal areas are more strongly connected with medial rather than lateral FEF, whereas lateral parietal areas are highly connected to the lateral FEF. Area VIP that is located in between medial and lateral parietal areas is functionally connected to both medial and lateral FEF. The same argument can be made regarding the FC of FEF with dorsal and ventral premotor areas. Area F2 is functionally connected to medial FEF more strongly than to lateral FEF, area F5 displays higher FC to lateral FEF, and area F4 is functionally connected to both FEF regions.

The results show that area LIP in the parietal cortex is also connected to both medial and lateral FEF. Microstimulation of the rostral area LIP triggers saccades in craniocentric rather than retinotopic coordinates (Kurylo and Skavenski 1991). Such a

craniocentric coding has also been observed in the ventral premotor cortex (Fujii et al. 1998). Interestingly, I found that rostral area LIP was also functionally connected to the small saccade region of FEF, whereas I found that the more caudal region showed FC with both medial and lateral FEF seeds.

Within subcortical areas, I observed significant positive FC between the caudal putamen and FEF. Interestingly, there is evidence from anatomic tracing studies that FEF projects to the caudal putamen in monkeys (Parthasarathy et al. 1992; Stanton et al. 1988). These projections might have a role in saccade control as well as in hand movements. In support of this notion, saccade-related and saccade outcome-related activity has recently been reported in the caudal macaque putamen (Phillips and Everling 2012), and Ueda and Kimura (2003) have proposed that the putamen may be involved in visuospatial processing of hand movements. I also observed that both medial and lateral FEF have negative FC with the caudate nucleus and the rostral putamen. Although still poorly understood, spontaneous anti-correlated activity at rest has been suggested to exist between systems with oppositely signed responses during task performance (Fox et al. 2009). However, previous studies have demonstrated that the caudate nucleus facilitates saccades (Hikosaka et al. 2000), whereas I found that the caudate had negative correlation with FEF. Further studies are needed to reveal the neural mechanisms underlying anti-correlated RS-fMRI activity.

FC as identified by RS-fMRI is based on the correlations of spontaneous low-frequency fluctuations of the BOLD fMRI signals between different brain areas and as such does not necessarily indicate that functionally connected brain areas are also anatomically linked by monosynaptic connections. However, systematic studies that

compare RS-fMRI FC with a large set of data from tracer studies in macaques have shown that FC patterns in RS-fMRI are dictated by the underlying neuroanatomic architecture (Adachi et al. 2012; Shen et al. 2012). This observation is consistent with an earlier RS-fMRI study that had placed a single seed in FEF and reported positive FC with known anatomically connected areas in the posterior and frontal cortex (Hutchison et al. 2012) and strong anti-correlated FC with areas in the lateral sulcus.

Resting-state FC maps could be affected by a variety of factors. For instance, if the physiological noise originating from cardiac and respiratory activity is not removed from the data, it would substantially affect the FC maps. Moreover, anesthesia can alter resting-state FC; for instance, it has been shown that the FC of posterior cingulate cortex in the default mode network was decreased under propofol (Boveroux et al. 2010) and sevoflurane administration (Martuzzi et al. 2010). Moreover, activity in executive control networks has been shown to be decreased under anesthesia (Boveroux et al. 2010). Animal studies have also shown that resting-state FC changes under anesthesia, and it has been posited that different levels of anesthesia change the specificity of FC maps (Liu et al. 2013). However, the same study has shown that the BOLD signal correlation is strongest between bilateral homotopic brain regions, even under deep anesthesia (Liu et al. 2013). Vanhaudenhuyse et al. (2010) have suggested that reductions in FC could be interpreted as reduced capacity for cognitive processing. The alternative explanation could be that although anesthesia can alter the resting-state FC, the physiologic “baseline” FC still persists regardless of the altered level of consciousness. This idea has been supported in previous RS-fMRI studies (e.g., Raichle et al. 2001). Similarly, Vincent et al. (2007) have shown that the coherent spontaneous BOLD fluctuations in the

monkey oculomotor system persist during light and deep anesthesia. Furthermore, resting-state FC that has been acquired in anesthetized monkeys corresponds well with the anatomic connectivity between brain areas, as mentioned above (Hutchison et al. 2012; Shen et al. 2012). In the present study, I have acquired the functional images under 1% isoflurane anesthesia, which is defined as light anesthesia (Vincent et al. 2007), minimizing the effects on resting-state FC.

The distinct FC pattern of medial and lateral FEF with other cortical areas is in good agreement with the results from anatomic tracer studies. A retrograde tracer study reported that lateral FEF projected to V3, V4, V4T, TE, FST, MT, MST, and rostral LIP, whereas medial FEF innervated V2, VIP, 23b, MDP, DP, 7a, and caudal LIP (Stanton et al. 1995). A similar anatomic connectivity pattern has been described for projections from posterior areas to FEF (Schall et al. 1995). Overall, that study demonstrated that medial FEF receives projections predominately from posterior regions representing the peripheral visual field, whereas lateral FEF receives inputs from areas that encode the central visual field (Schall et al. 1995). The FC patterns are also similar to the anatomic connectivity of FEF with frontal regions (Stanton et al. 1993), with the exception of the supplementary eye fields (6DR), which receive projections from medial and lateral FEF but which only showed FC with medial FEF. Functionally connected areas in the hemisphere contralateral to the seed ROIs were smaller in spatial extent compared with functionally connected areas in the ipsilateral hemisphere. Although it is possible that physiological noise may contribute to this finding, it is more likely that the finding has a neural origin. Anatomic tracing studies have posited that connectivity in the contralateral hemisphere is commonly restricted to geographically and architectonically homotopic

areas of the cortex (e.g., see Lewis and Van Essen 2000). Thus, the FC with contralateral heterotopic areas is likely polysynaptic, and this may explain the smaller functionally connected areas in the contralateral hemisphere.

The medial FEF network contained areas of the medial-dorsal stream, and the lateral FEF network included areas in the lateral-dorsal processing stream as well as areas in the ventral visual stream. Therefore, I speculate that the organization of these two networks reflects the alternating phases of vision for action in natural environments: a reorienting phase that is usually based on behavioral goals and which involves the generation of a large saccade or eye-head movement together with a reaching movement of the arm and a subsequent detailed object processing phase that involves small saccades, grasping, and manual manipulation.

## **2.6. REFERENCES:**

**Adachi Y, Osada T, Sporns O, Watanabe T, Matsui T, Miyamoto K, Miyashita Y.** Functional connectivity between anatomically unconnected areas is shaped by collective network-level effects in the macaque cortex. *Cereb Cortex* 22: 1586–1592, 2012.

**Amiez C, Joseph JP, Procyk E.** Reward encoding in the monkey anterior cingulate cortex. *Cereb Cortex* 16: 1040–1055, 2006a.

**Amiez C, Kostopoulos P, Champod AS, Petrides M.** Local morphology predicts functional organization of the dorsal premotor region in the human brain. *J Neurosci* 26: 2724–2731, 2006b.

**Angel RW, Alston W, Garland H.** Functional relations between the manual and oculomotor control systems. *Exp Neurol* 27: 248–257, 1970.

**Bahill AT, Clar MR, Stark L.** The main sequence, a tool for studying human eye movements. *Math Biosci* 24: 191–204, 1975.

**Ballard DH, Hayhoe MM.** Modelling the role of task in the control of gaze. *Vis Cogn* 17: 1185–1204, 2009.

**Biguer B, Jeannerod M, Prablanc C.** The coordination of eye, head, and arm movements during reaching at a single visual target. *Exp Brain Res* 46: 301–304, 1982.

**Boveroux P, Vanhaudenhuyse A, Bruno MA, Noirhomme Q, Lauwick S, Luxen A, Degueldre C, Plenevaux A, Schnakers C, Phillips C, Brichant JF, Bonhomme V, Maquet P, Greicius MD, Laureys S, Boly M.** Breakdown of within- and between-network resting state functional magnetic resonance imaging connectivity during propofol-induced loss of consciousness. *Anesthesiology* 113: 1038–1053, 2010.

**Bruce CJ, Goldberg ME.** Primate frontal eye fields. I. Single neurons discharging before saccades. *J Neurophysiol* 53: 603–635, 1985.

**Bruce CJ, Goldberg ME, Bushnell MC, Stanton GB.** Primate frontal eye fields. II. Physiological and anatomical correlates of electrically evoked eye movements. *J Neurophysiol* 54: 714–734, 1985.

**Cavina-Pratesi C, Goodale MA, Culham JC.** fMRI reveals a dissociation between grasping and perceiving the size of real 3D objects. *PLoS One* 2: e424, 2007.

**Churchill NW, Oder A, Abdi H, Tam F, Lee W, Thomas C, Ween JE, Graham SJ, Strother SC.** Optimizing preprocessing and analysis pipelines for single-subject fMRI. I. Standard temporal motion and physiological noise correction methods. *Hum Brain Mapp* 33: 609–627, 2012.

**Culham JC, Danckert SL, DeSouza JF, Gati JS, Menon RS, Goodale MA.** Visually guided grasping produces fMRI activation in dorsal but not ventral stream brain areas. *Exp Brain Res* 153: 180–189, 2003.

**Davare M, Kraskov A, Rothwell JC, Lemon RN.** Interactions between areas of the cortical grasping network. *Curr Opin Neurobiol* 21: 565–570, 2011.

**Desimone R, Schein SJ.** Visual properties of neurons in area V4 of the macaque: sensitivity to stimulus form. *J Neurophysiol* 57: 835–868, 1987.

**Dum RP, Strick PL.** Motor areas in the frontal lobe of the primate. *Physiol Behav* 77: 677–682, 2002.

**Elsley JK, Nagy B, Cushing SL, Corneil BD.** Widespread presaccadic recruitment of neck muscles by stimulation of the primate frontal eye fields. *J Neurophysiol* 98: 1333–1354, 2007.

**Emeric EE, Brown JW, Leslie M, Pouget P, Stuphorn V, Schall JD.** Performance monitoring local field potentials in the medial frontal cortex of primates: anterior cingulate cortex. *J Neurophysiol* 99: 759–772, 2008.

**Farber NE, Harkin CP, Niedfeldt J, Hudetz AG, Kampine JP, Schmeling WT.** Region-specific and agent-specific dilation of intracerebral microvessels by volatile anesthetics in rat brain slices. *Anesthesiology* 87: 1191–1198, 1997.

**Fattori P, Raos V, Breveglieri R, Bosco A, Marzocchi N, Galletti C.** The dorsomedial pathway is not just for reaching: grasping neurons in the medial parieto-occipital cortex

of the macaque monkey. *J Neurosci* 30: 342–349, 2010.

**Fattori P, Gamberini M, Kutz DF, Galletti C.** ‘Arm-reaching’ neurons in the parietal area V6A of the macaque monkey. *Eur J Neurosci* 13: 2309–2313, 2001.

**Foerster RM, Carbone E, Koesling H, Schneider WX.** Saccadic eye movements in the dark while performing an automatized sequential high-speed sensorimotor task. *J Vis* 12: 2012.

**Fogassi L, Gallese V, Buccino G, Craighero L, Fadiga L, Rizzolatti G.** Cortical mechanism for the visual guidance of hand grasping movements in the monkey: A reversible inactivation study. *Brain* 124: 571–586, 2001.

**Fox MD, Raichle ME.** Spontaneous fluctuations in brain activity observed with functional magnetic resonance imaging. *Nat Rev Neurosci* 8: 700–711, 2007.

**Fox MD, Zhang D, Snyder AZ, Raichle ME.** The global signal and observed anticorrelated resting state brain networks. *J Neurophysiol* 101: 3270–3283, 2009.

**Freedman EG, Sparks DL.** Eye-head coordination during head-unrestrained gaze shifts in rhesus monkeys. *J Neurophysiol* 77: 2328–2348, 1997.

**Fujii N, Mushiake H, Tanji J.** An oculomotor representation area within the ventral premotor cortex. *Proc Natl Acad Sci USA* 95: 12034–12037, 1998.

**Fuster J.** *The Prefrontal Cortex*. London: Elsevier, 2008.

**Gallese V, Murata A, Kaseda M, Niki N, Sakata H.** Deficit of hand preshaping after muscimol injection in monkey parietal cortex. *Neuroreport* 5: 1525–1529, 1994.

**Galletti C, Fattori P, Battaglini PP, Shipp S, Zeki S.** Functional demarcation of a border between areas V6 and V6A in the superior parietal gyrus of the macaque monkey. *Eur J Neurosci* 8: 30–52, 1996.

**Galletti C, Fattori P, Gamberini M, Kutz DF.** The cortical visual area V6: brain location and visual topography. *Eur J Neurosci* 11: 3922–3936, 1999.

**Galletti C, Kutz DF, Gamberini M, Breveglieri R, Fattori P.** Role of the medial parieto-occipital cortex in the control of reaching and grasping movements. *Exp Brain Res* 153: 158–170, 2003.

**Gilchrist ID.** Saccades. In: *The Oxford Handbook of Eye Movements*, edited by Liversedge SP, Gilchrist ID, and Everling S. Oxford: Oxford University Press, 2012, p. 85–94.

**Grefkes C, Fink GR.** The functional organization of the intraparietal sulcus in humans and monkeys. *J Anat* 207: 3–17, 2005.



**Greicius M.** Resting-state functional connectivity in neuropsychiatric disorders. *Curr Opin Neurol* 21: 424–430, 2008.

**Greicius MD, Supekar K, Menon V, Dougherty RF.** Resting-state functional connectivity reflects structural connectivity in the default mode network. *Cereb Cortex* 19: 72–78, 2009.

**Gribble PL, Everling S, Ford K, Mattar A.** Hand-eye coordination for rapid pointing movements. Arm movement direction and distance are specified prior to saccade onset. *Exp Brain Res* 145: 372–382, 2002.

**Hayden BY, Nair AC, McCoy AN, Platt ML.** Posterior cingulate cortex mediates outcome-contingent allocation of behavior. *Neuron* 60: 19–25, 2008.

**Hayhoe MM, Shrivastava A, Mruczek R, Pelz JB.** Visual memory and motor planning in a natural task. *J Vis* 3: 49–63, 2003.

**Hikosaka O, Takikawa Y, Kawagoe R.** Role of the basal ganglia in the control of purposive saccadic eye movements. *Physiol Rev* 80: 953–978, 2000.

**Honey CJ, Sporns O, Cammoun L, Gigandet X, Thiran JP, Meuli R, Hagmann P.** Predicting human resting-state functional connectivity from structural connectivity. *Proc Natl Acad Sci USA* 106: 2035–2040, 2009.

**Hutchison RM, Everling S.** Monkey in the middle: why non-human primates are needed to bridge the gap in resting-state investigations. *Front Neuroanat* 6: 29, 2012.

**Hutchison RM, Gallivan JP, Culham JC, Gati JS, Menon RS, Everling S.** Functional connectivity of the frontal eye fields in humans and macaque monkeys investigated with resting-state fMRI. *J Neurophysiol* 107: 2463–2474, 2012.

**Hutchison RM, Womelsdorf T, Gati JS, Everling S, Menon RS.** Resting-state networks show dynamic functional connectivity in awake humans and anesthetized macaques. *Hum Brain Mapp.* In press.

**Hutchison RM, Leung LS, Mirsattari SM, Gati JS, Menon RS, Everling S.** Resting-state networks in the macaque at 7 T. *Neuroimage* 56: 1546–1555, 2011a.

**Hutchison RM, Womelsdorf T, Gati JS, Leung LS, Menon RS, Everling S.** Resting-state connectivity identifies distinct functional networks in macaque cingulate cortex. *Cereb Cortex* 22: 1294–1308, 2011b.

**Ito S, Stuphorn V, Brown JW, Schall JD.** Performance monitoring by the anterior cingulate cortex during saccade countermanding. *Science* 302: 120–122, 2003.

**Itti L, Koch C.** A saliency-based search mechanism for overt and covert shifts of visual attention. *Vision Res* 40: 1489–1506, 2000.

**Jeannerod M, Arbib MA, Rizzolatti G, Sakata H.** Grasping objects: the cortical mechanisms of visuomotor transformation. *Trends Neurosci* 18: 314–320, 1995.

**Johansson RS, Westling G, Backstrom A, Flanagan JR.** Eye-hand coordination in object manipulation. *J Neurosci* 21: 6917–6932, 2001.

**Johnston K, Everling S.** Neurophysiology and neuroanatomy of reflexive and voluntary saccades in non-human primates. *Brain Cogn* 68: 271–283, 2008.

**Kurylo DD, Skavenski AA.** Eye movements elicited by electrical stimulation of area PG in the monkey. *J Neurophysiol* 65: 1243–1253, 1991.

**Land M, Mennie N, Rusted J.** The roles of vision and eye movements in the control of activities of daily living. *Perception* 28: 1311–1328, 1999.

**Land MF.** Vision, eye movements, and natural behavior. *Vis Neurosci* 26: 51–62, 2009.

**Land MF, Hayhoe M.** In what ways do eye movements contribute to everyday activities? *Vision Res* 41: 3559–3565, 2001.

**Leopold DA, Maier A.** Ongoing physiological processes in the cerebral cortex. *Neuroimage* 62: 2190–2200, 2011.

**Lewis JW, Van Essen DC.** Corticocortical connections of visual, sensorimotor, and multimodal processing areas in the parietal lobe of the macaque monkey. *J Comp Neurol* 428: 112–137, 2000.

**Liu X, Zhu XH, Zhang Y, Chen W.** The change of functional connectivity specificity in rats under various anesthesia levels and its neural origin. *Brain Topogr.* 26: 363–77, 2013.

**Luna B, Thulborn KR, Strojwas MH, McCurtain BJ, Berman RA, Genovese CR, Sweeney JA.** Dorsal cortical regions subserving visually guided saccades in humans: an fMRI study. *Cereb Cortex* 8: 40–47, 1998.

**Lund TE, Hanson LG.** Physiological noise reduction in fMRI using vessel time-series as covariates in a general linear model. *Proceedings of the International Society of Magnetic Resonance in Medicine, 9th Annual Meeting.* Glasgow, UK: ISMRM, 2001, p. 22.

**Luppino G, Murata A, Govoni P, Matelli M.** Largely segregated parieto- frontal connections linking rostral intraparietal cortex (areas AIP and VIP) and the ventral premotor cortex (areas F5 and F4). *Exp Brain Res* 128: 181–187, 1999.

**Margulies DS, Kelly AM, Uddin LQ, Biswal BB, Castellanos FX, Milham MP.** Mapping the functional connectivity of anterior cingulate cortex. *Neuroimage* 37: 579–588, 2007.

**Markov NT, Misery P, Falchier A, Lamy C, Vezoli J, Quilodran R, Gariel MA,**

**Giroud P, Ercsey-Ravasz M, Pilaz LJ, Huissoud C, Barone P, Dehay C, Toroczkai Z, Van Essen DC, Kennedy H, Knoblauch K.** Weight consistency specifies regularities of macaque cortical networks. *Cereb Cortex* 21: 1254–1272, 2011.

**Martuzzi R, Ramani R, Qiu M, Rajeevan N, Constable RT.** Functional connectivity and alterations in baseline brain state in humans. *Neuroimage* 49: 823–834, 2010.

**McCoy AN, Crowley JC, Haghighian G, Dean HL, Platt ML.** Saccade reward signals in posterior cingulate cortex. *Neuron* 40: 1031–1040, 2003. **Menon V.** Large-scale brain networks and psychopathology: a unifying triple network model. *Trends Cogn Sci* 15: 483–506, 2011.

**Mon-Williams M, McIntosh RD.** A test between two hypotheses and a possible third way for the control of prehension. *Exp Brain Res* 134: 268–273, 2000.

**Murata A, Gallese V, Luppino G, Kaseda M, Sakata H.** Selectivity for the shape, size, and orientation of objects for grasping in neurons of monkey parietal area AIP. *J Neurophysiol* 83: 2580–2601, 2000.

**Murphy K, Birn RM, Handwerker DA, Jones TB, Bandettini PA.** The impact of global signal regression on resting state correlations: are anti-correlated networks introduced? *Neuroimage* 44: 893–905, 2009.

**Nakamura K, Matsumoto K, Mikami A, Kubota K.** Visual response properties of single neurons in the temporal pole of behaving monkeys. *J Neurophysiol* 71: 1206–1221, 1994.

**Parthasarathy HB, Schall JD, Graybiel AM.** Distributed but convergent ordering of corticostriatal projections: analysis of the frontal eye field and the supplementary eye field in the macaque monkey. *J Neurosci* 12: 4468–4488, 1992.

**Paus T.** Location and function of the human frontal eye-field: a selective review. *Neuropsychologia* 34: 475–483, 1996.

**Phillips JM, Everling S.** Neural activity in the macaque putamen associated with saccades and behavioral outcome. *PLoS One* 7: e51596, 2012.

**Prablanc C, Echallier JF, Komilis E, Jeannerod M.** Optimal response of eye and hand motor systems in pointing at a visual target. I. Spatio-temporal characteristics of eye and hand movements and their relationships when varying the amount of visual information. *Biol Cybern* 35: 113–124, 1979.

**Raichle ME, MacLeod AM, Snyder AZ, Powers WJ, Gusnard DA, Shulman GL.** A default mode of brain function. *Proc Natl Acad Sci USA* 98: 676–682, 2001.

**Raos V, Franchi G, Gallese V, Fogassi L.** Somatotopic organization of the lateral part of area F2 (dorsal premotor cortex) of the macaque monkey. *J Neurophysiol* 89: 1503–1518, 2003.

**Raos V, Umiltà MA, Murata A, Fogassi L, Gallese V.** Functional properties of grasping-related neurons in the ventral premotor area F5 of the macaque monkey. *J Neurophysiol* 95: 709–729, 2006.

**Rizzolatti G, Luppino G.** The cortical motor system. *Neuron* 31: 889–901, 2001.

**Rizzolatti G, Matelli M.** Two different streams form the dorsal visual system: anatomy and functions. *Exp Brain Res* 153: 146–157, 2003.

**Robinson DA, Fuchs AF.** Eye movements evoked by stimulation of frontal eye fields. *J Neurophysiol* 32: 637–648, 1969.

**Sakata H, Taira M, Murata A, Mine S.** Neural mechanisms of visual guidance of hand action in the parietal cortex of the monkey. *Cereb Cortex* 5: 429–438, 1995.

**Schall JD, Morel A, King DJ, Bullier J.** Topography of visual cortex connections with frontal eye field in macaque: convergence and segregation of processing streams. *J Neurosci* 15: 4464–4487, 1995.

**Scholvinck ML, Maier A, Ye FQ, Duyn JH, Leopold DA.** Neural basis of global resting-state fMRI activity. *Proc Natl Acad Sci USA* 107: 10238–10243, 2010.

**Shen K, Bezgin G, Hutchison RM, Gati JS, Menon RS, Everling S, McIntosh AR.** Information processing architecture of functionally defined clusters in the macaque cortex. *J Neurosci* 32: 17465–17476, 2012.

**Shim G, Oh JS, Jung WH, Jang JH, Choi CH, Kim E, Park HY, Choi JS, Jung MH, Kwon JS.** Altered resting-state connectivity in subjects at ultra-high risk for psychosis: an fMRI study. *Behav Brain Funct* 6: 58, 2010.

**Shima K, Tanji J.** Role for cingulate motor area cells in voluntary movement selection based on reward. *Science* 282: 1335–1338, 1998.

**Shmuel A, Leopold DA.** Neuronal correlates of spontaneous fluctuations in fMRI signals in monkey visual cortex: Implications for functional connectivity at rest. *Hum Brain Mapp* 29: 751–761, 2008.

**Shmueli K, van Gelderen P, de Zwart JA, Horovitz SG, Fukunaga M, Jansma JM, Duyn JH.** Low-frequency fluctuations in the cardiac rate as a source of variance in the resting-state fMRI BOLD signal. *Neuroimage* 38: 306–320, 2007.

**Smeets JB, Brenner E.** A new view on grasping. *Motor Control* 3: 237–271, 1999.

**Stanton GB, Bruce CJ, Goldberg ME.** Topography of projections to posterior cortical areas from the macaque frontal eye fields. *J Comp Neurol* 353: 291–305, 1995.

**Stanton GB, Bruce CJ, Goldberg ME.** Topography of projections to the frontal lobe from the macaque frontal eye fields. *J Comp Neurol* 330: 286–301, 1993.

**Stanton GB, Goldberg ME, Bruce CJ.** Frontal eye field efferents in the macaque monkey. I. Subcortical pathways and topography of striatal and thalamic terminal fields. *J Comp Neurol* 271: 473–492, 1988.

**Strick PL, Dum RP, Picard N.** Motor areas on the medial wall of the hemisphere. *Novartis Found Symp* 218: 64–75; discussion 75–80, 104–108, 1998.

**Tatler BW, Hayhoe MM, Land MF, Ballard DH.** Eye guidance in natural vision: reinterpreting salience. *J Vis* 11: 5, 2011.

**Ueda Y, Kimura M.** Encoding of direction and combination of movements by primate putamen neurons. *Eur J Neurosci* 18: 980–994, 2003.

**Van Essen DC.** Surface-based approaches to spatial localization and registration in primate cerebral cortex. *Neuroimage* 23, Suppl 1: S97–S107, 2004.

**Van Essen DC, Dickson J, Harwell J, Hanlon D, Anderson CH, Drury HA.** An integrated software system for surface-based analyses of cerebral cortex. *J Am Med Inform Assoc* 8: 443–459, 2001.

**Van Essen DC, Glasser MF, Dierker DL, Harwell J.** Cortical parcellations of the macaque monkey analyzed on surface-based atlases. *Cereb Cortex* 22: 2227–2240, 2012.

**Vanhaudenhuyse A, Noirhomme Q, Tshibanda LJ, Bruno MA, Boveroux P, Schnakers C, Soddu A, Perlberg V, Ledoux D, Brichant JF, Moonen G, Maquet P, Greicius MD, Laureys S, Boly M.** Default network connectivity reflects the level of consciousness in non-communicative brain-damaged patients. *Brain* 133: 161–171, 2010.

**Vincent JL, Patel GH, Fox MD, Snyder AZ, Baker JT, Van Essen DC, Zempel JM, Snyder LH, Corbetta M, Raichle ME.** Intrinsic functional architecture in the anaesthetized monkey brain. *Nature* 447: 83–86, 2007.

**Wise SP, Boussaoud D, Johnson PB, Caminiti R.** Premotor and parietal cortex: corticocortical connectivity and combinatorial computations. *Annu Rev Neurosci* 20: 25–42, 1997.

**Woolrich MW, Behrens TE, Beckmann CF, Jenkinson M, Smith SM.** Multilevel linear modelling for fMRI group analysis using Bayesian inference. *Neuroimage* 21: 1732–1747, 2004.

## CHAPTER 3:

### 3. Theta and Beta synchrony coordinate frontal eye fields and anterior cingulate cortex during sensori-motor mapping<sup>2</sup>

#### 3.1. ABSTRACT:

The frontal eye fields (FEF) and the anterior cingulate cortex (ACC) are commonly co-activated for cognitive saccade tasks, but whether this joined activation indexes coordinated activity underlying successful guidance of sensorimotor mapping is unknown. Here I tested whether ACC and FEF circuits coordinate through phase synchronization of local field potential and neural spiking activity in macaque monkeys performing memory-guided and pro- and anti-saccades. I found that FEF and ACC showed prominent synchronization at a 3-9 Hz theta and a 12-30 Hz beta frequency band during the delay and preparation periods. The strength of theta- and beta-band coherence between ACC and FEF, but not variations in power predicted correct task performance. Taken together, the results support a role of ACC in cognitive control of fronto-parietal networks and suggest that narrow-band theta and to some extent beta rhythmic activity

---

<sup>2</sup> A version of Chapter 3 is submitted for publication as S. Babapoor-Farrokhran, M. Vinck, T. Womelsdorf, and S Everling, (2016): Theta and Beta synchrony coordinate frontal eye fields and anterior cingulate cortex during sensori-motor mapping. *Nature Communications*.

indexes the coordination of relevant information during periods of enhanced control demands.

### **3.2. INTRODUCTION:**

The frontal eye field (FEF) plays a crucial role in overt (Bruce et al. 1985; Wurtz and Mohler 1976) and covert orienting (Moore and Armstrong 2003; Thompson et al. 2005). Together with parietal and extrastriate visual areas, FEF is part of the dorsal attention network that provides top-down allocation of attention to contralateral space through long-range connections with visual cortical areas in humans and nonhuman primates (Bressler et al. 2008; Caspari et al. 2015; Corbetta and Shulman 2002). Activity in this fronto-parietal spatial priority network is modulated by cortical and subcortical inputs that are thought to encode behavioral rules, values, and motivational signals (Womelsdorf and Everling 2015). One cortical area that has anatomical connections with FEF is the anterior cingulate cortex (ACC) (Wang et al. 2004). Functional connectivity between ACC and FEF has also been demonstrated by resting-state functional magnetic resonance imaging (fMRI) in macaques (Babapoor-Farrokhran et al. 2013) and task-based fMRI studies commonly show co-activation of FEF and ACC in a variety of cognitive saccades task (McDowell et al. 2008). However, the neural mechanisms underlying the functional co-activation of ACC and FEF in behavioral tasks remain unknown.

One proposed mechanism for the communication of spatially dispersed neuronal groups is through synchronizing the excitability phases of band-limited activity (Fries 2005; Womelsdorf et al. 2007). Such long-range phase synchrony of rhythmic activation facilitates the efficient transmission of neuronal signals between brain regions (Akam and

Kullmann 2014; Fries 2005; Womelsdorf et al. 2014b). More specifically, the communication between brain areas involved in memory-guided and top-down control processes is thought to be facilitated in prefrontal cortices via synchronization at band limited rhythmic activity in a theta frequency band (3-9 Hz) (Liebe et al. 2012; Voloh et al. 2015; Womelsdorf et al. 2010b), and in a beta frequency band (12-30 Hz) (Brovelli et al. 2004; Engel and Fries 2010; Miller and Buschman 2013; Salazar et al. 2012; Womelsdorf et al. 2014a). However, the contribution of theta and beta frequency bands to the transmission of neural signals between ACC and other brain areas is still poorly understood.

Here I recorded local field potentials (LFPs) and spiking activity from FEF and ACC simultaneously and investigated task-dependent synchronization between the two areas while monkeys performed a memory-guided saccade task and a task with randomly interleaved pro- and anti-saccade trials. The results show that a narrow-band of theta rhythmic activity indexes the coordination of relevant information between FEF and ACC during periods of enhanced control demands. Furthermore, I found increased beta band (12-30 Hz) synchronization in the delay and preparatory periods of the memory-guided saccade task and pro-/anti-saccade task, respectively.

### **3.3. MATERIALS AND METHODS:**

Two male adult macaque monkeys (*M. mulatta* and *M. fascicularis*) weighing 7-9 kg were subjects in this study. All experimental procedures and animal care were implemented in accordance with the guidelines of the Canadian Council of Animal Care policy on the care and use of laboratory animals and an ethics protocol approved by the Animal Users Subcommittee of the University of Western Ontario Council on Animal



Care. I simultaneously recorded the LFP and unit activity in the ACC and FEF while monkeys performed a memory-guided saccade task and a randomly interleaved pro-/anti-saccade task (Figure 3.1 A-C). In this study, I performed spectral power analysis, field-field coherence analysis and spike-field coherence analysis using custom written Matlab code (Mathworks, Natick, MA) and fieldtrip toolbox (<http://www.ru.nl/fcdonders/fieldtrip/>). A detailed description of the experimental procedures and data analysis methods are included in the supplementary information.

### **3.4. RESULTS:**

I simultaneously recorded LFPs in the ACC (n=233 sites; n=87 and n=146 in monkey 1 and 2, respectively) and FEF (n=209 sites; n=62 and n=147 in monkey 1 and 2) while monkeys performed the memory-guided saccade task and the pro/anti-saccade task (Figure 3.1 A). Together with these LFPs, I simultaneously recorded the spiking activity of ACC (n=149 units; n=52 and n=97 in monkey 1 and 2) and FEF units (n=74 units; n=46 and n=28 in monkey 1 and 2; Figure 3.1 B-C).

LFP power and phase-synchronization spectra showed prominent peaks in the theta and beta band (Figures 3.2-3.3). I therefore focus the remainder of the results and discussion on these two bands. I also explored ACC-FEF interactions across delta, alpha and gamma (30-100 Hz) bands. In contrast to the theta and beta band, I observed no consistent modulation in these frequency ranges in different conditions (Figures 3.2-3.3, Supplementary Figures 3.2-3.7), suggesting that functionally meaningful interactions between ACC and FEF proceeds predominantly in the theta and beta frequencies (Womelsdorf and Everling 2015).

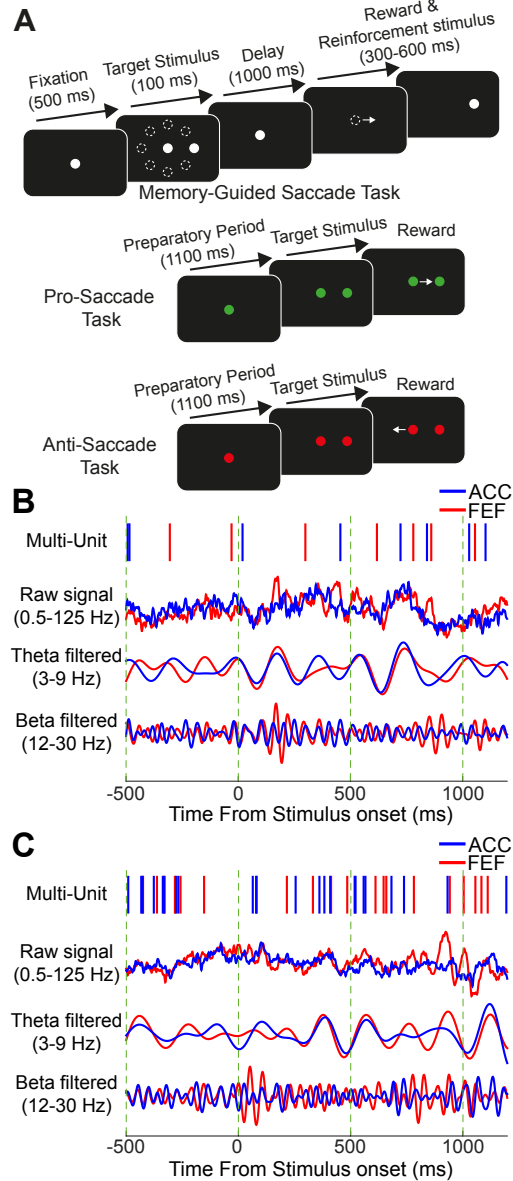


**Figure 3.1. Experimental paradigm and sample traces of simultaneously recorded activity in ACC and FEF.** (A) Schematic of the memory-guided saccade task and pro/anti-saccade task. (B) The traces show the multi-unit activity, raw LFP signal (0.5-125 Hz), theta band pass filtered signal (3-9Hz) and beta band pass filtered signal (12-30 Hz) in a trial of memory-guided saccade task. (C) Same as A in another memory-guided saccade task trial. The vertical green dashed lines indicate the 500ms time intervals aligned on stimulus onset.

#### ***3.4.1. Modulation of theta and beta power during the delay period:***

The memory-guided saccade task required the monkeys to maintain a spatial location in working memory and then to generate a saccade toward the remembered location after the imposed delay period. I first calculated the LFP power spectra during the delay period for correctly performed memory-guided saccade trials (horizontal and oblique targets). Both ACC and FEF LFPs showed a prominent increase in theta power (3-9 Hz) during the delay period (Figure 3.2 A & B). Additionally, a transient increase in 15-20 Hz beta frequency power was evident in the immediate post-stimulus period (Figure 3.2 A & B).

I further examined whether LFP power was tuned to the spatial target location. I found that a significant number of FEF (18/209; 8.61%,  $P < 0.05$ , Binomial test) but not ACC (11/233; 4.72% n.s.; ACC vs. FEF:  $P=0.099$ , Chi-Square test) channels showed significant spatial tuning of power within the theta frequency band (3-9Hz) during the delay period in the time window of 400-1100ms following target stimulus onset (Figure 3.2 A, one-way ANOVA,  $P < 0.05$ ). In addition, a significant number of FEF (50/209; 23.92%,  $P<0.05$ ) but not ACC channels (14/233; 6.08% n.s.; difference ACC vs. FEF:  $P<0.001$ ) showed significant tuning in the beta-band (12-30 Hz). Thus, I found spatial tuning of LFP power in theta and beta frequencies in FEF but not in ACC. The observed power modulation of the FEF LFPs is in line with previous FEF single unit recording results, which suggest a high degree of spatial tuning in FEF neurons (Bruce and Goldberg 1985).

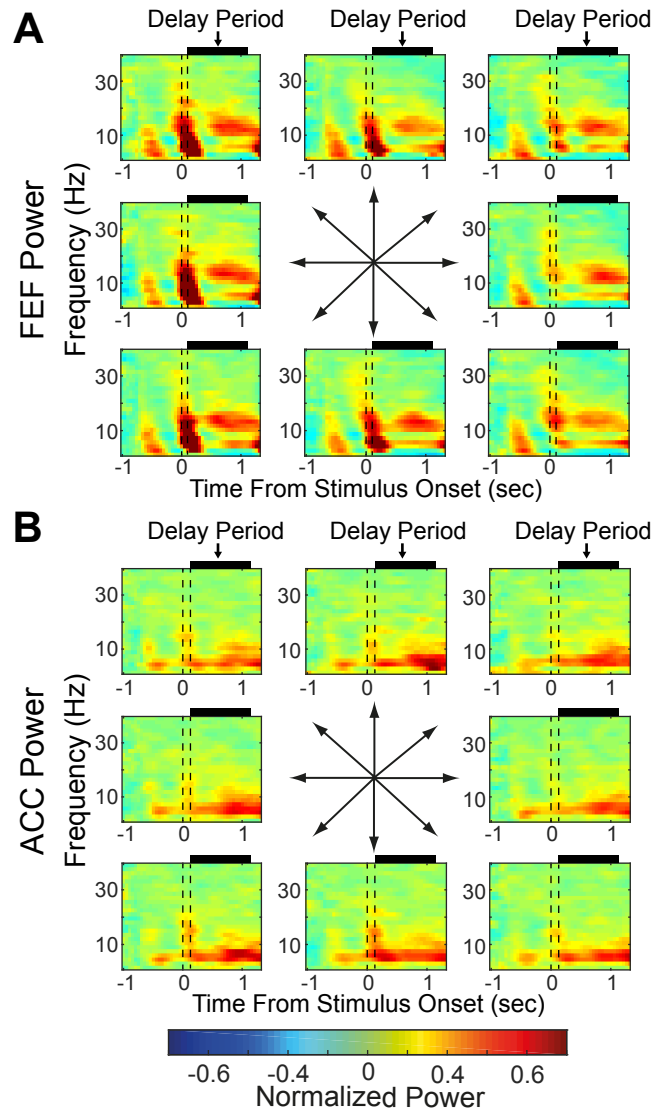


**Figure 3.2. LFP power in FEF and ACC during the memory-guided saccade task.** (A) Average time frequency spectra of the FEF LFP power across 8 target locations in the memory-guided saccade task. (B) Average time frequency spectra of ACC LFP power across 8 target locations in the memory-guided saccade task. The dashed lines demarcate the time of the onset and offset of the target stimulus. The black boxes on top of each graph demarcate the delay period.

### ***3.4.2. Task-dependent LFP-LFP coherence between ACC and FEF:***

I next tested whether ACC and FEF showed task dependent interactions in the theta (3-9Hz) and beta (12-30 Hz) band. For a large subset of inter-areal recording pairs, theta- and beta-band phase synchronization increased from the baseline (700ms prior to the fixation point onset in the inter-trial interval) to the delay period of the memory-guided saccade task (400 to 1100ms following stimulus onset in the delay period, *see* Methods). Of the 674 ACC-FEF LFP-LFP channel pairs, respectively 447 (66.32%) and 330 (48.96%) channel pairs displayed significant increases in theta- and beta-phase synchronization during the delay period (theta: 141/233 and 306/441 of monkey 1 and 2, respectively; beta: 91/233 and 239/441 of monkey 1 and 2;  $P < 0.001$ , permutation test, *see* Methods). On the other hand, respectively 128 (18.99%) and 179 (26.56%) pairs exhibited statistically significant decreased theta- and beta-synchrony in the delay period relative to the baseline (theta: 65/233 and 63/441 of monkey 1 and 2; beta: 71/233 and 108/441 of monkey 1 and 2;  $P < 0.001$ , permutation test). Furthermore, the population of ACC-FEF channel pairs exhibited increased theta- and beta-band synchrony in the delay period vs. baseline of the memory-guided saccade task (Figures 3.3 C, 3.3 D, 3.3 E, and 3.3 G). Consistent with these results, I found a prominent peak in the average inter-areal theta and beta, but not alpha (10-12 Hz) and gamma-band (30-100 Hz) phase synchronization across the population of pairs of recording sites in FEF and ACC (Figure 3.3 A-B, Supplementary Figure 3.2). This theta- and beta-band phase synchronization was evident in both monkeys (Figure 3.3 B). In addition, I observed increased inter-areal theta and beta band synchronization in the preparatory period (400 ms-1100ms following

fixation onset) of the pro-/anti-saccade task compared to baseline (Supplementary Figure 3.2 B).

Increased phase-synchronization between ACC and FEF might partially reflect an independent phase reset in both areas aligned on stimulus onset. To examine this, I subtracted the averaged stimulus aligned evoked LFP from the signals before calculating phase synchrony. This procedure resulted in decreased ACC-FEF theta band phase synchronization during the early delay period (Figure 3.3 C compared to Supplementary Figures 3.3 C) but did not affect the increased phase synchronization in the late delay period (400-1100ms following the stimulus onset). This finding suggests that the increased phase synchronization in the 400-1100ms following the stimulus period is not time locked to the stimulus onset and reflects genuine ACC-FEF synchronization (Supplementary Figure 3.3). On the other hand, I did not observe this decrease in the immediate post-stimulus beta-band phase synchronization of the average-subtracted data compared to that of the original data (Figure 3.3 D compared to Supplementary Figures 3.3 D). This suggests that beta-band ACC-FEF phase synchronization primarily represents an induced oscillatory response that is not evoked by the stimulus onset. In the following sections, I have performed the delay period analyses in the 400-1100ms following the stimulus onset to avoid stimulus-related evoked responses.

Finally, I asked whether inter-areal phase synchronization distinguished ipsi- and contra-verse saccade planning in the memory-guided saccade task. The difference in theta- and beta-phase synchronization was not significantly different between ipsi- and contra-verse saccades in the window of 400-1100ms following the stimulus onset (Figures 3.3 E, and 3.3 G).

To summarize, these findings indicate that there is a coordination of FEF and ACC activity in theta and beta-band frequencies during the delay period of the memory-guided saccade task and the preparatory period of the pro/anti-saccade task, which represent periods of enhanced control demands.

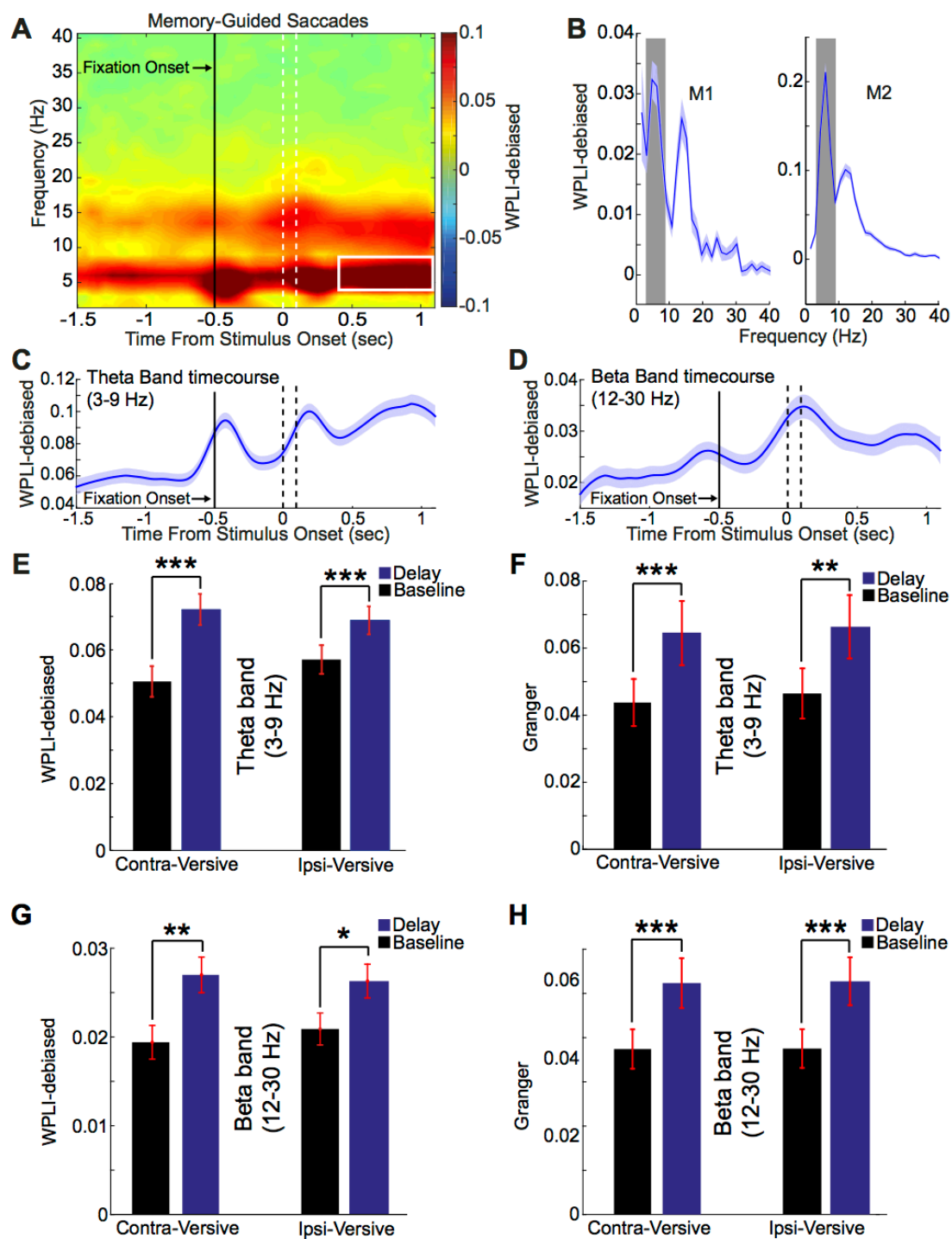




**Figure 3.3. Increased theta and beta coherence between ACC and FEF.** (A) Time-Frequency spectrum of the wpli-debiased coherence between the FEF and ACC in memory-guided saccade task for the population of ACC-FEF channel pairs (n=674). The white contour shows the area in which the subsequent analyses were performed (see Methods). The dashed lines demarcate the time of the onset and offset of the target stimulus. (B) WPLI-debiased FEF-ACC coherence spectrum of the individual monkeys in the delay period across all recording pairs (n=674). (C) Theta band (3-9 Hz) time course of the ACC-FEF WPLI-debiased phase synchronization. (D) Beta band (12-30 Hz) time course of the ACC-FEF WPLI-debiased phase synchronization. (E) Comparison of WPLI-debiased coherence between baseline and delay period of the contra-verse and ipsi-verse memory-guided saccades (\*\*\*:  $p < 0.001$ , t-test). Error bars indicate SEM. (F) Comparison of the overall Granger causality effect of ACC over FEF ( $G_{ACC \rightarrow FEF} - G_{FEF \rightarrow ACC}$ ) between baseline and delay period of the contra-verse and ipsi-verse memory-guided saccades (\*\*\*:  $p < 0.001$ , \*\*:  $p < 0.01$ , t-test, n=275). Error bars indicate SEM. (G) Comparison of beta band WPLI-debiased coherence between baseline and delay period of the contra-verse and ipsi-verse memory-guided saccades (\*\*:  $p < 0.01$ , \*:  $p < 0.05$ ; t-test). Error bars indicate SEM. (H) Comparison of the beta band overall Granger effect of ACC over FEF ( $G_{ACC \rightarrow FEF} - G_{FEF \rightarrow ACC}$ ) between baseline and delay period of the contra-verse and ipsi-verse memory-guided saccades (\*\*\*:  $p < 0.001$ ; t-test). Error bars indicate SEM.

### ***3.4.3. Task-dependent Granger-causality between ACC and FEF LFPs:***

I further investigated the directionality of the ACC-FEF interactions by performing Granger-causality analyses. Both during the delay and the baseline period, I observed bidirectional Granger-causal effects between ACC and FEF LFPs, with prominent peaks in the theta and beta range, and a stronger direction from ACC to FEF than vice versa (Supplementary Figure 3.4 A-C). During the delay period, as compared to the baseline period, the Granger-causal effect in the theta-band increased for both directions ( $G_{ACC \rightarrow FEF}$  and  $G_{FEF \rightarrow ACC}$ ) (Supplementary Figure 3.4 A-B). Yet, for the beta-band, I observed that the Granger causal effect increased from ACC to FEF, but not from FEF to ACC (Supplementary Figure 3.4 A-B). Correspondingly, I found that the Granger-causal effect in the theta- (paired t-test,  $P < 0.001$  in contra-verse and  $P < 0.01$  in ipsi-verse conditions, Figure 3.3 F) and beta-band (paired t-test,  $P < 0.001$  in both contra- and ipsi-verse trials, Figure 3.3 H) increased more strongly in the direction of ACC to FEF than vice versa ( $G_{ACC \rightarrow FEF} - G_{FEF \rightarrow ACC}$ ). The results also indicated that the causal effect of ACC on FEF is greater than that of FEF over ACC during the delay period across alpha, and gamma frequency ranges (paired t-test,  $P < 0.05$ ), as shown in Supplementary Figure 3.4 C. I computed the chance level Granger values by randomly shuffling the time-frequency domain of the raw data. Across theta and beta frequencies, the  $G_{ACC \rightarrow FEF}$  and  $G_{FEF \rightarrow ACC}$  values, both in the baseline and delay periods, were above the chance level. In summary, I observed that ACC-FEF interaction patterns changed during the delay period of the contra-verse and ipsi-verse saccade trials, with the Granger-causal effect from ACC to FEF becoming relatively stronger.

#### ***3.4.4. Decreased theta and beta-synchrony between ACC and FEF LFPs on error trials:***

I found that FEF and ACC LFPs exhibit phase-synchronization in the theta and beta frequency band during the delay period. My next question was whether this synchronization predicted behavioral task performance. To test whether the strength of phase synchronization affected performance in the memory-guided saccade task, I compared FEF-ACC phase synchronization between correct trials and error trials in which the animal made an eye movement toward the wrong stimulus location. I found that both theta and beta band coherence between the ACC and FEF were significantly larger on correct trials than error trials during the delay period (Figure 3.4 A; t-test,  $P < 0.001$ ). I validated the relationship of coherence with performance by using an anti-saccade task that triggered more directional error trials than the memory-guided saccade task. Similar to the memory-guided saccade task, the population of the ACC-FEF channel pairs showed significantly decreased theta- and beta-band phase synchronization in the error vs. correct anti-saccades during the 400-1100ms following the fixation onset during the preparatory period (Figure 3.4 A, t-test,  $P < 0.01$ ). I confirmed that these statistical differences were not the result of differences in sample size, by performing the same analysis using the same number of trials for correct and error trials.

I also asked how theta power is modulated in correct and error trials in the ACC and FEF. I found no significant differences in theta power between correct and error trials in the ACC or FEF (Figure 3.4 B-C, left two columns). However, there were significant differences of beta power across the delay periods of the memory-guided saccade task but not in the preparatory period of the anti-saccade task (Figure 3.4 B-C, right two

columns). This indicated that the changes in theta and beta band ACC-FEF phase-synchronization in either one (beta) or both (theta) behavioral tasks were dissociated from changes in local power.

Taken together, these results indicate that theta- and beta-band phase synchronization between ACC and FEF provide a better prediction of performance than local power in these areas. Higher phase-synchronization on correct trials than on error trials supports the hypothesis that ACC-FEF theta and beta phase-synchronization play functional roles in working memory as well as in cognitive control.

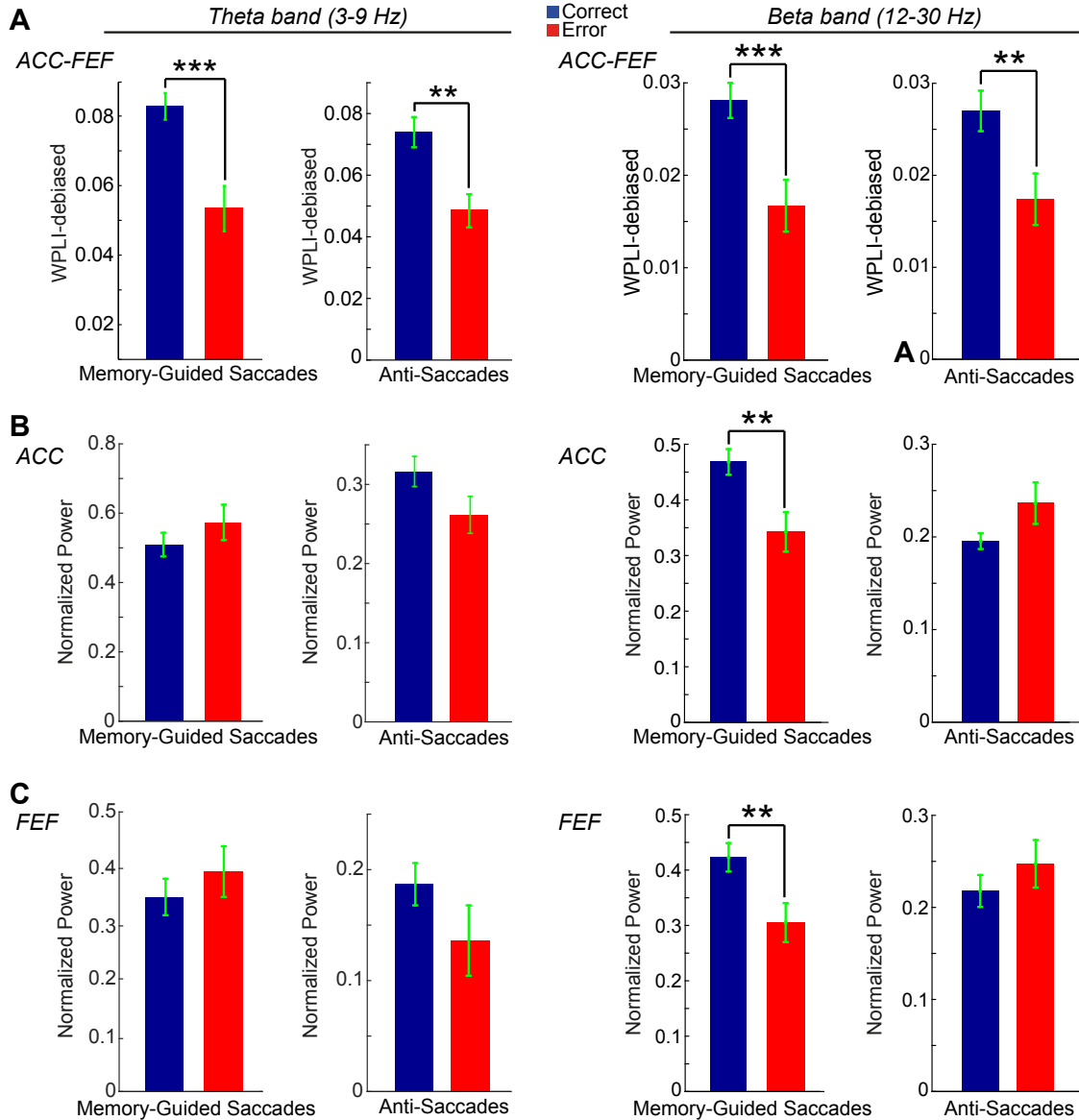


**Figure 3.4. Correct task performance is dependent on field-field coherence but not on LFP power.** (A) Shown the comparison of theta (columns 1 and 2) and beta-band (columns 3 and 4) WPLI-debiased coherence between correct and error memory-guided saccades in the delay period of the memory guided saccade task (400-1100ms following target stimulus onset) and the preparatory period (400-1100ms following fixation onset) of the anti-saccade task. (B) Same as A, but shown normalized ACC theta and beta-band power. (C) Same as A but for normalized FEF power. \*:  $p < 0.05$ ; \*\*:  $p < 0.01$ ; \*\*\*:  $p < 0.001$ , t-test. Error bars indicate SEM.

#### ***3.4.5. Modulation of spike-field synchrony during the delay period:***

Together, these results suggest that theta and beta-band frequencies play a prominent role in the neuronal communication between ACC and FEF. I hence predicted that theta-band LFP modulations in one area should be related to the spiking activity of neurons in the other area. I tested this using the pairwise phase consistency (PPC) as a measure of spike-field coherence (Vinck et al. 2012). I first examined whether there was a difference in spike-field synchrony between the baseline and delay periods.

A significant fraction of ACC-unit-to-FEF-LFP pairs and FEF-unit-to-ACC-LFP pairs exhibited significantly increased ( $P < 0.05$ , permutation test, Figure 3.5 A-B left and middle) theta band phase-coupling in the delay period vs. baseline of both contra-verse (ACC units:  $68/283 = 24.03\%$ ,  $P < 0.001$ , Binomial Test; FEF units:  $16/154 = 10.4\%$ ,  $P < 0.001$ ) and ipsi-verse trials (ACC units:  $45/326 = 13.8\%$ ,  $P < 0.001$ ; FEF units:  $17/204 = 8.33\%$ ,  $P < 0.001$ ). In contrast, I found no evidence for significant decreases in phase-locking (Figure 3.5 A-B left and middle). Furthermore I observed an increase in average spike-field coupling in a subset of theta frequencies (3-4 Hz) during delay vs. baseline of contra-verse, but not ipsi-verse memory trials (Figure 3.6 A-B left and middle).

In addition, I found a significant fraction of cells with increased but not decreased theta band phase-coupling during contra-verse as compared to ipsi-verse trials (ACC units:  $34/353 = 9.6\%$ ,  $P < 0.001$ ; FEF units:  $15/209 = 7.2\%$ ,  $P < 0.001$ , Figure 3.5 A-B right). Furthermore, I observed that the average spike-LFP phase-locking was increased during contra-verse as compared to ipsi-verse trials in a subset of theta frequencies (3-4 Hz; Figure 3.6 A-B right).

At beta-frequencies, I also found that a small but significant fraction of ACC-unit-to-FEF-LFP pairs and FEF-unit-to-ACC-LFP pairs showed increased phase-coupling in the beta-band (12-30 Hz) in the delay period vs. baseline of both contra-verse (ACC units: 17/283=6.0%,  $P<0.001$ ; FEF units: 15/154=9.8%,  $P<0.001$ ) and ipsi-verse trials (ACC units: 22/326=6.8%,  $P<0.001$ ; FEF units: 15/204=7.4%,  $P<0.001$ ), whereas I found no evidence for significant decreases (Figure 3.5 A-B left and middle). Although I found a trend for increased average spike-field phase locking at beta frequencies during the delay as compared to the baseline period, this effect only reached significance for the population of ACC-unit-to-FEF-LFP pairs (Figure 3.7 A, left). Furthermore, in contrast to the theta-band, I found no evidence for significant changes in beta-band spike-LFP phase-locking between ipsi and contra-verse trials for ACC-units-to-FEF-LFP (Figure 3.5 A, right). A small but significant fraction of FEF cells exhibited increased beta-band phase locking to ACC LFPs in ipsi-verse as compared to contra-verse trials (17/209=8.1%,  $P<0.001$ ) (Figure 3.5 B right). Moreover, I did not observe a significant difference in the average spike-LFP phase-locking during the delay periods of contra-verse as compared to ipsi-verse trials across beta band frequencies (Figure 3.7 A-B, right). Finally, I tested the spike-field coupling of the ACC and FEF units with FEF and ACC LFP respectively, across delta, alpha, and gamma bands and I did not observe significant effects (Figure 3.6, Supplementary Figures 3.5-3.7).

I also tested for possible influences of firing rate differences between units on the observed spike LFP synchronization. I repeated the spike-field analysis, but only including in the analysis those units with no significant difference of spike rates between

the tested conditions. The obtained effects were still statistically significant (*see* (Vinck et al. 2013) for a detailed description).

In summary, I found evidence for positive modulations in theta and beta phase-coupling both during contra- and ipsi-verse trials, consistent with the LFP-LFP phase-synchronization analysis. I found that increases in theta-band spike-LFP phase coupling were more prominent during contra-verse than ipsi-verse memory trials.



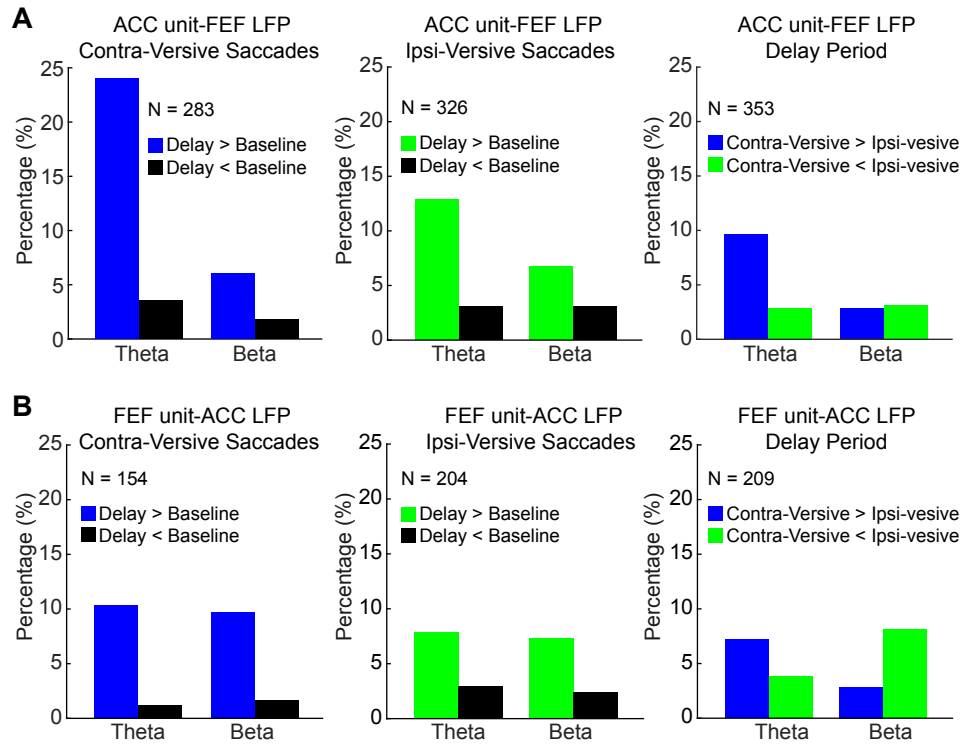


**Figure 3.5. Percentage of units with significant spike-field coupling in theta and beta band.** (A) Percentage of the ACC-units-to-FEF-LFP pairs showing significant changes in phase-locking across the theta and beta frequency range. Comparison between baseline and delay of contra-verse saccades (left), comparison between baseline and delay of ipsi-verse saccades (middle) and comparison between the contra- and ipsi-verse saccades in the delay period (right). (B) Same as (A), but now depicted the percentage of the FEF-units-to-ACC-LFP pairs showing significant changes in phase-locking across the theta and beta frequency range. Statistical testing was performed using two-sided permutation tests, such that chance level is 2.5%.

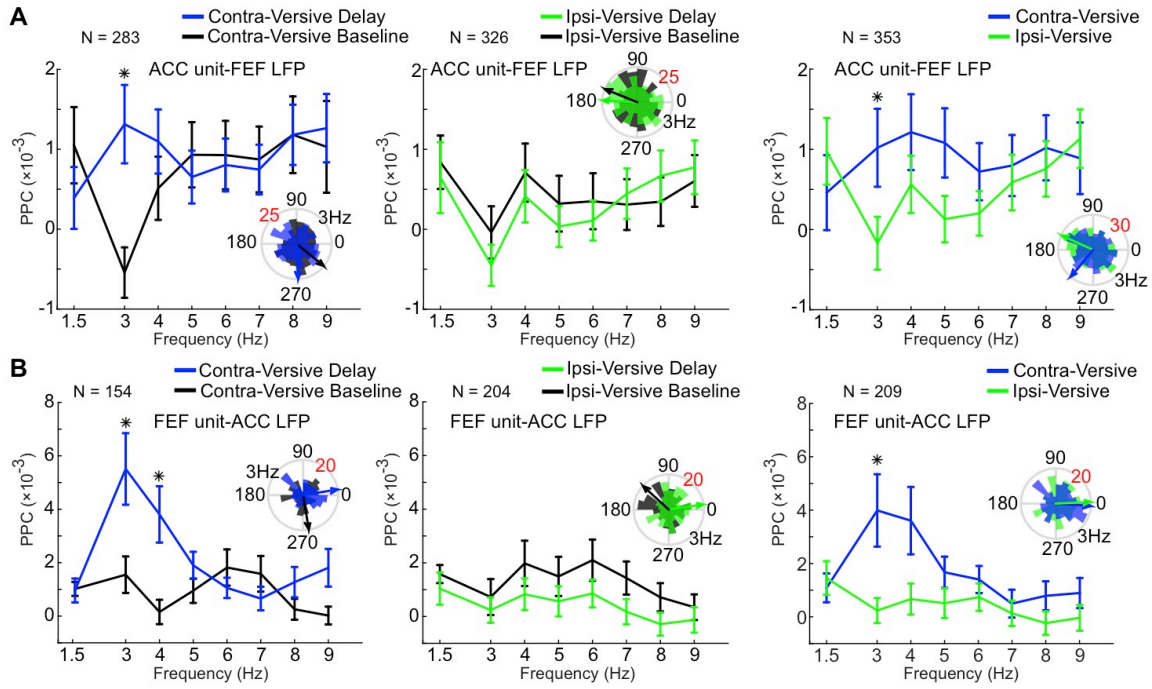


**Figure 3.6. Pairwise phase consistencies (PPCs) across delta and theta band.** (A) PPC spike-field coherence spectrum of the population of the ACC-units-to-FEF-LFP pairs across the delta and theta frequency range. Comparison between baseline and delay of contra-verse saccades (left), comparison between baseline and delay of ipsi-verse saccades (middle) and comparison between the contra- and ipsi-verse saccades in the delay period (right). (B) PPC spike-field coherence spectrum of the population of the FEF-units-to-ACC-LFP pairs across the delta and theta frequency range. Comparison between baseline and delay of contra-verse saccades (left), comparison between baseline and delay of ipsi-verse saccades (middle) and comparison between the contra- and ipsi-verse saccades in the delay period (right). It should be noted that the same significant differences between ipsi-verse and contra-verse trials were seen even after we compared the contra- versus ipsi-verse conditions using a permutation test as described in the methods section. Error bars denote SEM in all panels. \*:  $p < 0.05$ , paired t-test). The rose plots on the side of each graph show the histogram of the coupling angles of the population of the ACC/FEF units.

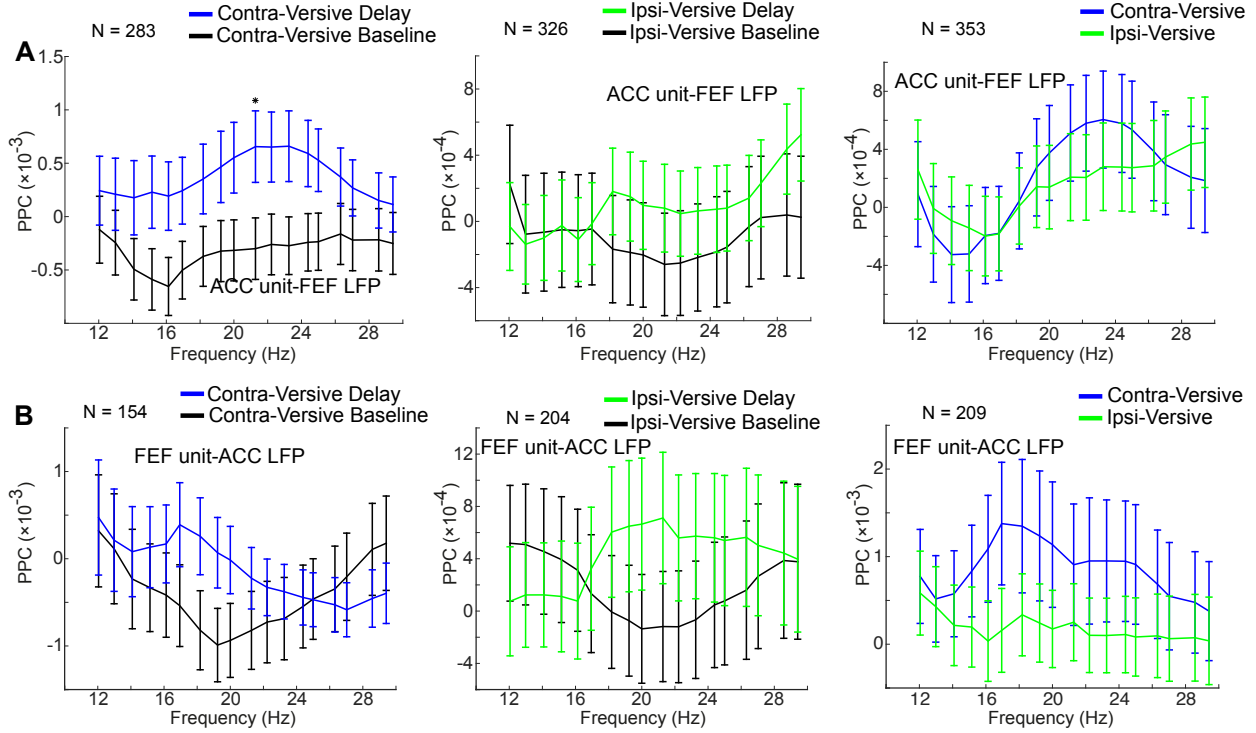


**Figure 3.7. Pairwise phase consistencies (PPCs) across beta band.** (A) PPC spike-field coherence spectrum of the population of the ACC-units-to-FEF-LFP pairs across the beta frequency range. Comparison between baseline and delay of contra-verse saccades (left), comparison between baseline and delay of ipsi-verse saccades (middle) and comparison between the contra- and ipsi-verse saccades in the delay period (right). (B) PPC spike-field coherence spectrum of the population of the FEF-units-to-ACC-LFP pairs across the beta frequency range. Comparison between baseline and delay of contra-verse saccades (left), comparison between baseline and delay of ipsi-verse saccades (middle) and comparison between the contra- and ipsi-verse saccades in the delay period (right). Error bars denote SEM in all panels. \*:  $p < 0.05$ , paired t-test).

### **3.5. DISCUSSION:**

Here, I have reported that neural circuits in the ACC and the FEF synchronize the phases of theta and beta specific activity during the short-term retention of stimulus locations in a working memory task. This working memory induced inter-areal synchronization (1) was evident in more than half of the LFP-LFP recording pairs, (2) translated to spiking activity in the ACC and FEF with significant inter-areal spike-LFP synchronization in both anatomical directions, i.e. with spikes from ACC coupled to LFPs in FEF and with FEF spikes coupling to LFPs from ACC, and (3) indexed correct versus erroneous working memory performance. These findings provide evidence that functional interactions between brain areas implementing (associated with FEF) and biasing (associated with ACC) working memory and also higher order cognitive performance proceed through phase synchronized activation at band-limited theta and beta rhythmic activity (Liebe et al. 2012; Lisman and Jensen 2013; Voloh et al. 2015). These results indicate how larger working memory networks coordinate their activity and constrain the possible cell- and circuit mechanisms that underlie successful working memory performance (Womelsdorf and Everling 2015).

Neuronal circuits in FEF are well known to encode target locations for overt orienting and covert stimulus selection during working memory, sustained attention and visual search tasks (reviewed e.g. in (Miller and Buschman 2013)). During working memory and stimulus selection, the long range synchronization of FEF with intra-parietal areas takes place at characteristic 12-30 Hz frequencies (Bastos et al. 2015; Buschman and Miller 2007; Dotson et al. 2014; Salazar et al. 2012), and at higher, gamma band frequencies with visual area V4 neurons that share similar spatial tuning to target

locations than the FEF circuits (Gregoriou et al. 2009; Gregoriou et al. 2014). Beyond these beta- and gamma- band mediated interactions across fronto-posterior brain areas with spatially tuned neuronal circuits, it has been unknown how more anterior structures including circuits in the anterior cingulate cortex are linked to the FEF during ongoing fronto-parietal network activation. My findings answer this question by documenting theta (3-9 Hz) and beta (12-30 Hz) frequency specific synchronization between neural circuits in FEF and in ACC. Band-limited synchronization at theta and beta frequencies could provide a temporal reference for coordinating spiking activity between both areas (Mizuseki et al. 2009; Salazar et al. 2012; Womelsdorf et al. 2010b). I discuss the results on beta and theta-band synchronization separately in what follows.

*Theta-band synchronization.* Transiently emerging LFP activity at a 3-9 Hz theta frequency band has been shown to characterize ACC circuits during preparatory states (Fujisawa and Buzsaki 2011; Womelsdorf et al. 2010a) and during top-down controlled stimulus selection (Voloh et al. 2015). Complementary to the latter study's findings, theta rhythmic activation in my task emerged in response to a sample stimulus that served as a cue to select a spatial target location as later saccadic target location. The theta rhythmic synchronization of ACC circuits with the FEF that I observed is thus directly related to the cognitive demands to establish and maintain an internal spatial target representation. Consistent with this functional interpretation I found that a failure to maintain the target location in working memory was evident in reduced theta rhythmic interactions of ACC and FEF, suggesting that phase synchronization between ACC and FEF is functionally important to successfully achieve the behavioral goal. Notably, similar to a previous study on theta activation in the ACC (Voloh et al. 2015), locally confined LFP theta

power modulations were not as informative to predict successful top-down performance compared to inter-areal theta band interactions (Figure 3.4; see also (Voloh et al. 2015)). I speculate that this set of results reveal that the mere activation of theta rhythmic circuit motifs within the ACC and FEF are not sufficient to support adaptive behavior (Womelsdorf et al. 2014b). Rather, these findings highlight that theta rhythmic circuit motifs need to be coordinated between areas to successfully maintain an internally generated top-down network state (Lisman and Jensen 2013; Phillips et al. 2014; Womelsdorf and Everling 2015; Womelsdorf et al. 2010c).

Could the observed theta-band synchronization between ACC and FEF be part of a larger functional network? I observed enhanced ACC-FEF phase synchronization during a working memory task that was originally used to discover persistent working memory activity in lateral prefrontal cortex (area 46/9 and anterior area 8b) (Funahashi et al. 1989; Goldman-Rakic 1990). Several studies have shown that this lateral PFC hot spot of working memory does not act as a discrete working memory module, but that it acts within a broad working memory network of brain areas that includes the FEF and the ACC (D'Esposito and Postle 2015; Ma et al. 2014). Such a network perspective is consistent with the dense anatomical inter-connectivity of ACC, FEF and lateral PFC (Barbas 2015). Functionally, this network perspective of working memory is supported by a study that documented increased 3-9 Hz theta LFP power and increased PFC-to-V4 theta band phase synchronization during the working memory delay of a match-to-sample task (Liebe et al. 2012). The convergence of these major findings about the inter-areal signature underlying successful working memory performance opens the possibility that all four brain areas, lateral PFC, FEF, ACC, and V4 phase synchronize their local

activities to a common theta rhythm during successful maintenance of working memory that would be measurable if all areas were recorded simultaneously. An important consequence of this scenario is that cellular and circuit mechanisms that generate and sustain theta rhythmic circuit activation would be key mechanisms underlying the inter-areal coordination of working memory representations (Wang 2010; Womelsdorf et al. 2014b).

I found that a moderate fraction of ACC and FEF units synchronized to theta LFP activity at distant sites (FEF and ACC, respectively) more strongly during the working memory delay than during the pre-delay baseline period (see Figures 3.5 and 3.6). This increase was particularly prominent for contra-versive memory locations, indicating that inter-areal spike-LFP synchronization carried top-down information similar to previous reports (Liebe et al. 2012; Womelsdorf et al. 2010a). These observations suggest that theta phases measured in LFP activity in the ACC and in the FEF during the delay period can be conceived of as a direct measure of coordination of spiking activity in the local circuits (Voloh et al. 2015). Theta phase indexed the spike-LFP synchronization from ACC to FEF and from FEF to ACC during retention of target locations. I speculate that this reciprocal interaction indexes the exchange of area specific information. For example FEF spikes carry location specific information about contralateral targets that could be conveyed to ACC circuits. ACC neurons typically containing spatially tuned targets only when those targets are linked to outcomes for top-down controlled behavior such as reward or attentional control demands (Hayden and Platt 2010; Johnston et al. 2007; Kaping et al. 2011; Kennerley et al. 2006; Shen et al. 2014; Shenhav et al. 2013). A linkage to these representations in the ACC could be crucial to prevent premature

responding during the working memory delay consistent with previous human and monkey results suggesting that ACC activation prevents impulsive responding (Agam et al. 2010; Brown et al. 2008; Milea et al. 2003). Indeed, it has been previously shown that neuronal spiking output can modulate the oscillatory activity by influencing the postsynaptic potentials (Pesaran et al. 2008). Thus, spiking activity that is synchronized between ACC and FEF could index the ongoing coupling of task relevant information required for successful working memory performance.

The role of frontal midline theta in working memory has been previously demonstrated in human studies and the ACC has been suggested as its main source (Gulbinaite et al. 2014; Kaplan et al. 2014; Meltzer et al. 2007). Moreover, the ACC has long been implicated in performance or conflict monitoring (Schall et al. 2002). In this regard, human studies have suggested that frontal midline theta is involved in the processing of conflict and errors (Cohen 2011; 2014). These reports suggest that the theta band plays a major role in the cognitive functioning of the ACC in humans, macaques, and rodents and my results provide further support for this claim.

*Beta-band synchronization.* As mentioned in the introduction, beta band synchronization is suggested to be involved in long-range transmission of information between brain areas (Engel and Fries 2010; Miller and Buschman 2013; Salazar et al. 2012; Womelsdorf et al. 2014a). In addition to theta band modulations, my study found a similarly prominent modulation of delay period activity in the beta frequency band. Enhanced ACC-FEF beta band specific coherence (1) was almost as prevalent as theta coherence (beta: 49% vs. theta: 66% of pairs), (2) showed significantly enhanced Granger-causality that pointed to a stronger directionality from ACC to FEF than vice



versa, and (3) was significantly reduced on error trials. These signatures resonate well with beta band spike-field coherence between FEF and parietal cortex and between ACC with lateral prefrontal cortex during goal directed task performance (Salazar et al. 2012; Womelsdorf et al. 2014b). Moreover, a previous study has documented that beta band specific activation is involved in the directional causal effect of the higher order association cortices over primary motor areas (Brovelli et al. 2004). My study suggests that the same frequency that characterizes these fronto-parietal interactions also incorporates interactions with medial frontal (ACC) and oculomotor (FEF) circuits. In a recent study, it has been shown that beta band synchrony is involved in cognitive and motor control during gait adaptation (Wagner et al. 2016). This report is in line with my findings suggesting the involvement of the ACC-FEF beta band synchronization in sensori-motor mapping. Furthermore, inter-areal beta synchrony is suggested to be enhanced with selective attention (Bastos et al. 2015; Buschman and Miller 2007; Micheli et al. 2015; Womelsdorf et al. 2014a). I observed increased beta synchrony both in the delay period of the memory-guided saccade task and the preparatory period of the anti saccade task. These findings suggest that the increased cognitive and attention demands of the tasks could underlie increased beta band synchronization between these areas. It will be an important task for future studies to characterize the extent and distribution of such a putative large-scale beta frequency band network and to disentangle the information carried in frequency specific coupling in such a beta network when compared to the network of brain areas that synchronize at theta frequency band (Womelsdorf and Everling 2015).

*Cellular mechanisms.* One possible mechanism for ACC-FEF phase-synchronization could be based on interactions of a subclass of parvalbumin expressing, fast spiking interneurons and subsets of pyramidal cells showing resonance to theta rhythmic inhibition (Stark et al. 2013). Stark and colleagues (2013) have documented that these interneurons induce theta rhythmic firing in pyramidal cells in the medial prefrontal cortex of rodents that is considered to be partly functional analogous to primate anterior cingulate cortices (Barbas 2015; Passingham and Wise 2012). Importantly, during 3-10 Hz theta rhythmic inhibition, pyramidal cell firing was not reduced as would be expected for an inhibitory regime, and even showed increased post-inhibitory firing, essentially implementing a theta mediated amplification of firing (Stark et al. 2013). Such theta-mediated amplification of spike output may facilitate and sustain long-range theta coherence between anterior cingulate, hippocampal, parietal and medial prefrontal structures of the rodent (Sirota et al. 2008). This widespread theta synchronization emerges in rodents during choice tasks that require working memory recall of spatial reward associations similar to spatial target associations that need to be maintained in my oculomotor response task (Benchenane et al. 2010; Siapas et al. 2005). I speculate that these rodent studies could therefore be informative about the cellular basis of working memory networks in primates. Consistent with this suggestion, a recent study in macaque ACC and lateral PFC identified two functional subclasses of a total of seven separable classes, one putative interneuron subclass and one putative pyramidal cell subclass, that showed a particular prominent phase synchronization with LFP's at theta band frequencies (Ardid et al. 2015). These theta band neurons segregated from other functional classes of neurons that either did not synchronize to the LFP at any frequency,

or that preferred to phase align their spiking activity with beta band oscillatory activity instead of theta frequencies (Ardid et al. 2015). Taken together, these findings suggest that frequency-specific synchronization of firing could be established by subsets of interneurons and pyramidal cells that share intrinsic resonance properties, and that are largely segregated from neuron populations that synchronize their firing to LFP activity at, e.g. beta band frequencies (Roux and Buzsaki 2015; Womelsdorf et al. 2014b)

*Summary.* In summary, the increased ACC-FEF phase synchrony and also increased causal effect of the ACC over FEF during the delay period suggests that the ACC-FEF interaction serves a functional role. The increased ACC unit-FEF LFP coupling in the delay period of the contra-verse saccades could indicate that the ACC biases FEF to generate a contra-verse saccade (Figure 3.8). My results also suggest that FEF sends target location signals to the ACC through increased FEF unit-ACC LFP coupling in the delay period of contra-verse saccades (Figure 3.8). I speculate that selective theta and beta frequency coherence of the FEF and ACC during working memory delays reveals how top-down information is actively coordinated to ensure the effective harvesting of rewards during top-down controlled behavior. I speculate that theta cycles may provide the critical reference for neuronal spikes in distributed brain systems to code for goal- and choice- relevant information (Kayser et al. 2012; Mizuseki et al. 2009; Pezzulo et al. 2014; Womelsdorf et al. 2014b).

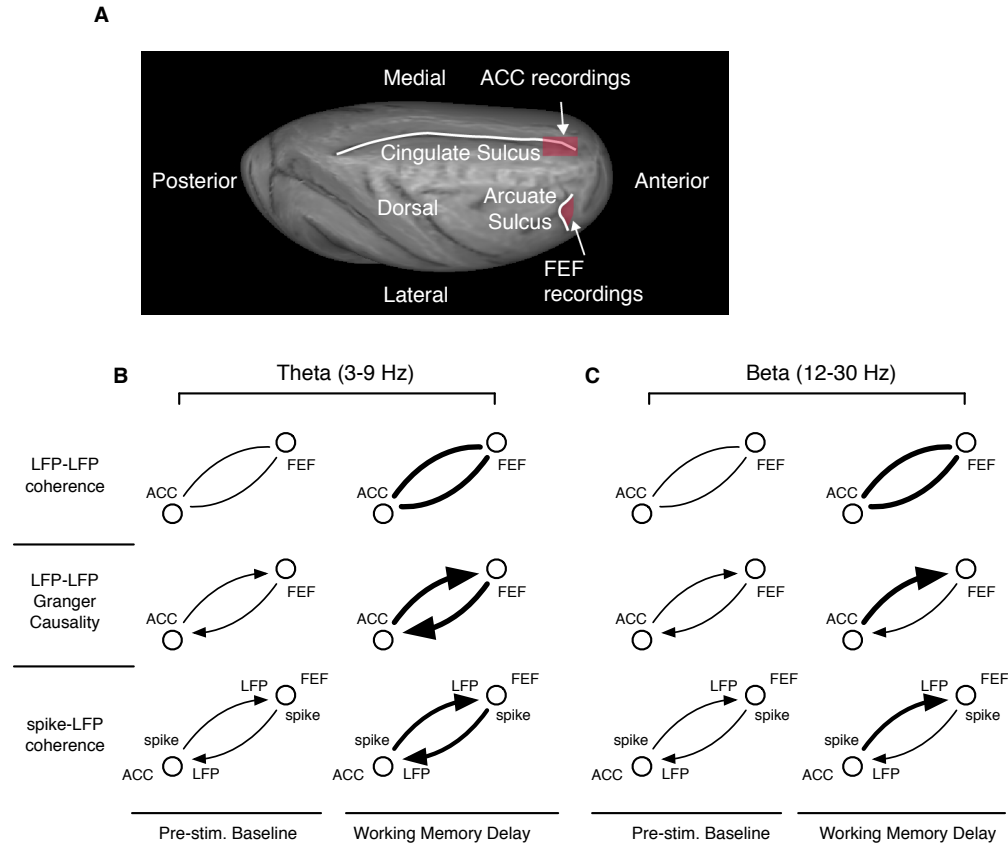


**Figure 3.8. Illustration of recorded brain area locations and summary of main inter-areal ACC-FEF modulations observed in this study.** (A) ACC and FEF recording locations (in red shading) shown on a rendering of a semi-inflated macaque brain. (B, C) Illustration of main inter-areal effects in the theta (B) and beta (C) band with the thickness of connections indicating the strength or prevalence of the effects. LFP-LFP coherence (top row) was modulated during the delay in > 75% of LFP-LFP pairs in both frequencies (with increased coherence in the largest majority). Granger causality (middle row) increased during the delay for both ACC-FEF and FEF-ACC directions, but the ACC to FEF granger causal flow was stronger than FEF to ACC granger causal flow at both, theta and beta frequencies. Spike-LFP coherence (bottom row) increased for both directions during the delay in the theta band, but was different between delay and baseline merely in one beta frequency bin (at 22Hz) for ACC spike to FEF LFP sites for contra-verse saccades. Reduced inter-area modulation prior to error commission was evident in both frequencies across different measures and is described in the text.

### 3.6. REFERENCES:

- Agam Y, Joseph RM, Barton JJ, and Manoach DS.** Reduced cognitive control of response inhibition by the anterior cingulate cortex in autism spectrum disorders. *Neuroimage* 52: 336-347, 2010.
- Akam T, and Kullmann DM.** Oscillatory multiplexing of population codes for selective communication in the mammalian brain. *Nature reviews Neuroscience* 15: 111-122, 2014.
- Ardid S, Vinck M, Kaping D, Marquez S, Everling S, and Womelsdorf T.** Mapping of functionally characterized cell classes onto canonical circuit operations in primate prefrontal cortex. *J Neurosci* 35: 2975-2991, 2015.
- Babapoor-Farrokhran S, Hutchison RM, Gati JS, Menon RS, and Everling S.** Functional connectivity patterns of medial and lateral macaque frontal eye fields reveal distinct visuomotor networks. *J Neurophysiol* 109: 2560-2570, 2013.
- Barbas H.** General Cortical and Special Prefrontal Connections: Principles from Structure to Function. *Annu Rev Neurosci* 2015.
- Bastos AM, Vezoli J, Bosman CA, Schoffelen JM, Oostenveld R, Dowdall JR, De Weerd P, Kennedy H, and Fries P.** Visual Areas Exert Feedforward and Feedback Influences through Distinct Frequency Channels. *Neuron* 85: 390-401, 2015.
- Benchenane K, Peyrache A, Khamassi M, Tierney PL, Gioanni Y, Battaglia FP, and Wiener SI.** Coherent Theta Oscillations and Reorganization of Spike Timing in the Hippocampal-Prefrontal Network upon Learning. *Neuron* 66: 921-936, 2010.
- Bressler SL, Tang W, Sylvester CM, Shulman GL, and Corbetta M.** Top-down control of human visual cortex by frontal and parietal cortex in anticipatory visual spatial attention. *Journal of Neuroscience* 28: 10056-10061, 2008.
- Brovelli A, Ding MZ, Ledberg A, Chen YH, Nakamura R, and Bressler SL.** Beta oscillations in a large-scale sensorimotor cortical network: Directional influences revealed by Granger causality. *P Natl Acad Sci USA* 101: 9849-9854, 2004.
- Brown MR, Vilis T, and Everling S.** Isolation of saccade inhibition processes: rapid event-related fMRI of saccades and nogo trials. *Neuroimage* 39: 793-804, 2008.
- Bruce CJ, and Goldberg ME.** Primate frontal eye fields. I. Single neurons discharging before saccades. *Journal of neurophysiology* 53: 603-635, 1985.
- Bruce CJ, Goldberg ME, Bushnell MC, and Stanton GB.** Primate frontal eye fields. II. Physiological and anatomical correlates of electrically evoked eye movements. *J Neurophysiol* 54: 714-734, 1985.
- Buschman TJ, and Miller EK.** Top-down versus bottom-up control of attention in the prefrontal and posterior parietal cortices. *Science* 315: 1860-1862, 2007.
- Caspari N, Janssens T, Mantini D, Vandenberghe R, and Vanduffel W.** Covert shifts of spatial attention in the macaque monkey. *J Neurosci* 35: 7695-7714, 2015.
- Cohen MX.** Error-related medial frontal theta activity predicts cingulate-related structural connectivity. *NeuroImage* 55: 1373-1383, 2011.
- Cohen MX.** A neural microcircuit for cognitive conflict detection and signaling. *Trends Neurosci* 37: 480-490, 2014.
- Corbetta M, and Shulman GL.** Control of goal-directed and stimulus-driven attention in the brain. *Nature reviews Neuroscience* 3: 201-215, 2002.

**D'Esposito M, and Postle BR.** The cognitive neuroscience of working memory. *Annu Rev Psychol* 66: 115-142, 2015.

**Dotson NM, Salazar RF, and Gray CM.** Frontoparietal Correlation Dynamics Reveal Interplay between Integration and Segregation during Visual Working Memory. *Journal of Neuroscience* 34: 13600-13613, 2014.

**Engel AK, and Fries P.** Beta-band oscillations--signalling the status quo? *Curr Opin Neurobiol* 20: 156-165, 2010.

**Fries P.** A mechanism for cognitive dynamics: neuronal communication through neuronal coherence. *Trends Cogn Sci* 9: 474-480, 2005.

**Fujisawa S, and Buzsaki G.** A 4 Hz oscillation adaptively synchronizes prefrontal, VTA, and hippocampal activities. *Neuron* 72: 153-165, 2011.

**Funahashi S, Bruce CJ, and Goldman-Rakic PS.** Mnemonic coding of visual space in the monkey's dorsolateral prefrontal cortex. *J Neurophysiol* 61: 331-349, 1989.

**Goldman-Rakic PS.** Cellular and circuit basis of working memory in prefrontal cortex of nonhuman primates. *Progress in brain research* 85: 325-335; discussion 335-326, 1990.

**Gregoriou GG, Gotts SJ, Zhou H, and Desimone R.** High-frequency, long-range coupling between prefrontal and visual cortex during attention. *Science* 324: 1207-1210, 2009.

**Gregoriou GG, Rossi AF, Ungerleider LG, and Desimone R.** Lesions of prefrontal cortex reduce attentional modulation of neuronal responses and synchrony in V4. *Nat Neurosci* 17: 1003-1011, 2014.

**Gulbinaite R, van Rijn H, and Cohen MX.** Fronto-parietal network oscillations reveal relationship between working memory capacity and cognitive control. *Front Hum Neurosci* 8: 2014.

**Hayden BY, and Platt ML.** Neurons in Anterior Cingulate Cortex Multiplex Information about Reward and Action. *Journal of Neuroscience* 30: 3339-3346, 2010.

**Johnston K, Levin HM, Koval MJ, and Everling S.** Top-down control-signal dynamics in anterior cingulate and prefrontal cortex neurons following task switching. *Neuron* 53: 453-462, 2007.

**Kaping D, Vinck M, Hutchison RM, Everling S, and Womelsdorf T.** Specific contributions of ventromedial, anterior cingulate, and lateral prefrontal cortex for attentional selection and stimulus valuation. *PLoS Biol* 9: e1001224, 2011.

**Kaplan R, Bush D, Bonnefond M, Bandettini PA, Barnes GR, Doeller CF, and Burgess N.** Medial prefrontal theta phase coupling during spatial memory retrieval. *Hippocampus* 24: 656-665, 2014.

**Kayser C, Ince RAA, and Panzeri S.** Analysis of Slow (Theta) Oscillations as a Potential Temporal Reference Frame for Information Coding in Sensory Cortices. *Plos Comput Biol* 8: 2012.

**Kennerley SW, Walton ME, Behrens TE, Buckley MJ, and Rushworth MF.** Optimal decision making and the anterior cingulate cortex. *Nat Neurosci* 9: 940-947, 2006.

**Liebe S, Hoerzer GM, Logothetis NK, and Rainer G.** Theta coupling between V4 and prefrontal cortex predicts visual short-term memory performance. *Nat Neurosci* 15: 456-U150, 2012.

**Lisman JE, and Jensen O.** The theta-gamma neural code. *Neuron* 77: 1002-1016, 2013.

**Ma WJ, Husain M, and Bays PM.** Changing concepts of working memory. *Nat Neurosci* 17: 347-356, 2014.

**McDowell JE, Dyckman KA, Austin BP, and Clementz BA.** Neurophysiology and neuroanatomy of reflexive and volitional saccades: evidence from studies of humans. *Brain Cogn* 68: 255-270, 2008.

**Meltzer JA, Negishi M, Mayes LC, and Constable RT.** Individual differences in EEG theta and alpha dynamics during working memory correlate with fMRI responses across subjects. *Clin Neurophysiol* 118: 2419-2436, 2007.

**Micheli C, Kaping D, Westendorff S, Valiante TA, and Womelsdorf T.** Inferior-frontal cortex phase synchronizes with the temporal-parietal junction prior to successful change detection. *Neuroimage* 119: 417-431, 2015.

**Milea D, Lehericy S, Rivaud-Pechoux S, Duffau H, Lobel E, Capelle L, Marsault C, Berthoz A, and Pierrot-Deseilligny C.** Antisaccade deficit after anterior cingulate cortex resection. *Neuroreport* 14: 283-287, 2003.

**Miller EK, and Buschman TJ.** Cortical circuits for the control of attention. *Curr Opin Neurobiol* 23: 216-222, 2013.

**Mizuseki K, Sirota A, Pastalkova E, and Buzsaki G.** Theta oscillations provide temporal windows for local circuit computation in the entorhinal-hippocampal loop. *Neuron* 64: 267-280, 2009.

**Moore T, and Armstrong KM.** Selective gating of visual signals by microstimulation of frontal cortex. *Nature* 421: 370-373, 2003.

**Passingham R, and Wise S.** *The Neurobiology of the Prefrontal Cortex: Anatomy, Evolution, and the Origin of Insight*. Oxford University Press, 2012.

**Pesaran B, Nelson MJ, and Andersen RA.** Free choice activates a decision circuit between frontal and parietal cortex. *Nature* 453: 406-409, 2008.

**Pezzulo G, van der Meer MAA, Lansink CS, and Pennartz CMA.** Internally generated sequences in learning and executing goal-directed behavior. *Trends Cogn Sci* 18: 647-657, 2014.

**Phillips JM, Vinck M, Everling S, and Womelsdorf T.** A long-range fronto-parietal 5- to 10-Hz network predicts "top-down" controlled guidance in a task-switch paradigm. *Cereb Cortex* 24: 1996-2008, 2014.

**Roux L, and Buzsaki G.** Tasks for inhibitory interneurons in intact brain circuits. *Neuropharmacology* 88: 10-23, 2015.

**Salazar RF, Dotson NM, Bressler SL, and Gray CM.** Content-specific fronto-parietal synchronization during visual working memory. *Science* 338: 1097-1100, 2012.

**Schall JD, Stuphorn V, and Brown JW.** Monitoring and control of action by the frontal lobes. *Neuron* 36: 309-322, 2002.

**Shen C, Ardid S, Kaping D, Westendorff S, Everling S, and Womelsdorf T.** Anterior Cingulate Cortex Cells Identify Process-Specific Errors of Attentional Control Prior to Transient Prefrontal-Cingulate Inhibition. *Cereb Cortex* 2014.

**Shenhav A, Botvinick MM, and Cohen JD.** The expected value of control: an integrative theory of anterior cingulate cortex function. *Neuron* 79: 217-240, 2013.

**Siapas AG, Lubenov EV, and Wilson MA.** Prefrontal phase locking to hippocampal theta oscillations. *Neuron* 46: 141-151, 2005.

**Sirota A, Montgomery S, Fujisawa S, Isomura Y, Zugaro M, and Buzsaki G.** Entrainment of neocortical neurons and gamma oscillations by the hippocampal theta rhythm. *Neuron* 60: 683-697, 2008.

**Stark E, Eichler R, Roux L, Fujisawa S, Rotstein HG, and Buzsaki G.** Inhibition-induced theta resonance in cortical circuits. *Neuron* 80: 1263-1276, 2013.

**Thompson KG, Biscoe KL, and Sato TR.** Neuronal basis of covert spatial attention in the frontal eye field. *J Neurosci* 25: 9479-9487, 2005.

**Vinck M, Battaglia FP, Womelsdorf T, and Pennartz C.** Improved measures of phase-coupling between spikes and the Local Field Potential. *J Comput Neurosci* 33: 53-75, 2012.

**Vinck M, Womelsdorf T, Buffalo EA, Desimone R, and Fries P.** Attentional Modulation of Cell-Class-Specific Gamma-Band Synchronization in Awake Monkey Area V4. *Neuron* 80: 1077-1089, 2013.

**Voloh B, Valiante TA, Everling S, and Womelsdorf T.** Theta,  $\gamma$  coordination between anterior cingulate and prefrontal cortex indexes correct attention shifts. *Proceedings of the National Academy of Sciences* 2015.

**Wagner J, Makeig S, Gola M, Neuper C, and Muller-Putz G.** Distinct beta Band Oscillatory Networks Subservicing Motor and Cognitive Control during Gait Adaptation. *J Neurosci* 36: 2212-2226, 2016.

**Wang XJ.** Neurophysiological and computational principles of cortical rhythms in cognition. *Physiol Rev* 90: 1195-1268, 2010.

**Wang Y, Matsuzaka Y, Shima K, and Tanji J.** Cingulate cortical cells projecting to monkey frontal eye field and primary motor cortex. *Neuroreport* 15: 1559-1563, 2004.

**Womelsdorf T, Ardid S, Everling S, and Valiante TA.** Burst firing synchronizes prefrontal and anterior cingulate cortex during attentional control. *Curr Biol* 24: 2613-2621, 2014a.

**Womelsdorf T, and Everling S.** Long-Range Attention Networks: Circuit Motifs Underlying Endogenously Controlled Stimulus Selection. *Trends Neurosci* 38: 682-700, 2015.

**Womelsdorf T, Johnston K, Vinck M, and Everling S.** Theta-activity in anterior cingulate cortex predicts task rules and their adjustments following errors. *P Natl Acad Sci USA* 107: 5248-5253, 2010a.

**Womelsdorf T, Schoffelen JM, Oostenveld R, Singer W, Desimone R, Engel AK, and Fries P.** Modulation of neuronal interactions through neuronal synchronization. *Science* 316: 1609-1612, 2007.

**Womelsdorf T, Valiante TA, Sahin NT, Miller KJ, and Tiesinga P.** Dynamic circuit motifs underlying rhythmic gain control, gating and integration. *Nat Neurosci* 17: 1031-1039, 2014b.

**Womelsdorf T, Vinck M, Leung LS, and Everling S.** Selective theta-synchronization of choice-relevant information subserves goal-directed behavior. *Front Hum Neurosci* 4: 2010b.

**Womelsdorf T, Vinck M, Leung LS, and Everling S.** Selective theta-synchronization of choice-relevant information subserves goal-directed behavior. *Front Hum Neurosci* 4: 210, 2010c.

**Wurtz RH, and Mohler CW.** Enhancement of visual responses in monkey striate cortex and frontal eye fields. *J Neurophysiol* 39: 766-772, 1976.



### **3.7. SUPPLEMENTARY METHODS:**

#### **3.7.1. Subjects:**

Two male adult macaque monkeys (*M. mulatta* and *M. fascicularis*) weighing 7-9 kg were subjects in this study. Recording chambers were implanted over the right arcuate sulcus and right anterior cingulate sulcus based on previously obtained MRIs. Details for the surgical procedures have been described previously (Phillips et al. 2014). Postsurgical MRIs were obtained to confirm the location of the recording chambers and to allow reconstruction of the recording sites. All experimental procedures and animal care were implemented in accordance with the guidelines of the Canadian Council of Animal Care policy on the care and use of laboratory animals and an ethics protocol approved by the Animal Users Subcommittee of the University of Western Ontario Council on Animal Care. The monkeys were under close supervision by the university veterinarians.

#### **3.7.2. Behavioral Task:**

Animals were trained to perform a standard memory-guided saccade (Figure 3.1 A). Each trial started with the presentation of a white central fixation point ( $0.15^\circ$ ). Once monkeys fixated this spot within a  $0.5^\circ \times 0.5^\circ$  window for 500ms, a white target stimulus ( $0.15^\circ$ ) was presented for 100ms with equal probability in one of 8 cardinal directions ( $0^\circ, 45^\circ, 90^\circ, 135^\circ, 180^\circ, 225^\circ, 270^\circ, 315^\circ$ ) at a distance of  $9^\circ$  from the central fixation point. The animals were required to maintain fixation during the stimulus presentation and during the 1000ms period following stimulus presentation, which I define as the delay period of the task. During the delay period the central fixation point remained illuminated and the target stimulus was not visible. The offset of the central fixation point

instructed the monkeys to perform a saccade toward the remembered target location. To obtain a water reward, the monkeys were required to perform a saccade within 500ms after the offset of the central fixation point toward the remembered location (window of  $5^{\circ} \times 5^{\circ}$ ) and to maintain fixation at the remembered target location for a random period of 300-600ms. If the animal correctly performed all the required steps, the target stimulus reappeared and the animal received a water reward (Figure 3.1 A). Eye movements were recorded at 500Hz and 1000 Hz using video eye trackers (EyeLink II and EyeLink 1000, Kanata, ON, Canada). Presentation of the behavioral stimuli, monitoring of the responses and reward delivery were controlled using CORTEX as the experimental control software (NIMH, Bethesda, MA, USA). Task events, vertical and horizontal eye positions and digitized neural signals were stored together using either a Plexon MAP or Omniplex system (Plexon Inc., Dallas, TX). I visually inspected the eye traces and the trials in which the eye movement trajectory deviated from the normal pathway were excluded. Monkey 1 correctly performed 94.68% and monkey 2 correctly performed 89.97% of memory-guided saccade trials.

The animals did not make many errors in the memory-guided saccade task and this makes the analysis of performance-related effects challenging. To overcome this shortcoming of the memory-guided saccade task, I also used a randomly interleaved pro-/anti-saccade task and the anti-saccade task led to more direction error trials. In this task, each trial started with the appearance of a central fixation point ( $0.15^{\circ}$ ) the color of which instructed the monkeys to perform a pro- or anti-saccade on stimulus presentation. The fixation point remained illuminated for a period of 1100-1400ms, which I designate as the preparatory period. The monkeys were required to maintain fixation during the

preparatory period and then the target stimulus appeared at a distance of 9° either to the right or left of the central fixation point. In pro-saccade trials, the monkeys were required to saccade towards the target stimulus and in anti-saccade trials they had to make a saccade towards the mirror location of the target stimulus (Figure 3.1 A). To obtain a water reward, the monkeys were required to maintain fixation at the target location for a random period of 300-600ms. Monkey 1 correctly performed 76.85% and monkey 2 correctly performed 82.63% of anti-saccade trials.

### ***3.7.3. Electrophysiological Recordings:***

FEF and ACC recordings were performed by advancing tungsten microelectrodes (FHC, Bowdoinham, ME) through guide tubes into the brain using software controlled precision micro-drives (NAN Instruments Ltd., Israel) on a daily basis. The micro-drives were assembled on a plastic grid with 1mm inter-hole distance. At the beginning of each experimental session, 2-4 electrodes were advanced into the FEF and ACC. The coordinates of the ACC recording sites for monkey 1 were 5-17 mm anterior, 8-12 mm dorsal and 2-4 mm to the right side of the anterior commissure. Similarly, the coordinates of the ACC recording sites for monkey 2 were 7-17 mm anterior, 12-16 mm dorsal and 2-4 mm to the right side of the anterior commissure. The coordinates of the FEF recording sites for monkey 1 were 1 mm anterior, 8-12 mm dorsal and 13-16 mm to the right side of the anterior commissure. The coordinates of the FEF recording sites for monkey 2 were 2-4 mm anterior, 10-16 mm dorsal and 12-16 mm to the right side of the anterior commissure. The ACC recording sites included areas 24d, 24b and 10m according to the composite monkey brain atlas of Van Essen et al.(Van Essen et al. 2012). The proper location of the FEF electrodes was confirmed by electrical micro-stimulation as

previously described (Bruce et al. 1985) (train duration of 70 ms set at 300 Hz, biphasic pulses of 0.2 ms duration, current < 50 $\mu$ A). Supplementary Figure 3.1 shows a reconstruction of the ACC and FEF recording sites.

The signal from each electrode was pre-amplified (Plexon Inc.) and band-pass filtered between 0.5-250 Hz for LFP signals and between 250-8000 Hz for the single-/multi-units and digitized at the frequency of 40kHz. Each area's signal was referenced separately against the corresponding recording chamber. The sampling rate for LFP signals was set at 1000 Hz. ACC and FEF multi-neuron activity was isolated offline by applying a threshold  $\pm$  3-5 standard deviations above or below the average raw signal to separate the multi-neuron activity from noise. I further visually inspected the waveforms to confirm that this procedure resulted in normal waveforms and the multi-units with abnormal waveform shape were excluded from the analysis. I will refer to multi-neuron activity as units throughout the paper.

#### **3.7.4. Data Analysis:**

*Spectral Power Analysis.* All of the data analyses were performed with custom written Matlab code (Mathworks, Natick, MA) using the fieldtrip toolbox (<http://www.ru.nl/fcdonders/fieldtrip/>) (Oostenveld et al. 2011). I first performed an artifact rejection procedure. In this procedure, the trials in which the LFP power exceeded 4 standard deviations from the average were excluded from the analysis. Then, I performed Fast Fourier transformation following hanning tapering of the data (Bosman et al. 2012) (a multi-taper method with a discrete prolate spheroidal sequence was used to analyze 40-100Hz frequencies) around the time of the target stimulus onset and the delay period. The analysis window started at 1500 ms prior to and ended at 1200ms after the

target stimulus onset. The analysis time window did not have any overlap with the reward presentation to avoid contamination of the data with possible reward consumption artifacts. I performed the frequency analysis using a 670 ms sliding time window in 50ms steps. The power spectra for individual channels were z-score normalized using a baseline of 500-1000 ms prior to the fixation point onset in both memory-guided saccade task and pro/anti-saccade task.

*Field-Field coherence analysis.* I performed a phase coherence analysis between FEF and ACC electrodes using Weighted Phase Lag Index (Lipsman et al. 2014; Phillips et al. 2014; Vinck et al. 2011) (WPLI-debiased; see (Vinck et al. 2011) for a detailed mathematical definition of the method). Briefly, WPLI is exclusively based on the imaginary component of the cross-spectrum and it is insensitive to volume conduction from a single source or a common reference. Furthermore, the WPLI is more robust to noise and is invariant when two dependent sources mix linearly and thus, it is more sensitive in detection of the true interactions between two signals (Lipsman et al. 2014; Vinck et al. 2011). WPLI is defined:

$$\frac{\sum_{j=1}^N \Im \{X_j\}}{\sum_{j=1}^N |\Im \{X_j\}|} \quad (1)$$

Here,  $\Im \{X_j\}$  is the imaginary component of the cross-spectrum in the  $j$ -th trial. Sample size is a concern when using WPLI and hence, I used WPLI-debiased which estimates the squared WPLI. WPLI-debiased has negligible sample size bias for datasets of small sample size (Vinck et al. 2011). In order to test for the difference in WPLI-debiased coherence across experimental conditions, I first averaged the WPLI-debiased theta band coherence across the appropriate time window for each channel pair (e.g. 400-1100ms following the target stimulus as the delay related WPLI-debiased theta coherence and

700ms prior to fixation point onset as the baseline WPLI-debiased coherence in the memory-guided saccade task). Then, I performed a t-test to investigate whether there is a statistically significant difference across experimental conditions. I performed the comparison of WPLI-debiased coherence between correct and error trials with the adjusted number of correct trials relative to errors and the results showed significant effects as I have reported in this manuscript. I also used a permutation test to further validate the results obtained by the t-tests. In this test, I pooled the data from two conditions and randomly split the pooled data into two groups with the same sample sizes for a minimum of 1000 times. Afterwards, I obtained a distribution of the difference in the means of the shuffled groups. If the difference of the means of the original samples fell at least  $> 95\%$  of the generated distribution ( $>97.5\%$  for two-tailed tests), I considered the difference between groups as significant. I obtained statistically significant results in all the comparisons that t-test yielded statistical significance; thus, I could validate the t-test results with this permutation test.

The WPLI-debiased method outputs a single value for a given trial set and thus, I cannot perform a traditional statistics to test whether there is a difference in WPLI-debiased coherence between the baseline and delay period of a single channel pair. To test for a statistically significant difference in coherence between baseline (700ms before fixation onset) and delay (400-1100ms after stimulus onset) period in a single channel pair, I used a bootstrapping approach. I created 1000 bootstraps with replacement of the original trial set and obtained a distribution of the WPLI-debiased for the baseline and delay periods. The difference between baseline and delay was determined to be significant if the mean of the WPLI-debiased in the delay period fell above or below the

99.9<sup>th</sup> percentile of the WPLI-debiased distribution of the baseline period. In order to further confirm the results of the bootstrapping procedure, I pooled the baseline and delay WPLI-debiased results and randomly assigned them into two groups. Then, I tested whether the mean difference between the original baseline and delay period falls above or below the 99.9<sup>th</sup> percentile of the mean difference of the randomly generated groups. The results of this procedure yielded nearly identical results to the bootstrapping procedure I have described above.

*Granger causality analysis:* To analyze the directionality of interactions, I performed Granger-causality analysis. Granger-causality analysis is based on modeling the two time series as a vector autoregressive model,

$$\begin{aligned} x_1(t) &= \sum_{m=1}^M (A_{11}(\tau) x_1(t-\tau) + \sum_{m=1}^M (A_{12}(\tau) x_2(t-\tau) + \varepsilon_1(t) \\ x_2(t) &= \sum_{m=1}^M (A_{22}(\tau) x_2(t-\tau) + \sum_{m=1}^M (A_{21}(\tau) x_1(t-\tau) + \varepsilon_2(t). \end{aligned} \quad (2)$$

In this equation, the two signals are predicted by a linear combination of their own past values, and the past values of the other time series. The residual errors (unexplained variance) are captured by the variables  $\varepsilon_1(t)$  and  $\varepsilon_2(t)$ , with covariance matrix  $\Sigma$ . I estimated the coefficients for the VAR model by setting the order  $M=32$  and using the *armorf* function in the BSMART toolbox (Cui et al. 2008) to find the least-squares solution to equation (2). I then used the standard decomposition of Granger's time domain causality into frequency-domain Granger-causality, as developed by Geweke et al. (1982) (Geweke 1982). Fourier transformation of equation (2) yields the spectral decomposition

$$\mathbf{S}(f) = \mathbf{H}(f)\Sigma\mathbf{H}^*(f) \quad (3)$$

The frequency-domain Granger-causality from  $x_2$  to  $x_1$  is now defined as

$$I_{2 \rightarrow 1} = \ln \frac{S_{11}(f)}{S_{11}(f) - \left( \Sigma_{22} - \frac{\Sigma_{12}^2}{\Sigma_{11}} \right) |H_{12}(f)|^2} \quad (4)$$

This expression can be understood as the log fraction of intrinsic power in the first signal at frequency  $f$  over the amount of power that remains after the predictions from the second signal have been factored in.

It is well established that Granger-causality can be sensitive to both uncorrelated and correlated noise that is superimposed on the measurements of the signals of interest. This can lead to a substantial amount of false alarms in the identification of Granger-causality relationships (see (Haufe et al. 2013; Javor-Duray et al. 2015; Nolte et al. 2008; Vinck et al. 2015; Winkler et al. 2015)). I have recently shown that an effective control for the noise problem can be achieved by using the time reversal of signals. If the Granger-causality from  $x_1$  to  $x_2$  is stronger than the Granger-causality from  $x_2$  to  $x_1$ , then I expect that the reverse holds true when I time-reverse the signals. Thus, I only accept conclusions about the asymmetry of Granger-causality when both conditions hold true. For the analysis of the present dataset, I determined for each channel combination whether the asymmetry in Granger-causality values in the theta-frequency range flipped after time-reversing the signals. I only selected those ACC-FEF channel combinations for which this held true. In other words, if an ACC (FEF) channel tended to Granger-cause the FEF (ACC) channel in the theta-range, then I expected that the FEF (ACC) channel would Granger-cause the ACC (FEF) channel after time-reversing the signals. As shown by (Vinck et al. 2015), this provides a highly effective procedure to diminish the influence of correlated and uncorrelated noise.

The Granger causal effect of the ACC over FEF is shown as  $G_{ACC \rightarrow FEF}$  and the Granger causal effect of FEF over ACC is denoted as  $G_{FEF \rightarrow ACC}$ . The overall causal



effect of ACC over FEF was derived by implementing the ( $G_{ACC \rightarrow FEF} - G_{FEF \rightarrow ACC}$ ) equation. The results shown in Figures 3.3 F and 3.3 H are obtained by implementing the ( $G_{ACC \rightarrow FEF} - G_{FEF \rightarrow ACC}$ ) equation. The results shown in Supplementary Figure 3.4 A depicts  $G_{ACC \rightarrow FEF}$ , Supplementary Figure 3.4 B shows  $G_{FEF \rightarrow ACC}$ , and Supplementary Figure 3.4 C shows both  $G_{ACC \rightarrow FEF}$  (blue) and  $G_{FEF \rightarrow ACC}$  (red). I tested the difference between the baseline (700 ms before fixation onset) and the delay period (400-1100 ms following stimulus onset), using a t-test. I further confirmed the results of the t-test by implementing a permutation test. The permutation test procedure is described in detail above.

I also shuffled the time-frequency transformed raw data and computed the corresponding Granger values to obtain the chance level Granger. Then I compared the chance level  $G_{ACC \rightarrow FEF}$  and  $G_{FEF \rightarrow ACC}$  values to the original Granger values from the non-shuffled dataset. I observed that across theta and beta frequencies, both the  $G_{ACC \rightarrow FEF}$  and  $G_{FEF \rightarrow ACC}$  values in the baseline and delay periods were above the chance level.

*Spike-Field coherence analysis.* I used the Pairwise Phase consistency PPC as a measure of spike-field synchrony; for a detailed mathematical definition see (Vinck et al. 2012). Briefly, the PPC measure is robust to variations in the neuronal spike rate and to possible inter-dependencies of the spike-LFP phases (Vinck et al. 2013). It is defined as

$$PPC = \frac{\sum_{i=1}^M \sum_{j \neq i}^M U_i U_j}{M*(M-1)}$$

Here, M is the number of spikes,  $U_i$  is the vector describing the x and y component of the spike-LFP phase for the i-th. I only included units with at least 50 spiking events in the tested conditions to obtain a reliable and robust results and increase the statistical power of the analysis as has been shown before (Cabral et al. 2014; Liebe et al. 2012;

Womelsdorf et al. 2012). I performed a paired t-test and also a permutation test to probe the significant difference of the PPC across experimental conditions. I have described the permutation procedure above. In order to correct for multiple comparisons, I have implemented the false discovery rate (FDR) algorithm as described by Benjamini and Yekutieli (2001) (Benjamini and Yekutieli 2001).

In order to test for significant spike-field coupling across single ACC-unit-to-FEF-LFP and FEF-unit-to-ACC-LFP, I performed a permutation test. I first randomly shuffled the spikes across the tested conditions (e.g. baseline and delay) and obtained a distribution of the PPC values in the randomized experimental conditions. Then, I tested whether the PPC values of the original non-randomized conditions fell above or below the 2.5<sup>th</sup> percentile of the randomization distribution. If so, I designated that unit-LFP pair as having a significant modulation across the tested conditions.

### ***3.7.5. Supplementary references:***

**Benjamini Y, and Yekutieli D.** The control of the false discovery rate in multiple testing under dependency. *Ann Stat* 29: 1165-1188, 2001.

**Bosman CA, Schoffelen JM, Brunet N, Oostenveld R, Bastos AM, Womelsdorf T, Rubehn B, Stieglitz T, De Weerd P, and Fries P.** Attentional stimulus selection through selective synchronization between monkey visual areas. *Neuron* 75: 875-888, 2012.

**Bruce CJ, Goldberg ME, Bushnell MC, and Stanton GB.** Primate frontal eye fields. II. Physiological and anatomical correlates of electrically evoked eye movements. *J Neurophysiol* 54: 714-734, 1985.

**Cabral HO, Vinck M, Fouquet C, Pennartz CM, Rondi-Reig L, and Battaglia FP.** Oscillatory dynamics and place field maps reflect hippocampal ensemble processing of sequence and place memory under NMDA receptor control. *Neuron* 81: 402-415, 2014.

**Cui J, Xu L, Bressler SL, Ding M, and Liang H.** Bsmart: A Matlab/C Toolbox for Analysis of Multichannel Neural Time Series. *Neural Networks* 21: 1094-1104, 2008.

**Geweke J.** Measurement of Linear-Dependence and Feedback between Multiple Time-Series. *J Am Stat Assoc* 77: 304-313, 1982.

**Haufe S, Nikulin VV, Muller KR, and Nolte G.** A critical assessment of connectivity measures for EEG data: a simulation study. *Neuroimage* 64: 120-133, 2013.

**Javor-Duray BN, Vinck M, van der Roest M, Mulder AB, Stam CJ, Berendse HW, and Voorn P.** Early-onset cortico-cortical synchronization in the hemiparkinsonian rat model. *J Neurophysiol* 113: 925-936, 2015.

**Liebe S, Hoerzer GM, Logothetis NK, and Rainer G.** Theta coupling between V4 and prefrontal cortex predicts visual short-term memory performance. *Nat Neurosci* 15: 456-U150, 2012.

**Lipsman N, Kaping D, Westendorff S, Sankar T, Lozano AM, and Womelsdorf T.** Beta coherence within human ventromedial prefrontal cortex precedes affective value choices. *Neuroimage* 85: 769-778, 2014.

**Nolte G, Ziehe A, Nikulin VV, Schlogl A, Kramer N, Brismar T, and Muller KR.** Robustly estimating the flow direction of information in complex physical systems. *Phys Rev Lett* 100: 234101, 2008.

**Oostenveld R, Fries P, Maris E, and Schoffelen JM.** FieldTrip: Open source software for advanced analysis of MEG, EEG, and invasive electrophysiological data. *Comput Intell Neurosci* 2011: 156869, 2011.

**Phillips JM, and Everling S.** Neural activity in the macaque putamen associated with saccades and behavioral outcome. *PloS one* 7: e51596, 2012.

**Phillips JM, Vinck M, Everling S, and Womelsdorf T.** A long-range fronto-parietal 5- to 10-Hz network predicts "top-down" controlled guidance in a task-switch paradigm. *Cereb Cortex* 24: 1996-2008, 2014.

**Van Essen DC, Glasser MF, Dierker DL, and Harwell J.** Cortical parcellations of the macaque monkey analyzed on surface-based atlases. *Cereb Cortex* 22: 2227-2240, 2012.

**Vinck M, Battaglia FP, Womelsdorf T, and Pennartz C.** Improved measures of phase-coupling between spikes and the Local Field Potential. *J Comput Neurosci* 33: 53-75, 2012.

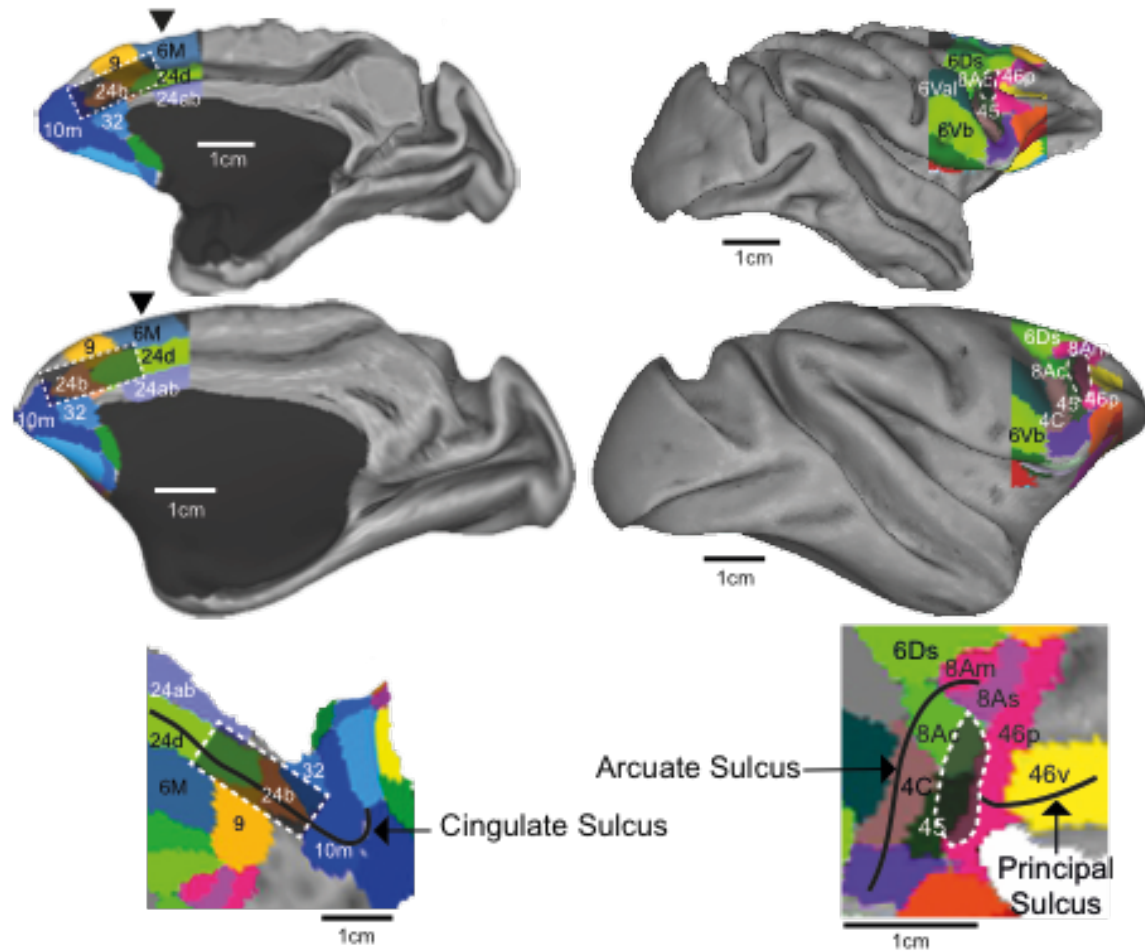
**Vinck M, Huurdeman L, Bosman CA, Fries P, Battaglia FP, Pennartz CMA, and Tiesinga PH.** How to detect the Granger-causal flow direction in the presence of additive noise? *Neuroimage* 108: 301-318, 2015.

**Vinck M, Oostenveld R, van Wingerden M, Battaglia F, and Pennartz CM.** An improved index of phase-synchronization for electrophysiological data in the presence of volume-conduction, noise and sample-size bias. *Neuroimage* 55: 1548-1565, 2011.

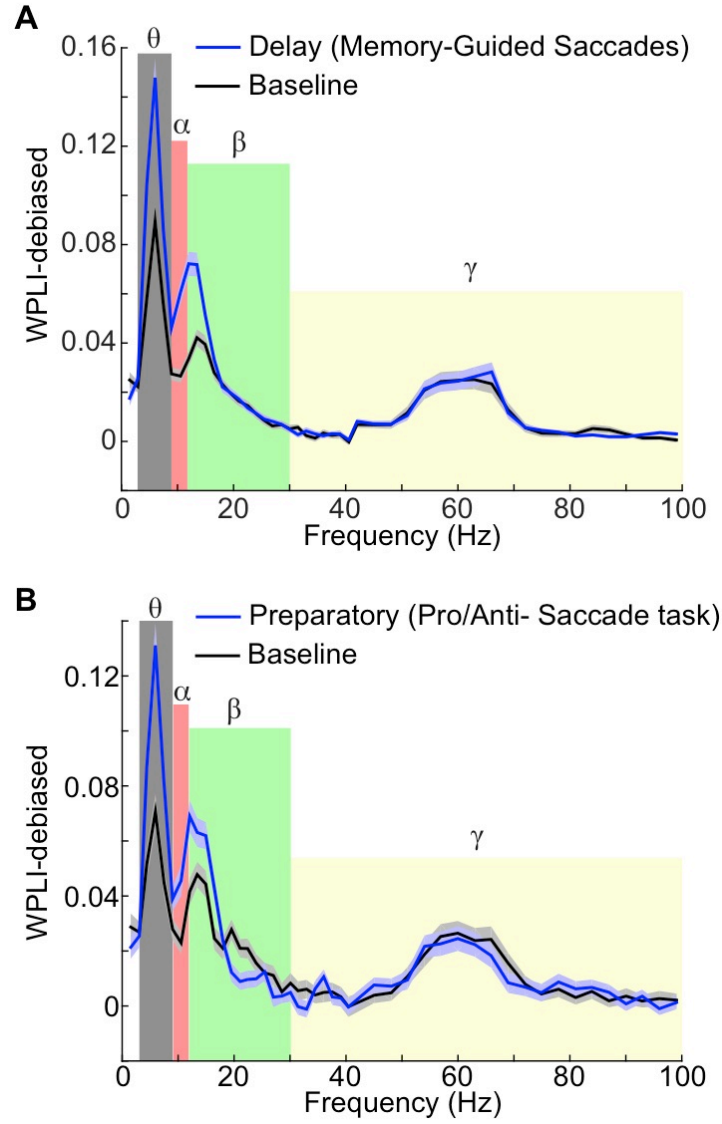
**Vinck M, Womelsdorf T, Buffalo EA, Desimone R, and Fries P.** Attentional Modulation of Cell-Class-Specific Gamma-Band Synchronization in Awake Monkey Area V4. *Neuron* 80: 1077-1089, 2013.

**Winkler I, Haufe S, Porbadnigk AK, Muller KR, and Dahne S.** Identifying Granger causal relationships between neural power dynamics and variables of interest. *Neuroimage* 111: 489-504, 2015.

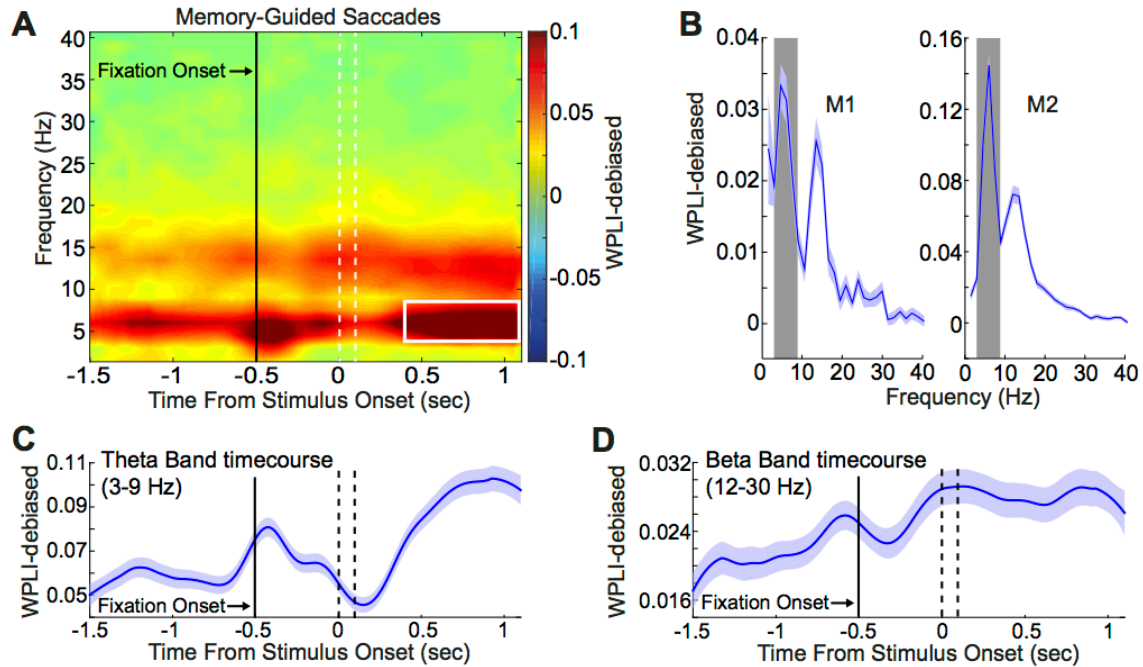
**Womelsdorf T, Lima B, Vinck M, Oostenveld R, Singer W, Neuenschwander S, and Fries P.** Orientation selectivity and noise correlation in awake monkey area V1 are modulated by the gamma cycle. *P Natl Acad Sci USA* 109: 4302-4307, 2012.



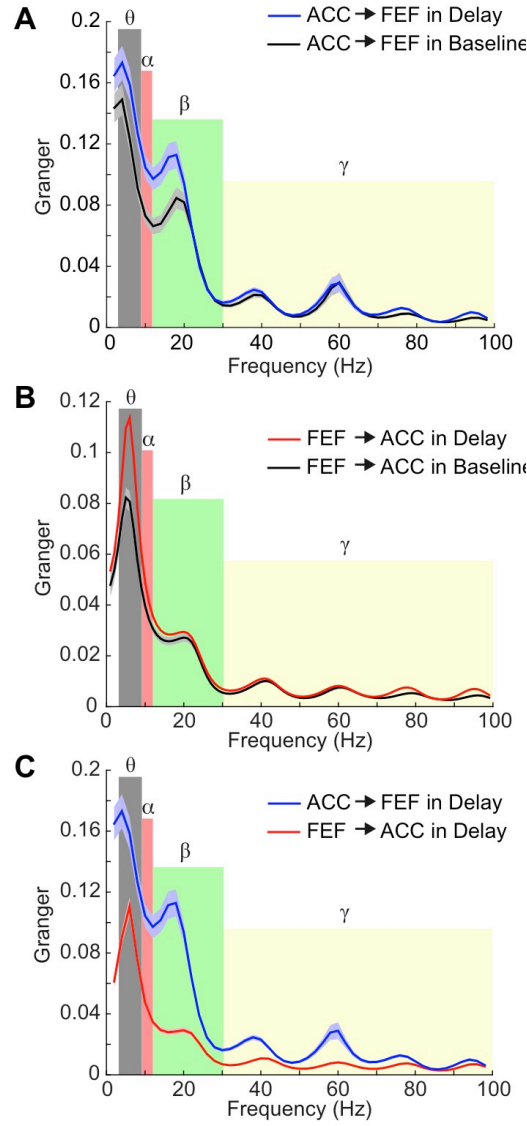
**Supplementary Figure 3.1. Schematic reconstruction of the recording sites.** The recording sites are overlaid on the F99 surface (using Caret software, Van Essen lab) according to the composite atlas of Van Essen et al. (2012)<sup>2</sup>. The left column is the reconstruction of the ACC recording sites shown on a fiducial (up), inflated (middle) and flat surface map. The arrows on the top and middle panels denote the location of the angle of the Arcuate sulcus. Similarly, the left column shows the reconstruction of the FEF recording sites.



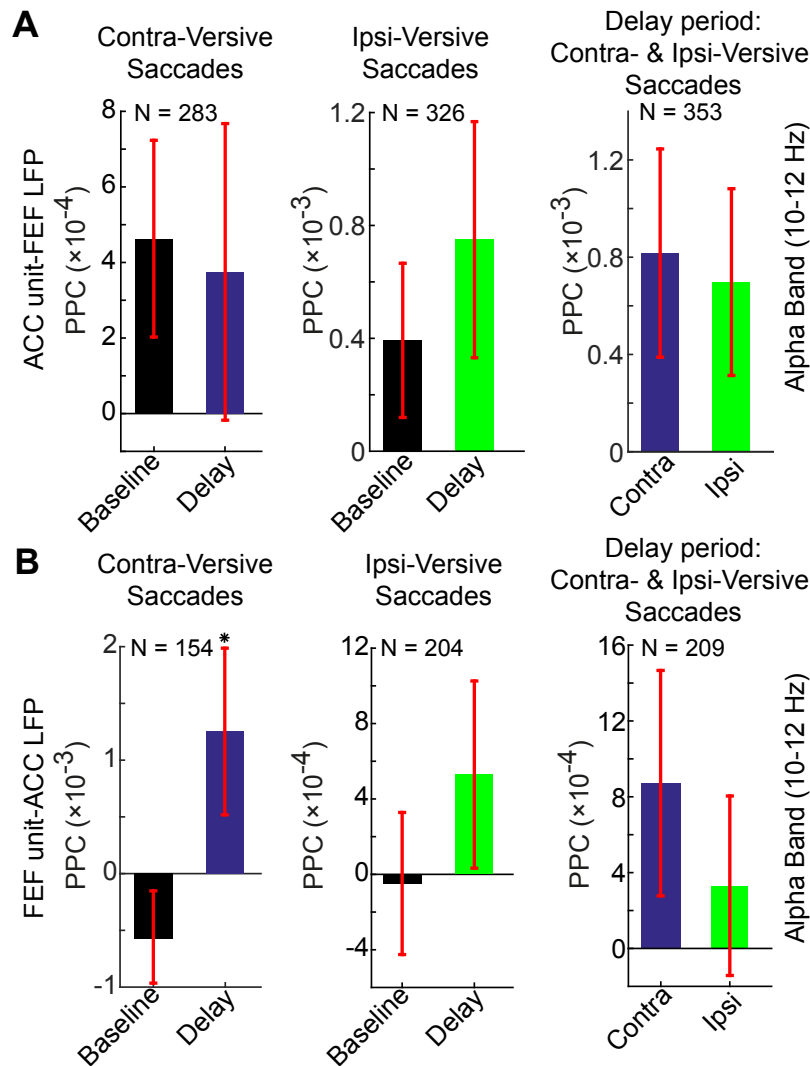
**Supplementary Figure 3.2. WPLI-debiased spectrum.** (A) The phase synchronization spectrum between ACC and FEF in memory-guided saccades is depicted across all recording pairs ( $n=674$ ). The panel shows larger ACC-FEF phase synchronization across theta and beta bands in the delay period (400-1100ms following the stimulus onset, blue) compared to the baseline (700ms prior to the fixation onset, black). (B) The phase synchronization spectrum between ACC and FEF in pro-/anti-saccades is depicted across all recording pairs ( $n=674$ ). The panel shows larger ACC-FEF phase synchronization across theta and beta bands in the preparatory period (400-1100 ms following the fixation onset, blue) compared to the baseline (700 ms prior to the fixation onset, black). The shading shows  $\pm$  SEM.



**Supplementary Figure 3.3. Increased theta-coherence between ACC and FEF after event-related signal subtraction.** (A) Time-Frequency spectra of the WPLI-debiased coherence between the FEF and ACC in memory-guided saccade task after subtraction of the averaged event-related potentials from the raw signal. The white contour shows the area in which the subsequent analyses were performed (see Methods). The dashed lines demarcate the time of the onset and offset of the target stimulus. (B) WPLI-debiased FEF-ACC coherence spectrum of the individual monkeys in the delay period across all recording pairs ( $n=674$ ). (C) Theta band (3-9 Hz) time course of the ACC-FEF WPLI-debiased phase synchronization. (D) Beta band (12-30 Hz) time course of the ACC-FEF WPLI-debiased phase synchronization.

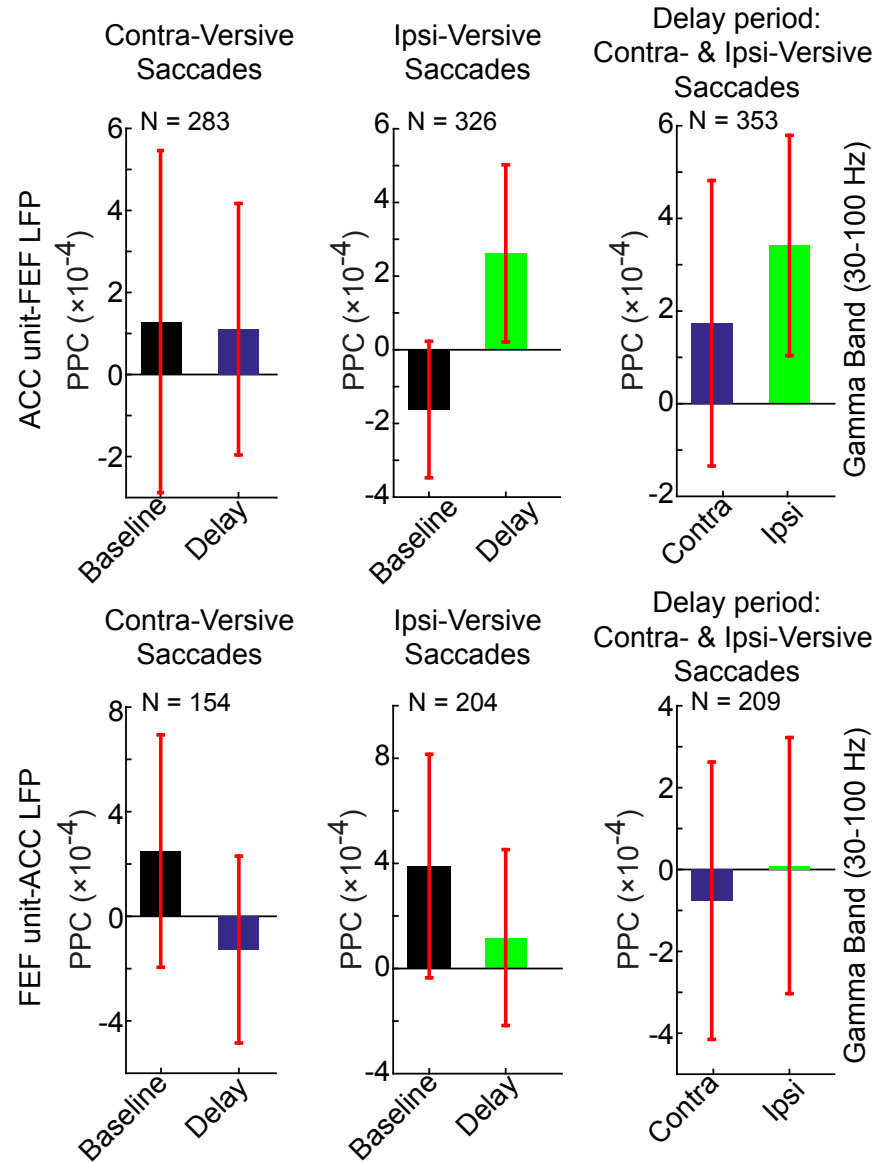


**Supplementary Figure 3.4. Granger causality spectrum between ACC and FEF.** (A) Causal effect of ACC over FEF ( $G_{ACC \rightarrow FEF}$ ) in the delay period (400-1100ms following the stimulus onset, blue) and the baseline (700 ms prior to fixation onset, black). The causal effect of ACC over FEF is larger in the delay period across theta and beta frequency range. (B) Causal effect of FEF over ACC ( $G_{FEF \rightarrow ACC}$ ) in the delay period (red) and the baseline (black). The causal effect of FEF over ACC is larger in the delay period across theta and beta frequency range. (C) Causal effect of ACC over FEF ( $G_{ACC \rightarrow FEF}$ , blue) is higher than the causal effect of FEF over ACC ( $G_{FEF \rightarrow ACC}$ , red) in the delay period across theta and beta frequency range. The shading depicts  $\pm$  SEM. The ACC-FEF channel pairs ( $n=275$ ) that displayed reversed Granger causality following the reversal of time series are included in this figure.

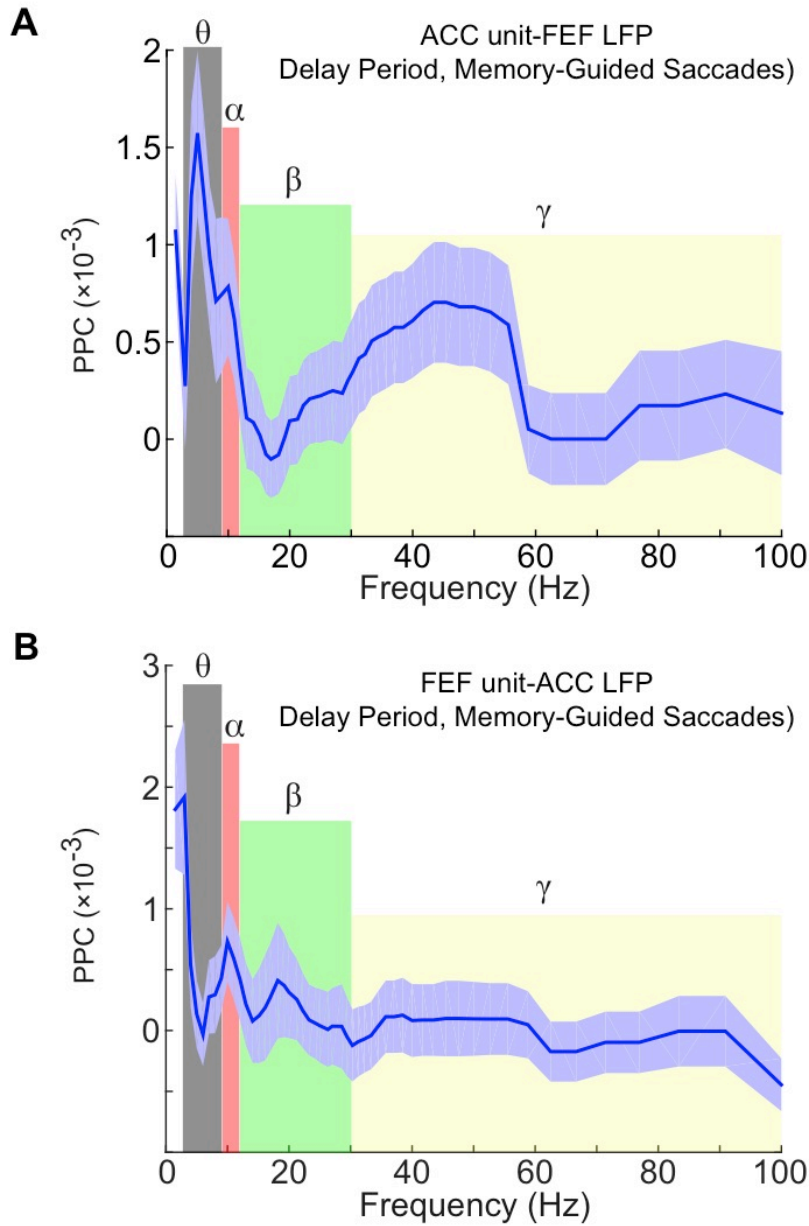


**Supplementary Figure 3.5. Pairwise phase consistencies (PPCs) across alpha band.** (A) PPC spike-field coherence spectrum of the population of the ACC units with the LFP's recorded in the FEF across the alpha frequency range. Comparison between baseline and delay of contra-verse saccades (left), comparison between baseline and delay of ipsi-verse saccades (middle) and comparison between the contra- and ipsi-verse saccades in the delay period (right). (B) PPC spike-field coherence spectrum of the population of the FEF units with the LFP's recorded in the ACC across the alpha frequency range. Comparison between baseline and delay of contra-verse saccades (left), comparison between baseline and delay of ipsi-verse saccades (middle) and comparison between the contra- and ipsi-verse saccades in the delay period (right). Error bars denote SEM in all panels. \*:  $p < 0.05$ , paired t-test).





**Supplementary Figure 3.6. Pairwise phase consistencies (PPCs) across gamma band.** (A) PPC spike-field coherence spectrum of the population of the ACC units with the LFP's recorded in the FEF across the gamma frequency range. Comparison between baseline and delay of contra-verse saccades (left), comparison between baseline and delay of ipsi-verse saccades (middle) and comparison between the contra- and ipsi-verse saccades in the delay period (right). (B) PPC spike-field coherence spectrum of the population of the FEF units with the LFP's recorded in the ACC across the gamma frequency range. Comparison between baseline and delay of contra-verse saccades (left), comparison between baseline and delay of ipsi-verse saccades (middle) and comparison between the contra- and ipsi-verse saccades in the delay period (right). Error bars denote SEM in all panels. \*:  $p < 0.05$ , paired t-test).



**Supplementary Figure 3.7. Pairwise phase consistencies (PPCs) spectrum.** (A) PPC spike-field coherence spectrum of the population of the ACC units with the LFP's recorded in the FEF across the frequency range of 1.5-100 Hz in the delay period of memory-guided saccade task. (B) PPC spike-field coherence spectrum of the population of the FEF units with the LFP's recorded in the ACC across the frequency range of 1.5-100 Hz in the delay period of memory-guided saccade task. In both panels, the peak spike-field coupling is observed in theta frequency range. Shades denote  $\pm$  SEM.

## **CHAPTER 4:**

### **4. GENERAL DISCUSSION:**

#### ***4.1. SUMMARY OF THE MAIN FINDINGS:***

##### ***4.1.1. FEF is functionally connected to the ACC and there is a difference between the functional connectivity of the medial and lateral FEF:***

The detailed explanation of the medial and lateral functional connectivity results is discussed in chapter 2. Here, I will provide more details specifically regarding the functional connectivity of the medial and lateral FEF with ACC. I observed that areas in the medial wall of the hemispheres, namely anterior and posterior cingulate cortices, show a higher degree of functional connectivity with medial than lateral FEF. Specifically in the anterior cingulate cortex, our maps show that caudal area 24 and areas of the cingulate cortex rostral to the genu of corpus callosum are functionally connected to the medial FEF. Schall and colleagues have shown that medial FEF is connected with area 23, that corresponds to the posterior cingulate cortex (Schall et al. 1995). However, the authors did not report the connectivity of the FEF with ACC. In another study conducted by Bates and Goldman-Rakic, tracer injection in area 8a (that corresponds to our medial FEF seed) led to anterograde and retrograde labeling throughout much of the cingulate cortex (Bates and Goldman-Rakic 1993). Although in that study the investigators did not inject tracers in area 8Av, which corresponds to our lateral FEF

seed, Bates and Goldman-Rakic reported that area 12 which is located rostral to the inferior limb of the arcuate sulcus has very weak connections with cingulate cortex (Bates and Goldman-Rakic 1993). In another study, Wang et al. found two areas in the anterior cingulate cortex, which were retrogradely labeled following FEF tracer injection, but the injection was not confined exclusively to the medial or lateral FEF (Wang et al. 2004). None of the above mentioned studies differentiated the connectivity of medial and lateral FEF throughout the cingulate areas, thus I cannot directly compare my findings with traditional tracing studies.

Furthermore, my findings demonstrated that SMA and area 46 are functionally connected to the medial FEF. Similarly, Bates and Goldman-Rakic have reported that area 8a is connected to the SMA (Bates and Goldman-Rakic 1993). In addition, Tian and Lynch have also shown that FEF is connected to area 46 but they have not distinguished the connectivity of medial vs. lateral FEF with area 46 (Tian and Lynch 1996). The fact that medial FEF is connected to both dl-PFC and ACC, but not the ventro-lateral prefrontal cortex (vl-PFC), suggests that these areas might share common physiological and functional characteristics. The dl-PFC has been documented to have extensive anatomical connectivity with the ACC, whereas vl-PFC does not appear to send/receive extensive projections to/from ACC (Petrides 2005). This finding is in line with my results and could suggest that medial FEF is connected with ACC and dl-PFC through mono- or polysynaptic projections. The next question arises is, does the anatomical connectivity between medial FEF, dl-PFC and ACC lead to shared functional properties across these frontal areas?

It has been suggested that the dl-PFC is involved in working memory performance. Although dl-PFC lesions do not result in complete loss of working memory capability, the capacity to maintain working memory of multiple objects is substantially reduced (Petrides 2000). Axonal fibers originating in dl-PFC, but not vl-PFC, pass medially and caudally to target cingulate cortex and then, follow through the retrosplenial areas and end in hippocampal regions (Petrides and Pandya 2004). These connections could aid dl-PFC in effective performance of working memory functions, especially because ACC is also suggested to be involved in working memory functions (Brignani et al. 2010).

The other consequence of the connectivity between ACC and medial prefrontal areas could be explained through the shared involvement of these areas in monitoring the consequences of actions. In a study conducted by Petrides et al., it was shown that vl-PFC was activated in response to a task in which subjects were required to distinguish between novel and familiar objects (Petrides et al. 2002). However, when the task involved monitoring the previous selection of the familiar objects, both the vl-PFC and dl-PFC were co-activated. This indicated that dl-PFC could be involved in monitoring the previous actions and their consequences. Such a performance monitoring role has also been described for ACC (Johnston et al. 2007; Procyk et al. 2016) and discussed in more detail in the general introduction section.

Taken together, my results indicated that medial FEF, dl-PFC and ACC are parts of a broader functional network. Additionally, my results support the notion that the functional connectivity of these areas may underlie their co-activation in tasks with higher cognitive demands, and that both dl-PFC and ACC are involved in monitoring the

efficient performance of tasks. In the next section, I will present the proposed mechanisms by which these areas communicate with each other in order to correctly perform behavioral tasks.

#### ***4.1.2. Theta and beta band synchronization is involved in the communication between FEF and ACC:***

We have demonstrated that the ACC and FEF display synchronized activity across theta and beta frequency bands and the strength of synchronization could predict the correct performance of the tasks. Even further, the ACC and FEF units were synchronized to FEF and ACC theta, and to a lesser extent beta activity. We have also previously demonstrated that ACC and FEF (especially the medial FEF) are parts of a functional network that include dl-PFC and also posterior parietal areas. I discussed in chapter 3 that the communication between ACC and FEF has a functional role in working memory performance. However, I also observed strong theta and to some extent beta band synchronization in the preparatory periods of pro-/anti-saccade task. This finding suggests that the functional network, of which ACC and FEF are parts, is not only involved in working memory, but also involved in other processes with varying cognitive demands. The activation of the same brain regions across different tasks has been previously reported, e.g. by Duncan and Owen (2000). The authors concluded that although each prefrontal region has been implicated in specialized cognitive functions, the involvement of prefrontal areas in diverse cognitive domains could be indicative of recruitment of a network of lateral prefrontal and dorsal cingulate areas in performance of cognitively demanding tasks. Our results provide evidence in support of this hypothesis

and we suggest that theta and beta synchrony could facilitate the communication between these areas.

My results also provide indirect evidence with regards to the physiological correlates of resting-state fMRI functional connectivity. The physiological mechanisms underlying resting-state fMRI functional connectivity has been a puzzling question in the field of neuroimaging. Logothetis and colleagues published one of the first papers that addressed this issue (Logothetis et al. 2001). The authors observed that the BOLD signal has the highest correlation with the local field potential (LFP) activity compared to the multi-unit activity. The authors concluded that the BOLD signal fluctuations in a given brain area are the product of the input and local neural processing rather than spiking output (Logothetis et al. 2001).

The question arises here is, which frequency band in LFP signal better correlates with the BOLD signal fluctuations? There have been several studies with somewhat contrasting results addressing this question. Leopold and colleagues (2003) have shown that the gamma band LFP power at a particular moment further fluctuates at a low frequency ( $< 0.1$  Hz). Furthermore, the slow fluctuations across gamma band follow the characteristic  $1/f$  pattern similar to the BOLD signal fluctuations (Leopold et al. 2003). In another study, a simultaneous LFP and fMRI recording experiment was conducted to investigate the correlation of neural activity with the BOLD signal (Shmuel and Leopold 2008). The investigators recorded the multi-unit activity and also LFP signal in the area V1 (primary visual area) and then, correlated this activity with the BOLD signal. They found that the relative multi-unit power fluctuations and particularly the gamma band power fluctuations correlated with time-lag BOLD signal. The correlation was strongest

with a ~6 seconds time lag between the BOLD signal and electrophysiological measures. This time lag corresponds well with the characteristic BOLD signal hemodynamic response function.

In a different study, the authors have performed fMRI and electrophysiological recordings in separate sessions (Wang et al. 2012). The electrophysiological recordings were performed in four distributed network sites. It was observed that these distant sites displayed phase synchronization mainly across lower frequency ranges ( $<20\text{Hz}$ ). Therefore, the authors suggested that lower frequencies might be responsible for the coherent BOLD signal fluctuations across distant areas (Wang et al. 2012). This finding is apparently in contrast to the previous studies demonstrating the correlation of BOLD signal with gamma power. However, it was shown that there was a strong cross-frequency coupling between phase of the lower frequencies and gamma power. The authors argued that the cross-frequency coupling could explain the gamma power correlation between distant brain areas, i.e. distant brain areas synchronize through lower frequencies and the gamma band synchronizes locally with the lower frequencies (Wang et al. 2012).

In a study conducted in our lab, simultaneous LFP and fMRI recordings were performed to further investigate the origin of the resting-state BOLD signal fluctuations. The results suggested that the spontaneous BOLD signal fluctuations exhibited positive correlation with the beta-low gamma band limited power (BLP) and negative correlation with that of the delta-theta band (Hutchison et al. 2015). It should be noted that the LFP signal was recorded in the prefrontal cortex (area 9/46d). The fact that different areas and neural circuits in the brain function through interactions across different frequency bands



has been previously described (Siegel et al. 2012). This could partially explain the discrepancy between the aforementioned studies, because each study has examined a different brain area through a variety of recording and analytical techniques.

Taken together, my results are in favor of theta and beta band synchronization as the underlying physiological correlate of the resting-state fMRI functional connectivity between FEF and ACC. However, this cannot be generalized to the functional connectivity between other brain regions, because each brain area might have varying oscillatory properties that are different than that of the ACC and FEF.

#### ***4.1.3. ACC affects FEF in memory-guided saccade task:***

The results of Granger causality analysis showed that the causal effect of ACC over FEF is higher than that of the FEF over ACC. This was an expected result given the role of ACC in higher cognitive functions. However, I still found that the FEF affects ACC, although to a lower extent than ACC affects FEF. The content of the FEF → ACC signal could be information regarding target location, given the extensive input FEF receives from visual areas (Ungerleider et al. 2008). Furthermore, FEF could send information regarding the subsequent motor plans to the ACC, so that ACC can process the expected outcome of these plans. The content of information sent from ACC to FEF could be a cognitive control signal related to the retained location of the saccade target in the memory-guided saccade task or the task rule in pro-/anti-saccade task. The causal effect of the ACC over FEF and vice versa seem to be conducted through theta and to a lesser extent beta band.

The involvement of beta band frequency in top-down control has received more attention than the theta band in the literature. For instance, it has been shown that the beta

band directional causal effect is asymmetric between PFC and posterior parietal cortex (PPC) (Salazar et al. 2012). Furthermore, it has been suggested that lower beta range frequencies (10-20 Hz) are involved in top-down control of visual selective attention (Bressler and Richter 2015). Correspondingly, the low beta activity is suggested to be involved in facilitating the influence of higher order visual areas over area V1 during attentional selection of visual stimuli (Bressler and Richter 2015). There is a recent emerging hypothesis suggesting that low beta band top-down control is mediated through the interaction with bottom-up gamma band oscillations (Wang 2010). According to this hypothesis which is so-called the Wang circuit, gamma band activity is generated in supragranular neurons in lower level cortical areas and relayed via layer II/III projection neurons to the layer IV input of the higher order cortical areas (Roopun et al. 2008). Conversely, the beta band activity of the infragranular layer in the higher level cortical area propagates through layer V neurons to the supragranular layer of the lower level area (Buffalo et al. 2011). The Wang circuit predicts that the stimulus related information is relayed from lower level to higher level areas through gamma band mediated mechanisms. This prediction has been shown to hold true; i.e. it has been demonstrated that the gamma band synchrony between V1 and V4 is essentially a bottom-up mechanism connecting the V4 with relevant retinotopic location of the attended stimuli in V1 (Bosman et al. 2012).

My findings are in line with the role of beta band synchrony in top-down control, i.e. the net direction of causal effect was from ACC to FEF across beta frequency range. However, I also found a strong causal effect of ACC over FEF across theta range frequencies. Even further, the spike-field coherence of ACC and FEF units with FEF and

ACC LFPs respectively, were more reliable across theta than beta range frequencies. This could be explained by the various patterns of oscillatory activity in different brain areas (Siegel et al. 2012). For instance, it has been repeatedly shown that the theta band is involved in the communication between prefrontal cortex and hippocampus (Hyman et al. 2005; Siapas et al. 2005; Siegel et al. 2012). Also, as mentioned in the introduction, the ACC displays prominent theta band activity (Womelsdorf et al. 2010), however, the involvement of theta band in top-down control of ACC over other frontal areas has not been thoroughly explored and my results provide evidence in this regard.

## ***4.2. CAVEATS AND LIMITATIONS:***

### ***4.2.1. Limited ability to record from multiple sites:***

The first caveat of this thesis is that it involves recordings only in sub-regions of the ACC and FEF. In order to explore the synchronization between ACC and frontal cortex, it would be ideal to record simultaneously from multiple sub-regions of ACC, multiple areas in dl-PFC and vl-PFC, as well as in the FEF. This would allow us to investigate synchronization across these sub-regions and examine whether there is a distinct synchronization pattern in each area, or the synchronization patterns are homogeneous across these frontal areas. However, there were technical constraints in doing so. I used computer-controlled micro-drives to advance tungsten microelectrodes into the brain. These micro-drives are relatively large and it is practically difficult to fit a large number of these drives over the target recording sites. One solution for this caveat could be using implanted chronic microelectrode arrays that would enable us to record from a large

number of electrodes distributed across a larger surface area of the cortex. The other solution could be using a semi-chronic recording system that again makes it possible to record across multiple electrodes.

#### ***4.2.2. Lack of specificity with regards to the recorded layer of the cortex:***

As mentioned above, each layer of the neocortex oscillates at a certain frequency range (Buffalo et al. 2011). Furthermore, different cortical regions send reciprocal projections through varying laminar layers of the cortex (Wang 2010). It would be of great interest if one could record from different laminas of the ACC and FEF cortices, and probe whether the so-called “Wang circuit” is also the underlying mechanism of communication between ACC and FEF. In order to do this, I should have used laminar high impedance electrodes in both sites to be able to record the single unit activity and also recognize the cortical layer of the recorded units. I could then understand in further detail the origin of theta and beta band in ACC and FEF, and the dynamics of the theta-beta band interaction in these areas. Indeed, very little is known regarding the theta-beta band interaction and the laminar recording could provide valuable information. It should be mentioned that recording from multiple cortical layers of the anterior bank of the arcuate sulcus could impose a technical challenge due to the anatomical constraints.

### **4.3. FUTURE DIRECTIONS:**

#### ***4.3.1. Investigating the theta- and beta band synchronization of medial and lateral***

##### ***FEF with ACC:***

As shown in chapter 2, the medial and lateral FEF exhibit distinct resting-state fMRI functional connectivity patterns. The medial FEF shows a stronger functional connectivity with ACC and even stronger with posterior cingulate cortex, whereas the lateral FEF does not exhibit a great deal of connectivity with ACC. The question that arises here is, is the synchronization pattern of the medial FEF different from that of the lateral FEF? One future direction will be to further analyze the data to answer this question. The results of this analysis could provide further evidence regarding the physiological mechanisms underlying resting-state fMRI functional connectivity. Furthermore, the results could further elucidate the dynamics of the communication between sub-regions of the large-scale brain networks.

#### ***4.3.2. Investigating the beta and theta band synchronization in pro-/anti-saccade task:***

In the third chapter of this thesis, I have performed the analyses mainly for the memory-guided saccade task. I also performed similar simultaneous recordings between the FEF and ACC across a pro-/anti-saccade task. The next future direction will be performing similar analyses across pro-/anti-saccade trials and examine whether the observed results are similar or different than what we have reported for the memory-guided saccade task. I predict that the results of the pro-/anti-saccade task will be very similar to the results reported in chapter 3. The reason for this prediction is that I speculate the theta and beta band synchrony provide a temporal framework through which different sub-regions of the prefrontal functional networks in the brain interact. Therefore, the synchronization

patterns will be expected to persist regardless of the task conditions. Indeed, such an observation would be consistent with the idea of a core-network of cortical areas that are co-activated for various task demands (Crittenden et al. 2016; Duncan and Owen 2000; Humphreys and Lambon Ralph 2015).

#### ***4.3.3. Identifying specific sub-classes of single units in the ACC and FEF that are coupled with different frequency bands:***

It can be hypothesized that different neuronal subtypes are coupled with certain frequency bands and their activity is modulated across specific task conditions and/or task epochs. We can classify neurons based on the shape of the action potential waveforms into putative interneurons and pyramidal neurons. Subsequently, we can investigate the synchronization pattern of each neuronal subtype and whether the synchronization pattern can predict certain functional properties in each subclass of neurons. The results of this analysis can provide valuable information with respect to the generators of certain frequency bands in the prefrontal cortex.

#### ***4.4. REFERENCES:***

- Bates JF, and Goldman-Rakic PS.** Prefrontal connections of medial motor areas in the rhesus monkey. *The Journal of comparative neurology* 336: 211-228, 1993.
- Bosman CA, Schoffelen JM, Brunet N, Oostenveld R, Bastos AM, Womelsdorf T, Rubehn B, Stieglitz T, De Weerd P, and Fries P.** Attentional stimulus selection through selective synchronization between monkey visual areas. *Neuron* 75: 875-888, 2012.
- Bressler SL, and Richter CG.** Interareal oscillatory synchronization in top-down neocortical processing. *Current opinion in neurobiology* 31: 62-66, 2015.
- Brignani D, Bortoletto M, Miniussi C, and Maioli C.** The when and where of spatial storage in memory-guided saccades. *NeuroImage* 52: 1611-1620, 2010.
- Buffalo EA, Fries P, Landman R, Buschman TJ, and Desimone R.** Laminar differences in gamma and alpha coherence in the ventral stream. *Proceedings of the National Academy of Sciences of the United States of America* 108: 11262-11267, 2011.

**Crittenden BM, Mitchell DJ, and Duncan J.** Task Encoding across the Multiple Demand Cortex Is Consistent with a Frontoparietal and Cingulo-Opercular Dual Networks Distinction. *The Journal of neuroscience : the official journal of the Society for Neuroscience* 36: 6147-6155, 2016.

**Duncan J, and Owen AM.** Common regions of the human frontal lobe recruited by diverse cognitive demands. *Trends in neurosciences* 23: 475-483, 2000.

**Humphreys GF, and Lambon Ralph MA.** Fusion and Fission of Cognitive Functions in the Human Parietal Cortex. *Cerebral cortex* 25: 3547-3560, 2015.

**Hutchison RM, Hashemi N, Gati JS, Menon RS, and Everling S.** Electrophysiological signatures of spontaneous BOLD fluctuations in macaque prefrontal cortex. *NeuroImage* 113: 257-267, 2015.

**Hyman JM, Zilli EA, Paley AM, and Hasselmo ME.** Medial prefrontal cortex cells show dynamic modulation with the hippocampal theta rhythm dependent on behavior. *Hippocampus* 15: 739-749, 2005.

**Johnston K, Levin HM, Koval MJ, and Everling S.** Top-down control-signal dynamics in anterior cingulate and prefrontal cortex neurons following task switching. *Neuron* 53: 453-462, 2007.

**Leopold DA, Murayama Y, and Logothetis NK.** Very slow activity fluctuations in monkey visual cortex: implications for functional brain imaging. *Cerebral cortex* 13: 422-433, 2003.

**Logothetis NK, Pauls J, Augath M, Trinath T, and Oeltermann A.** Neurophysiological investigation of the basis of the fMRI signal. *Nature* 412: 150-157, 2001.

**Petrides M.** Dissociable roles of mid-dorsolateral prefrontal and anterior inferotemporal cortex in visual working memory. *The Journal of neuroscience : the official journal of the Society for Neuroscience* 20: 7496-7503, 2000.

**Petrides M.** Lateral prefrontal cortex: architectonic and functional organization. *Philosophical transactions of the Royal Society of London Series B, Biological sciences* 360: 781-795, 2005.

**Petrides M, Alivisatos B, and Frey S.** Differential activation of the human orbital, mid-ventrolateral, and mid-dorsolateral prefrontal cortex during the processing of visual stimuli. *Proceedings of the National Academy of Sciences of the United States of America* 99: 5649-5654, 2002.

**Petrides M, and Pandya DN.** The frontal cortex. In: *The frontal cortex*, edited by Paxinos G. MJK. San Diego: Elsevier Academic Press, 2004, p. 950-972.

**Procyk E, Wilson CR, Stoll FM, Faraut MC, Petrides M, and Amiez C.** Midcingulate Motor Map and Feedback Detection: Converging Data from Humans and Monkeys. *Cerebral cortex* 26: 467-476, 2016.

**Roopun AK, Kramer MA, Carracedo LM, Kaiser M, Davies CH, Traub RD, Kopell NJ, and Whittington MA.** Period concatenation underlies interactions between gamma and beta rhythms in neocortex. *Frontiers in cellular neuroscience* 2: 1, 2008.

**Salazar RF, Dotson NM, Bressler SL, and Gray CM.** Content-specific fronto-parietal synchronization during visual working memory. *Science* 338: 1097-1100, 2012.

**Schall JD, Morel A, King DJ, and Bullier J.** Topography of visual cortex connections with frontal eye field in macaque: convergence and segregation of processing streams.

*The Journal of neuroscience : the official journal of the Society for Neuroscience* 15: 4464-4487, 1995.

**Shmuel A, and Leopold DA.** Neuronal correlates of spontaneous fluctuations in fMRI signals in monkey visual cortex: Implications for functional connectivity at rest. *Human brain mapping* 29: 751-761, 2008.

**Siapas AG, Lubenov EV, and Wilson MA.** Prefrontal phase locking to hippocampal theta oscillations. *Neuron* 46: 141-151, 2005.

**Siegel M, Donner TH, and Engel AK.** Spectral fingerprints of large-scale neuronal interactions. *Nature reviews Neuroscience* 13: 121-134, 2012.

**Tian JR, and Lynch JC.** Corticocortical input to the smooth and saccadic eye movement subregions of the frontal eye field in Cebus monkeys. *Journal of neurophysiology* 76: 2754-2771, 1996.

**Ungerleider LG, Galkin TW, Desimone R, and Gattass R.** Cortical connections of area V4 in the macaque. *Cerebral cortex* 18: 477-499, 2008.

**Wang L, Saalmann YB, Pinsk MA, Arcaro MJ, and Kastner S.** Electrophysiological low-frequency coherence and cross-frequency coupling contribute to BOLD connectivity. *Neuron* 76: 1010-1020, 2012.

**Wang XJ.** Neurophysiological and computational principles of cortical rhythms in cognition. *Physiological reviews* 90: 1195-1268, 2010.

**Wang Y, Matsuzaka Y, Shima K, and Tanji J.** Cingulate cortical cells projecting to monkey frontal eye field and primary motor cortex. *Neuroreport* 15: 1559-1563, 2004.

**Womelsdorf T, Johnston K, Vinck M, and Everling S.** Theta-activity in anterior cingulate cortex predicts task rules and their adjustments following errors. *Proceedings of the National Academy of Sciences of the United States of America* 107: 5248-5253, 2010.



## APPENDIX A: Documentation of Ethics Approval

**From:** eSiriusWebServer [mailto:[esiriusadmin@uwo.ca](mailto:esiriusadmin@uwo.ca)]

**Sent:** March 7, 2016 2:32 PM

**To:** [severlin@uwo.ca](mailto:severlin@uwo.ca)

**Cc:** [auspc@uwo.ca](mailto:auspc@uwo.ca); [auspc@uwo.ca](mailto:auspc@uwo.ca)

**Subject:** eSirius Notification - Annual Protocol Renewal APPROVED by the AUS 2008-125::7



2008-125::7:

**AUP Number:** 2008-125

**AUP Title:** Role of Frontal Cortex in Cognitive Control

**Yearly Renewal Date:** 02/01/2016

**The YEARLY RENEWAL to Animal Use Protocol (AUP) 2008-125 has been approved, and will be approved for one year following the above review date.**

1. This AUP number must be indicated when ordering animals for this project.
2. Animals for other projects may not be ordered under this AUP number.
3. Purchases of animals other than through this system must be cleared through the ACVS office. Health certificates will be required.

### REQUIREMENTS/COMMENTS

Please ensure that individual(s) performing procedures on live animals, as described in this protocol, are familiar with the contents of this document.

The holder of this Animal Use Protocol is responsible to ensure that all associated safety components (biosafety, radiation safety, general laboratory safety) comply with institutional safety standards and have received all necessary approvals. Please consult directly with your institutional safety officers.

Submitted by: Kinchlea, Will D  
on behalf of the Animal Use Subcommittee

*The University of Western Ontario*  
Animal Use Subcommittee / University Council on Animal Care  
Health Sciences Centre, • London, Ontario • CANADA – N6A 5C1  
PH: 519-661-2111 ext. 86768 • FL 519-661-2028  
Email: [auspc@uwo.ca](mailto:auspc@uwo.ca) • <http://www.uwo.ca/animal/website/>

# CURRICULUM VITAE

## Sahand Babapoor-Farrokhran

**Language Skills:** English, Farsi (Persian), Azerbaijani, Turkish, Arabic

### EDUCATION

April 2012 Transferred to Neuroscience PhD Program  
Jan 2011 Western University, Neuroscience graduate program  
Supervisor: Dr. Stefan Everling  
2001-2009 Tehran University of medical sciences, Tehran, Iran, MD degree  
2016-2021 Psychiatry residency program, Western University, London, ON, Canada

### AREAS OF RESEARCH INTEREST

Neuroimaging (resting-state fMRI), Electrophysiology and Neurophysiology, Cognitive Control

### THESIS & TITLE

PhD-project Role of Anterior Cingulate Cortex in Saccadic Eye Movements: a Resting-State fMRI and Single Neuron Recording Study; *Western University, Graduate Program in Neuroscience, London, Ontario, Canada*

MD Involvement of dopaminergic system of the ventral hippocampus in anxiety-related behavior; *Department of Pharmacology, School of Medicine, Tehran University of Medical Sciences, Tehran, Iran*

### AWARDS AND SCHOLORSHIPS

- 2014-2015 Winning **Ontario Graduate Scholarship (OGS)**; amount: **\$15000/year**. This scholarship is extremely competitive for international students and is awarded to only **8 out of more than one thousand international graduate students** at Western University
- 2011-2013 Western Graduate Research Scholarship (**WGRS**).
- 2001-2009 Educational Student Scholarship, Ministry of Health and Medical Sciences of Iran, MD program, Tehran University of Medical Sciences
- 2008 Being accepted in Iran's National Elites' Foundation (Bonyade Mellie Nokhbehan; [www.bmn.ir](http://www.bmn.ir)): A centre for outstanding students, scientists, artists and university faculties
- 2003 One of the 10 top students of Tehran university medical students

- 2001                      Ranked 83rd among 450000 participants in the nationwide Iranian university entrance exam and being accepted in Tehran University of Medical Sciences (The best and most competitive medical school in Iran)
- 1997-2001              Studying High school in National Organization for Developing Exceptional Talents (NODET) School (Shahid Beheshti, Oroumieh) after passing entrance exam
- 2000                      Winning **Silver Medal** of Iranian chemistry Olympiad

## **RESEARCH SKILLS**

- **Methods and Skills:** Monkey electrophysiology; Monkey resting-state fMRI; Antidromic Stimulation Technique; Single Neuron recording; Single cell data analysis, spectral analysis, field-to-field coherence and spike-to-field coherence analysis; fMRI data analysis using FSL and Matlab; Behavioral (Elevated Plus Maze, Conditioned place preference, pro-anti saccade task, memory guided saccade task); patient history taking and physical examination; Monkey, Rat and Mouse stereotaxic surgery; Matlab and Python programming
- **Statistics:** Statistics for Neuroscience, Biostatistics Courses (Tehran University and Institute for Cognitive Science Studies); fluency in SPSS and JMP, programming in R-software, Computation Neuroscience course (Python Programming), Computational Modeling and Neural Networks analysis using Matlab and Python
- **Operating Systems:** MS-Dos, Windows (2000, XP, Vista), Mac OS, UNIX, Linux
- **Other Skills:** Scientific writing (One course in Tehran University Students Research Center)

## **PROFESSIONAL AND RESEARCH EXPERIENCE**

- 2011-2015              *Western University, London, Ontario, Canada; Everling lab.* Performing electrophysiological recordings on non-human primates and single cell and LFP data analysis.
- 2011-2015              *Western University, London, Ontario, Canada; Everling lab.* Resting-state fMRI data collection on non-human primates and fMRI data analysis.
- March 2013              *York University, Toronto, Ontario, Canada.* Attending Fieldtrip workshop; Fieldtrip is a matlab toolbox for frequency and connectivity analysis
- Spring 2008-End of Summer 2009              Medical internship in Tehran University's hospitals (Including Imam Khomeini, Shariati, Razi, Pediatric medical center, Sina and Ruzbeh hospitals)
- 2009                      *Imam Khomeini hospital , Tehran, Iran*  
Advisor: Dr. Baheri and Dr. Shirzad  
Evaluation of the consequences of opium addiction in multiple body organs in the admitted opium addict patients of the Imam Khomeini hospital
- 2008-Spring 2009              *Department of Pharmacology, School of Medicine and Iranian National Center for Addiction Studies, Tehran University of Medical Sciences, Tehran, Iran*

Advisors: M.R Zarrindast and Ameneh Rezayof  
Interaction of dopaminergic and GABAergic systems of the ventral hippocampus in anxiety-related behavior

- 2008 *Pediatric medical center hospital, Tehran, Iran*  
Advisor: Mahmood Reza Ashrafi  
Case Report of the first reported Iranian cases of Pantothenate Kinase Associated Neurodegeneration (Formerly named Hallervorden-Spatz syndrome)
- 2007-2008 *Department of Pharmacology, School of Medicine and Iranian National Center for Addiction Studies, Tehran University of Medical Sciences, Tehran, Iran*  
Advisors: M.R Zarrindast and Ameneh Rezayof  
Performed research about involvement of dopaminergic system of the ventral hippocampus in anxiety-related behavior
- 2006 *Iranian center for neurological research, Imam Khomeini hospital, Tehran, Iran*  
Advisor: Mohammad Harirchian  
Evaluation of melatonin level in multiple sclerosis patients
- 2004-Spring 2007 *Department of Pharmacology, School of Medicine and Iranian National Center for Addiction Studies, Tehran University of Medical Sciences, Tehran, Iran*  
Advisors: M.R Zarrindast and Ameneh Rezayof  
Performed research about involvement of opioidergic system of the ventral hippocampus, the nucleus accumbens or the central amygdala in anxiety-related behavior

## **TEACHING EXPERIENCE**

- 2015-2016 *Western University, London, Ontario, Canada.*  
Instructor: Dr. Brian Corneil  
Lab Instructor. Neuroscience 2000 course.
- 2013-2014 *Western University, London, Ontario, Canada.*  
Instructor: Dr. Riley Hinson  
Lab Instructor. Psychology 2820; Research methods and statistics in psychology course.
- 2012-2013 *Western University, London, Ontario, Canada.*  
Instructor: Dr. Mike Atkinson.  
Teaching Assistant. Psychology 1000 course.
- 2011-2012 *Western University, London, Ontario, Canada.*  
Instructor: Dr. Laura Fazakas-Dehoog.  
Teaching Assistant. Psychology 1000 course.
- Winter 2011 *Western University, London, Ontario, Canada.*  
Instructor: Dr. Yves Bureau.

Teaching Assistant. Introduction to Behavioural and Cognitive Neuroscience course, Psych 2220B.

- 2004-2009        *Dr. Zarrindast's lab, Department of Pharmacology, School of Medicine, Tehran University of Medical Sciences, Tehran, Iran.*  
Teaching behavioral methods for the new comer researchers.
- 2001-2004(spring time)        *Oroumieh (my birth place) youngsters club, Oroumieh, Iran.*  
Teaching for preparation of chemistry Olympiad for high school students.
- 2001-2003        Teaching chemistry for high school students preparing for Iranian University entrance exam.

### **LEADERSHIP AND VOLUNTEERING EXPERIENCE**

- 2015        Public talk on behalf of Epilepsy support center to raise the awareness of the society about importance of epilepsy research; Western University, London ON, Canada
- 2014-2015        Neuroscience Program Grad student Representative, Western University, London ON, Canada
- 2014        Volunteering in Epilepsy support center; GAME ON program for children with epileptic disorders, London ON, Canada
- 2013-2014        Neuroscience steward in GTA (Graduate Teaching Assistant) union, Western University, London ON, Canada
- 2009        Chief of Interns in the Dermatology and Infectious disease ward, Tehran University of Medical Sciences, Tehran, Iran

### **PUBLICATIONS**

- **Sahand Babapoor-Farrokhran**, R. Matthew Hutchison, Joseph S. Gati, Ravi S. Menon, Stefan Everling; Functional connectivity patterns of medial and lateral macaque frontal eye fields reveal distinct visuomotor networks. *Journal of Neurophysiology*, 109:2560-2570, 2013
- Mohammad-Reza Zarrindast, **Sahand Babapoor-Farrokhran**, Savalan Babapoor-Farrokhran, Ameneh Rezayof; Involvement of opioidergic system of the ventral hippocampus, the nucleus accumbens or the central amygdala in anxiety-related behavior; *Life Sciences* 82 (2008) 1175–1181
- **Sahand Babapoor-Farrokhran**, Martin Vinck, Thilo Womelsdorf, Stefan Everling; Theta synchrony coordinates frontal eye fields and anterior cingulate cortex prior to memory-guided sensori-motor mapping tasks. Under review in *Nature Communications*.
- **Sahand Babapoor-Farrokhran**, Stefan Everling; Role of anterior cingulate cortex in saccade control. Under preparation.

## TALKS AND CONFERENCE PRESENTATIONS

- **Sahand Babapoor-Farrokhran**, Stefan Everling; Theta-band coherent activity is involved in transmission of between frontal eye field and anterior cingulate cortex, Epilepsy research day, 2015, Western University, London, Ontario, Canada (Talk)
- **Sahand Babapoor-Farrokhran**, Stefan Everling; Role of anterior cingulate cortex in saccade control, Epilepsy research day, 2015, Western University, London, Ontario, Canada (Talk)
- **Sahand Babapoor-Farrokhran**, Martin Vinck, Thilo Womelsdorf, Stefan Everling; Spike-field coupling of the anterior cingulate cortex and frontal eye field in goal-directed eye movements, Society for Neuroscience, 2015; Chicago, IL, USA (Poster)
- **Sahand Babapoor-Farrokhran**, Stefan Everling; Antidromic and orthodromic identification of anterior cingulate cortex neurons with projection to and from frontal eye fields, Electrophysiology workshop, 2014, Western University, London, Ontario, Canada (Talk)
- **Sahand Babapoor-Farrokhran**, Thilo Womelsdorf, Martin Vinck, Kevin Johnston, Stefan Everling; Theta-band coherent activity is involved in transmission of task relevant information between frontal eye field and anterior cingulate cortex, Society for Neuroscience, 2014; Washington DC, USA (Poster)
- **Sahand Babapoor-Farrokhran**, Kevin Johnston, Stefan Everling; Resting-state fMRI and electrophysiological characterization of connectivity between anterior cingulate cortex and frontal eye fields, Federation of European neuroscience Society, 2014; Milan, Italy (Poster)
- **S. Babapoor-Farrokhran**, K. Johnston, S. Everling; Beta-band Coherence Between Frontal Eye Field and Anterior Cingulate Cortex in Oculomotor Tasks, Society for Neuroscience, 2013; San-Diego, USA (Poster)
- **S. Babapoor-Farrokhran**, K. Johnston, S. Everling; Putative saccade-related area in cingulate cortex identified by resting-state fMRI in macaques, Society for Neuroscience, 2012; New Orleans, USA (Poster)
- **S. Babapoor-Farrokhran**, R. Hutchison, J. S. Gati, R. S. Menon, S. Everling; Resting state fMRI as a tool to localize putative saccade related brain areas in non-human primates, Society for Neuroscience, 2011; Washington, USA (Poster)
- **Sahand Babapoor-Farrokhran**, Savalan Babapoor-Farrokhran, Mohammad-Reza Zarrindast, Ameneh Rezayof; poster presentation: Bicuculine counteracts the anxiolytic effects of SCH23390 microinjection in the rat ventral hippocampus; FENS 2008; Geneva; Switzerland. (Poster)
- Savalan Babapoor-Farrokhran, **Sahand Babapoor-Farrokhran**, Mohammad-Reza Zarrindast, Ameneh Rezayof; poster presentation: Role of the opioidergic system in the rat nucleus accumbens on anxiety related behavior; FENS 2008; Geneva; Switzerland. (Poster)
- **Sahand Babapoor-Farrokhran**, Savalan Babapoor-Farrokhran, Mohammad-Reza Zarrindast, Ameneh Rezayof; poster presentation: The Nucleus accumbens and the Ventral Tegmental area are involved in morphine induced anxiolytic behavior; IBRO 2007, Melbourne, Australia (Poster)
- **Sahand Babapoor-Farrokhran**, Savalan Babapoor-Farrokhran, Mohammad-Reza Zarrindast, Ameneh Rezayof; poster presentation: The ventral hippocampus is involved in morphine-induced anxiolytic behavior. Mashhad (Iran) 18th physiology and pharmacology congress(2007) (Poster)

- **Sahand Babapoor-Farrokhran**, Mohammad-Reza Zarrindast, Ameneh Rezayof; poster presentation: The Dopaminergic system of ventral hippocampus is involved in anxiety related behavior. 3rd International congress on brain and behavior. Thessaloniki, Greece,(2007) (Poster)

### **PROFESSIONAL ASSOCIATION MEMBERSHIPS**

- 2016 College of Physicians and Surgeons of Ontario (CPSO)
- 2016 Professional Association of Residents of Ontario (PARO)
- 2012 Medical Council of Canada (MCC)
- 2011-2015 Member of Society of Graduate Studies (SOGS), Western University, London,
- 2011-2015 Member of Graduate Teaching Assistants (GTA) union, Western University, London, ON, Canada.
- 2011-2015 Member of Society for Neuroscience (SFN).
- 2008 Being accepted in Iran's National Elites' Foundation (Bonyade Mellie Nokhbeghan; [www.bmn.ir](http://www.bmn.ir)) ; A centre for outstanding students, scientists, artists and university faculties

### **HOBBIES AND INTERESTS:**

- Car racing
- Skiing
- Camping (including fishing, winter camping and ice fishing)